INVESTIGATION OF IN SITU PHYSICAL PROPERTIES OF SURFACE AND SUBSURFACE SITE MATERIALS BY ENGINEERING GEOPHYSICAL TECHNIQUES

Project Quarterly Report
October 1, 1965 to December 31, 1965

Joel S. Watkins, Editor and Project Chief

U.S. Department of the Interior
Geological Survey
Flagstaff, Arizona

February 1966

Work done on behalf of
National Aeronautics and Space Administration
Manned Spacecraft Center
Houston, Texas

NASA Contract T-25091 (G)

INVESTIGATION OF IN SITU PHYSICAL PROPERTIES OF SURFACE AND SUBSURFACE SITE MATERIALS BY ENGINEERING GEOPHYSICAL TECHNIQUES

Project Quarterly Report
October 1, 1965 to December 31, 1965

Joel S. Watkins, Editor and Project Chief

U.S. Department of the Interior
Geological Survey
Flagstaff, Arizona

February 1966

Work done on behalf of
National Aeronautics and Space Administration
Manned Spacecraft Center
Houston, Texas

NASA Contract T-25091 (G)

CONTENTS

Contents--continued

Contents--continued

ILLUSTRATIONS

Illustrations--continued

TABLES

HIGHLIGHTS AND SUMMARY

by Joel S. Watkins

The landing of the Russian Luna 9 spacecraft on the lunar surface as this report was going to press focuses the spotlight of immediate interest on two of the enclosed reports. One deals with the subsurface structure of the Southern Coulee of the Mono Craters, California, and the other describes a possible mechanism to account for the material of extremely low density thought to exist at the lunar surface.

Mono Craters Data

The Southern Coulee of the Mono Craters of eastern California is one of the best examples of a terrestrial pumice flow. On the basis of speculation by prominent geoscientists involved in the Space program that at least part of the mare surface is covered with pumiceous rock, In Situ Project personnel began studies on the rocks of the Southern Coulee in 1964. The recent landing of the Luna 9 spacecraft and the pictures transmitted back from the lunar surface add weight to the argument that parts of the lunar surface may indeed resemble the pumice of the Southern Coulee. Pictures of the surface of this flow are shown in figures 1 and 2. Figure 1 shows a generalized view of the rugged topography of the higher part of the Southern Coulee and figure 2 is a close-up of the blocks of pumice covering the surface.

The first report on Southern Coulee was by Loney (1964), who found that the Southern Coulee could be logically divided on the basis of morphologic or lithologic units.

Seismic data on Southern Coulee are few because poor trafficability on the Coulee has made it impossible to obtain data on all of Loney's units. However, available data suggest a relation between lithologic units (which are differentiated primarily on the basis of average densities).

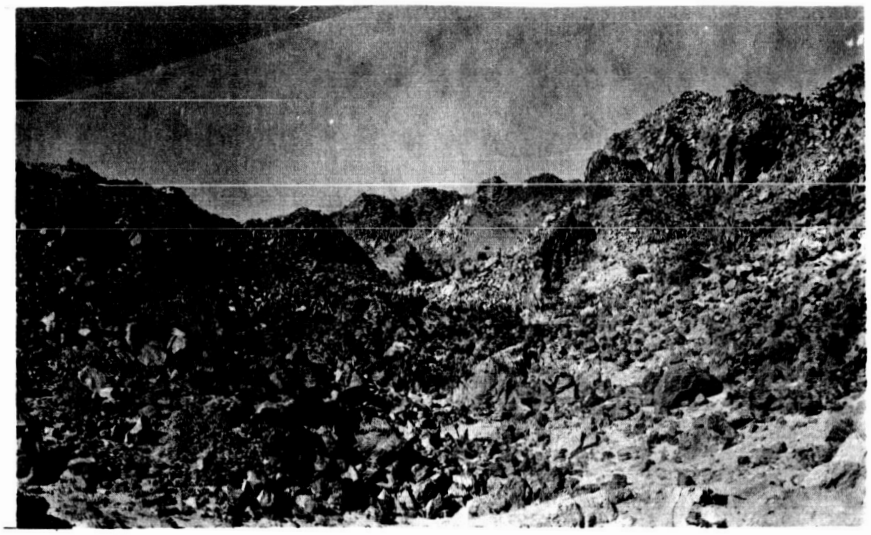

Figure 1.--Rugged topography in higher part of Southern Coulee (dome).

Figure 2.--Interbedded light-gray, dense pumice and black obsidian, unit of highest density, Southern Coulee.

Seismic sampling of major morphologic units revealed associated structures or substructures. For example, a velocity increase was detected within the dome and adjacent parts of the flow. Depth and velocity of the layers suggested a denser, more highly indurated rock mass beneath these units. The talus slope and the lower portion of the flow showed relatively uniform velocity distributions; and the fine ash fall overlying parts of the flow was distinguished by an anomalously low seismic velocity.

Inferred densities and structures were in general compatible with limited coring data. The data also indicate that sufficient vertical velocity differences exist in pumiceous lava flows to permit deduction of useful depth data from seismic refraction surveys.

Data currently available may be of value for testing lunar landing vehicles, studies of extraterrestrial vehicular or pedestrian activity and evaluation of remote-sensing equipment.

Density of Lunar Surface Materials

Recent excavation on S P flow north of Flagstaff suggests that low-density materials, such as the pumice of Mono Crater, if packed as loosely as blocks found on S P flow, may provide an explanation for lunar surface densities as low as 0.3 g per cc.

Members of the In Situ Project found that the bulk density of blocky, andesitic lava lying within 3 m of the surface of S P flow was only 1.23 g per cc, although the bulk density of individual blocks was 2.22 g per cc. Replacement of these blocks in the same packing arrangement with blocks of pumice from Mono Craters, whose measured bulk densities are as low as 0.49 g per cc, would yield an average bulk density slightly less than 0.3 g per cc.

To obtain the measurements at S P flow, L. A. Walters excavated a hole in the shape of an inverted, truncated four-sided pyramid with base edge dimensions of approximately 3 m, altitude 3 m, and upper (or lower, depending on how one looks at it) edge dimensions of approximately 1.5 m. The volume of the hole was determined by lining it with heavy plastic and filling it with a measured quantity of water. Surface

irregularities were similarly taken into account by covering the surface with plastic prior to excavation, then filling the plastic to a predetermined level on a surrounding frame. Blocks were weighed as they were removed from the excavation.

A similar excavation will be undertaken at the Southern Coulee of the Mono Craters as soon as the snow melts (estimated to occur in late May or early June).

Results of Seismic Investigations

Following the discovery that SH waves could be detected to the virtual exclusion of P waves by angular accelerometers, numerous measurements have now been completed on various rock units of the test sites described in previous reports.

Perhaps the most exciting recent results consist of the discovery that the shear modulus and Young's modulus of materials under investigation can be estimated with reasonable certainty from the shear-wave velocities without consideration of any of the other parameters indicated by elastic theory. The fact that these moduli can be estimated from the SH-wave velocity is thought to be related to the fact that the granular and fractured materials investigated thus far are not truly elastic bodies. A more detailed description of the relationship between the shear modulus, Young's modulus, and the SH-wave velocity are included in a subsequent paper in this report. Laboratory data from some of the same sites yield elastic moduli which differ significantly from in situ elastic moduli; the difference is thought to be caused by the void spaces and fracturing within the materials. A parameter, θ, has been defined as the dry bulk density divided by Poisson's ratio. Qualitatively, it appears that θ is a function of the degree of fracturing and void space in the material.

Although analyses are still provisional and no formal report has been prepared for this quarter, the P-wave velocity of dry granular materials appears to be primarily a function of the bulk density. Preliminary analyses suggest that bulk density can be determined with a mean relative error of about 7 percent for rock samples taken from eight of the sites studied thus far.

P- and S-wave velocity data have been collected this quarter from the Middle Mesa site, Sierra Ancha site, a site near Kingman, Arizona, consisting of weakly consolidated to unconsolidated alluvium; and S-wave velocity data has been obtained from the Sonora Pass granite, the Mono Ash, the Southern Coulee and the Bishop Tuff.

Status of studies of programmed test sites is shown in table 1.

Geologic and Physical Properties Data

Laboratory measurements of the bulk density, grain density, permeability and pore geometry have been completed for core samples taken from the Amboy basaltic lava, the Bishop Tuff, the S P andesitic lava, and the Sonora Pass granite. These data represent the continuation of our efforts to develop a badly needed catalog of physical properties data for lunar analog materials. Details of these measurements and tabulations of the data from these sites constitute a significant section of this quarter's report.

During the quarter, coring has been completed at the Kaibab test site, and a 350-ft core hole is under way on the south rim of Meteor Crater. Cores from the Mono Ash, Sonora Pass granite, Bishop Tuff, and Southern Coulee pumice were taken and transmitted to the laboratory for the measurements mentioned above. Some shot-hole drilling was also done for seismic operations.

Petrographic studies are under way on samples taken from the Mono Ash, Sonora Pass, and Bishop Tuff sites.

Automatic Data Processing

Seismic data are currently digitized in a format compatible with the CDC 3600 operated by the Bureau of Standards in Boulder, Colorado. The In Situ Project has access to this computer for processing all data as well as access to IBM 1620 with DISCPACK at Arizona State College in Flagstaff, Arizona. The IBM 1620 is used primarily for writing and debugging programs, although limited data can be processed on this if prepared in card form.

Within the next quarter it is hoped that physical properties data

Table 1.--Status of lunar analog site studies

Site	Seismic Data	Geologic Map	Cores	Petrography	Phys. Prop.
Kana-a flow	X	X	X	X	X
Cinder Hills	X	0	4	4	/
S P flow	X	X	4	X	X
Kaibab Limestone	X	0	X	0	X
Mono Ash	X	0	X	/	X
Southern Coulee	X	X	X	/	X
Bishop Tuff	X	0	X	/	X
Sonora Pass	X	0	X	/	X
Amboy flow	X	/2	/	/2	X
Pisgah flow	X	/2		/2	
Meteor Crater	X1	X2	/	/2	/
Middle Mesa	X				
Sierra Ancha	X	0			
Kingman alluvium	X	0			

Explanation

X = complete.

/ = partially complete.

0 = not applicable.

1 = gravity, magnetic and radiation surveys are also under way.

2 = relatively complete reports available from other sources.

3 = surface sample data, no core data as yet.

4 = no adequate means of coring exists, petrography must be done from surface samples.

will be committed to punch cards and that the programs necessary to perform statistical analyses required for these data will be written. Some programs already in existence in various libraries can be modified to meet project needs; other programs must be written.

Existing programs include Fourier transforms for windows of varying size, autocorrelation function, cross-correlation function, and a velocity filter program. These programs provide an automatically plotted graph. A digital filtering program is being developed and we have obtained from Dr. Harkrider, formerly of the California Institute of Technology, programs for analysis of surface waves. Some minor changes are still required to adapt these programs to the CDC 3600.

Meteor Crater

In addition to coring on the south rim of Meteor Crater, Arizona, project personnel have conducted refraction and reflection studies of rim and subcrater structures. Travel time delays both on the rim and in the crater have been interpreted in terms of limiting depths of pulverization and brecciation. Anomalously low velocities beneath the overturned and brecciated material of the south rim and travel-time delays suggest that moderate fracturing may extend several hundred meters beyond the rim of the crater. Extreme fracturing and pulverization are thought to be limited to overturned rim deposits and materials within the crater.

A few discontinuous reflections were observed in the south rim materials.

Reference

Loney, R. A., 1964, Geology--Southern Coulee site, in Watkins J. S., Loney, R. A., Whitcomb, J. H., and Godson, R. H., Investigation of in situ physical properties of surface and subsurface site materials by engineering geophysical techniques--Project quarterly report, Oct. 1 to Dec. 31, 1964, p. 5-36.

FIELD VERIFICATION OF IN SITU PHYSICAL PROPERTIES

by Carl H. Roach and Gordon R. Johnson

ABSTRACT.--Bulk densities, grain densities, porosities, effective porosities, and permeabilities have been determined for core samples obtained from basaltic lava near Amboy, California, rhyolitic tuff north of Bishop, California, granite from Sonora Pass in the Sierra Nevada of eastern California, pumice from the Southern Coulee of Mono Craters, California, and andesitic basalt from S P flow north of Flagstaff, Arizona. These parameters have been related to local variations in geologic structure and constitute an initial effort in the compilation of physical properties of a suite of probable lunar analog rock types and structures.

A brief description of techniques precedes discussion of results.

Introduction

The purpose of the field verification of in situ physical properties investigations is to establish the engineering-geophysical properties of surface and near-surface rock materials in terrestrial geologic environments. These environments were chosen to represent possible analogs to lunar environments that may be selected for Early Apollo landing sites. More specifically, the engineering properties pertaining to surface bearing strength and general trafficability of lunar surface materials are being emphasized to provide data needed for the safe completion of Early Apollo missions.

The method of study will be to take sufficient analytical equipment to field locations (in mobile laboratories) to conduct detailed physical properties investigations of terrestrial materials. These test site investigations will be comprehensive enough to allow rigorous analysis of all physical and chemical data by statistical techniques (analysis of variance, trend analysis, and multiple regression analysis), so that the interrelations and natural variability of the physical properties can be scientifically determined and properly related to the terrestrial geologic environment.

During this report period, most of the effort was given to completing

physical properties measurements on drill cores previously obtained. More extensive analysis of the physical properties of these rocks will be conducted in the future. The results presented in this report then are only initial steps in the process of investigating the engineering-geophysical properties of rock materials from these sites.

Physical Properties Techniques

Porosity-density measurements

Porosity can be defined as that fraction of the bulk volume of a rock that is void space. Since porosity is the relationship between the bulk volume of a sample and either its grain volume or pore volume, bulk and grain density measurements are usually obtained as porosity is determined. Porosity, in percent, is determined by either of the following equations:

$$\% \text{ porosity} = 100 \times \frac{\text{bulk volume} - \text{grain volume}}{\text{bulk volume}} \qquad (1)$$

or

$$\% \text{ porosity} = 100 \times \frac{\text{pore volume}}{\text{bulk volume}} \; ;$$

$$\% \text{ porosity} = 100 \left(1 - \frac{\text{grain volume}}{\text{bulk volume}}\right). \qquad (2)$$

In the above equations the grain and bulk densities, if known, may be substituted for the grain and bulk volumes respectively.

There are two types of porosity--total and effective. The effective porosity accounts for only those pores which are interconnected, regardless of the length or complexity of the connections. In many rocks there are pores which are physically isolated from other pore spaces. These pores, in addition to the interconnected pore spaces constitute the total porosity. To obtain accurate determinations of total porosity the samples must be pulverized enough to destroy all minute isolated pore spaces so that accurate grain density or grain volume measurements may be made.

To determine the total porosity of samples from various test sites, the bulk and grain densities were ascertained on 2- to 3-inch segments of NX core (2.1-inch diameter). The core segments were first dried at

105°C for 48 hours to eliminate the moisture in the rocks. The dry weights (in grams) of the samples were next obtained and, finally, the volumes (in cubic centimeters) were determined by direct measurement with calipers. The bulk densities (in grams per cubic centimeter) were computed by using the formula, density = $\frac{\text{weight}}{\text{volume}}$. The grain densities were determined by pulverizing the samples, weighing the powder, and obtaining the volume of the powder by a liquid displacement technique. More specifically, the method was as follows: A 50-ml volumetric flask was exactly filled with a suitable liquid such as kerosene. The flask and kerosene were weighed on an analytical balance and this weight was recorded as W_1. The flask was then partially emptied and weighed again. About 10 g of the powdered sample was added and the flask and powder were weighed. The difference between empty flask and flask plus powder weights was recorded as W_2. The flask was then subjected to a vacuum for about 30 minutes to expel any trapped air from around the grains. After removal from the vacuum chamber the flask was again exactly filled with kerosene and weighed. This weight was recorded as W_3. The formula used for determining the density of the powdered sample was

$$\text{grain density} = \frac{\dfrac{W_2}{W_1 + W_2 - W_3}}{\text{specific gravity of kerosene}} . \qquad (3)$$

The specific gravity of kerosene is best determined by running a kerosene blank with a batch of about 12 samples. The kerosene blank flask is weighed empty and full. If this flask is previously calibrated to an exact volume the difference in these two weights divided by the calibrated volume is equal to the specific gravity of the kerosene.

Kerosene is used for grain density determinations because of its great affinity for wetting the grain surfaces and because it is readily available and inexpensive. Temperature fluctuations during the procedure can cause small but significant errors in the weighings due to variations in the density of kerosene and small variations in volume of the flasks at different temperatures. For this reason, a constant temperature bath would improve the precision of this method of obtaining

grain density. Nevertheless, grain densities of 2 to 3 g per cc are generally reproducible within about ± 0.03 g per cc by the present procedure.

After the grain and bulk densities have been determined, the total porosities of the samples can be computed by substituting these densities for bulk and grain volumes respectively in either equation (1) or (2) as follows:

$$\text{total porosity} = 100 \times \frac{\text{grain density - bulk density}}{\text{grain density}}$$

or

$$\text{total porosity} = 100 \left(1 - \frac{\text{bulk density}}{\text{grain density}} \right) .$$

Effective porosity can be measured in a number of ways, but all methods involve injecting a gas or liquid into the open pores or removing and measuring the air from the pore spaces. A convenient instrument for measuring effective porosity of many rock types is the Ruska field porometer (model 1070). The field porometer consists of a manifold block to which is attached a metering cylinder and piston assembly with a measuring screw and micrometer sleeve for measuring displacement volumes. A core sample is placed into a cup which in turn is connected to the manifold so as to be airtight. The pressure is raised to a reference pressure by screwing in the micrometer sleeve. This reading, which is proportional to the grain volume, is recorded as "R core." The core sample is then immersed in a mercury pycnometer, and the displaced mercury, which is equal to the bulk volume of the core, is measured in the same manner as the core. The mercury reading, which is proportional to the bulk volume of the core, is recorded as "R hg."

An alternate and simpler method of obtaining R hg is to find the calipered bulk volume of the core sample and determine the R hg number from a calibration chart supplied with the instrument. This alternate method of obtaining R hg is especially useful in rocks with large pores that admit mercury and introduce error.

Since R core and R hg are proportional to the grain and bulk volumes of the core, the porosity can be determined by substituting these values

in equation (2) giving the equation

$$\% \text{ effective porosity} = 100 \left(1 - \frac{R \text{ core}}{R \text{ hg}} \right) .$$

The Ruska field porometer is a reliable and reasonably reproducible method for measuring porosity and has an advantage over other porosity techniques in that it is nondestructive to the sample. In some rock types, such as vesicular lava, the porometer is especially useful since good porosity measurements on this type of rock are difficult to obtain by most other techniques.

Permeability measurements

Permeability is a measure of the ability of a porous material to transmit fluids. Permeability of rocks is expressed in darcys or, more commonly, millidarcys. A rock having a permeability of 1 darcy will transmit 1 ml per second of a fluid of 1 centipoise viscosity through a cross-sectional area of 1 cm^2 under a pressure gradient of 1 atm. It is assumed that as long as the flow is viscous, permeability of a rock is independent of the fluid being used. However, most liquids interact with the rock material and the permeability thus measured is commonly lower than the permeability measured using a dry gas. Any moisture within a rock may react with a gas, and a lower permeability measurement results. Permeability, then, measured on a dried rock specimen using a dry gas is usually the maximum value that can be obtained and is referred to as the "absolute" permeability.

Gas permeability measurements were made on all small cores for which porosity was measured with a Ruska gas permeameter (model 1011). This instrument consists basically of a core holder, three calibrated flowmeters, a hand-calibrated Bourdon tube pressure gauge, and a pressure regulator with a gas inlet. These components are mounted and permanently interconnected on a bakelite panel. The cores are sealed with rubber stoppers in the core holder so that any gas entering must pass through the length of the core before escaping to the atmosphere.

The Ruska gas permeameter has a permeability range from about 0.4

millidarcy to 5 darcys. The permeability is calculated by using the formula

$$(K) = \frac{\mu \bar{Q} L}{A P},$$

where

(K) = Permeability in darcys;

μ = Viscosity in centipoises of the gas used;

$\bar{Q}$ = Average rate of flow in cubic centimeters per second in the sample derived from the flowmeter reading;

L = Length of sample in centimeters;

A = Cross-sectional area of sample in square centimeters;

P = Pressure gradient in atmospheres as indicated by the pressure gauge.

Nitrogen is most commonly used since it is safe and nonreactive in the rocks. Friable rocks can be mounted in sealing wax to facilitate measurement.

Liquid permeability measurements were made on some core samples with a Ruska liquid permeameter (model 1013). This instrument, similar in appearance to the gas permeameter, consists basically of a core holder with a fill connection, cutoff valve and burette supported by its lower end in the core holder and by its upper end in a discharge-fill valve to which the gas pressure line from the pressure regulator is connected. Permeability measurements are made by determining the time necessary for a specific amount of liquid at a given temperature to pass through the core when a given pressure gradient is applied. The core sample is sealed in the core holder with a rubber stopper as in the gas permeameter.

The formula for calculating the liquid permeability is

$$K = \frac{\mu V L}{A P T}$$

where

K = Permeability in darcys;

μ = Viscosity in centipoises of the liquid used for making the measurements;

V = Volume of liquid (in cubic centimeters) transmitted through sample;

L = Length of sample in centimeters;

A = Cross-sectional area of the sample in square centimeters;

P = Pressure gradient in atmospheres as read on the pressure gauge;

T = Time in seconds for the fixed volume of liquid to flow through the sample.

To minimize chemical interactions between liquid and rock materials, tap water (rather than distilled water) was used to measure the permeabilities of samples studied. However, resulting permeabilities were low when compared with the gas permeabilities of the same samples. Also, reproducible liquid permeabilities could not be as easily obtained as could reproducible gas permeabilities. Because of these factors, liquid permeability measurements were not emphasized during the present period.

Capillary pressure curves

Capillary pressure curves can be obtained by forcing mercury at various pressure increments into the evacuated pores of a rock sample, and plotting the pressure-volume relationship. The instrument used by the U.S. Geological Survey is a Ruska Purcell-type capillary pressure apparatus (model 1057M), which consists of a Ruska 100-cc volumetric pump with a high-pressure pycnometer attached to the pump. This volumetric measuring unit is attached to a vacuum and pressure control assembly by means of a flexible high-pressure hose. The volumetric pump has a precision metering plunger and metering screw. A movable pump scale and hand wheel micrometer dial permit direct volume readings to 0.01 cc and indicate volume of mercury added to or withdrawn from the pycnometer by movement of the plunger.

Capillary pressure measurements are obtained by placing a sample (usually a core 1 inch in diameter and 1 inch long) in the pycnometer and evacuating the system to an absolute pressure of 20 microns. After the vacuum valve is closed, the pycnometer is filled with mercury by advancing the metering plunger, and the bulk volume of the sample is read directly on the pump scale and micrometer dial. The pump scale and dial

are reset to zero and the pressure in the system is raised to a convenient level. The metering plunger is next adjusted to compensate for the mercury injected into the sample and the volume of mercury injected is read directly on the dial. The pressure is again raised in increments and the volume of mercury injected at each increment is recorded until a desired upper pressure is reached. The system is designed to operate up to 150 atm absolute.

Capillary pressure curves are a convenient method to study pore size distribution of various rock types. Also, since the mercury will invade virtually any open pore in most samples, accurate effective porosity measurements can be directly obtained on the apparatus. However, only two or three pressure-volume curves can be obtained from the capillary pressure apparatus per day, so this method cannot be conveniently used for routine measurement of porosity. Porosities obtained on the apparatus can be useful though as control for the less precise porosity measurements obtained on the Ruska field porometer described earlier in this report.

Results of Physical Properties Measurements

Results of physical properties measurements of core samples previously obtained from drill cores at a number of test sites in the western United States have been assembled for interpretation and are discussed by locality below.

Mass physical properties such as porosity, dry bulk density, grain density, nitrogen permeability, and mercury capillary pressure curves were obtained on core samples from each site studied in order to develop methods of classifying the pore geometry of each rock type being studied. A method of classifying the pore geometry of a porous rock is desirable so that interrelationships between pore geometry and bearing strength can be better understood.

At each site, two types of samples were selected for physical properties measurements. Segments of NX-diameter core 2 to 3 inches long were selected to obtain bulk density and porosity measurements that would best represent the porosity and density of the rocks in situ. Two small cores 1 inch long and 1 inch in diameter were removed from

each of these larger core samples for studying the interrelationships between porosity, density, and nitrogen permeability. These two smaller cores were taken parallel and perpendicular to the axis of the drill core. The directional cores were obtained to determine if the permeability was directionally controlled within the rocks in situ.

Amboy basalt

The best estimate of the in situ porosity and dry bulk density of basalt at the Amboy site can be obtained from physical measurements of segments of the NX cores obtained during drilling operations at this site. NX cores are the largest samples available for physical measurements, and their use greatly reduces errors related to natural variability over very small distances. Density and porosity measurements were made on a number of NX core samples obtained from each of four drill holes at the Amboy site. Data are tabulated in table 1. Physical measurements on 29 NX core samples show that the dry bulk density varies from 1.80 to 2.79 g per cc and has an average of 2.43 g per cc. The porosity of these NX cores varies from a low of 4.2 to a high of 37.7 percent, and the average porosity is 17.0 percent. In each of the four drill holes, core samples near the ground surface tend to have a higher porosity and a lower dry bulk density than those from greater depths (table 1). The porosity near the ground surface in each drill hole is high probably because the drill holes started near the tops of individual flows and therefore would naturally have higher original porosities because of gas evolution or vesiculation along the tops of the flows as they cooled when exposed to the atmosphere.

Small cores were taken normal and parallel to the NX core axis to determine if the basalt at the Amboy site had any directional permeability and if there is a relation between permeability and porosity on the same core specimen. The results of the physical measurements on these small oriented cores indicate the following: (1) basalt with measurable permeability occurs in the upper portions of each drill hole and extends to a depth of about 20 feet only; (2) a comparison of the permeability of parallel and normal cores indicates that the basalt

has no pronounced directional permeability, and (3) there seems to be no relation between permeability and porosity for the cores studied (table 2 and fig. 1). A correlation coefficient of -0.280 was calculated for these porosity-permeability measurements.

Mercury capillary pressure curves indicate that the pore system of the Amboy basalt consists almost entirely of large and small pores with almost no pores of intermediate size. Seventy percent of all pores in this basalt can be saturated with mercury at pressures less than 1 atm.

As a result of these preliminary studies, the Amboy basalt can be described as a dense, relatively impermeable basalt containing mostly isolated pores in the lower parts, and somewhat interconnecting pores in the upper parts, of the flows.

Bishop Tuff

Density and porosity measurements on NX cores indicate that, to a depth of about 61 ft, the Bishop Tuff has an average dry bulk density of 1.52 g per cc and an average porosity of 37.4 percent (table 3). However, at a depth of about 50 ft the tuff becomes more ashy, and porosity increases as dry bulk density decreases. Below a depth of 61 ft the material was so incoherent that useful samples could not be collected. Therefore, the density-porosity data will be useful only down to a depth of about 61 ft.

Density and permeability measurements on small oriented cores of Bishop Tuff indicate no pronounced directional permeability to nitrogen (table 4). The ashy tuff in the lower part of the drill hole does, however, become much more permeable to nitrogen and probably reflects a change in pore geometry as a result of the more unconsolidated nature of the material at that depth. A semilogarithmic plot of the nitrogen permeability and porosity data indicates no apparent relationship between these two parameters for the tuff samples (fig. 2). A relation between nitrogen permeability and porosity for six ashy tuff samples from this drill hole may exist (fig. 2), but too few samples were available to establish it. An attempt will be made to collect adequate samples of ashy tuff from the Bishop site for a correlation study of

the porosity and permeability of this rock type. These studies will be conducted in order to classify pore geometry and to relate these characteristics to the bearing strength characteristics.

Mercury capillary pressure curves indicate that the Bishop Tuff has a pore system that consists of pores whose sizes are distributed almost uniformly throughout the intermediate and small ranges.

Sonora Pass granite

Density-porosity measurements on NX core samples from the Sonora Pass granite show that the granite is extremely uniform in its density and porosity (table 5). The dry bulk density ranges from 2.61 to 2.64 g per cc and averages 2.62 g per cc. The total porosity ranges from 0.4 to 2.6 percent and averages 1.8 percent. These density-porosity data indicate that the Sonora Pass granite is extremely uniform and dense relative to granite bodies in other localities in the western United States.

None of the samples from the small oriented cores of Sonora Pass granite had measurable permeability (table 6). The dry bulk density of the small oriented cores averages the same as for the large NX cores, but the average effective porosity for the oriented cores is 0.1 percent, whereas the average total porosity of the larger NX cores is 1.8 percent. The low effective porosity of the small oriented cores is due largely to the fact that most of the pore space in the granite is isolated.

Mercury capillary pressure curves were not obtained for this granite because of its extremely low effective porosity.

Southern Coulee pumice and ash site

Density-porosity measurements on NX cores from the Southern Coulee site indicate that pumice from the ground surface to shallow depths has a much higher porosity, and correspondingly a lower dry bulk density, than does the pumice at greater depths (table 7). The dry bulk density of the pumice from Southern Coulee ranges from 0.49 to 2.17 g per cc and averages 1.06 g per cc. The porosity of the pumice varies from

13.2 to 79.2 percent and averages 55.7 percent. The density-porosity data obtained on the Southern Coulee pumice indicates that this material is suitable for the engineering-geophysical properties studies that will soon be undertaken on high-porosity and low-density materials.

Density, porosity, and nitrogen permeability measurements made on small oriented cores of the Southern Coulee pumice indicate that the nitrogen permeability of the pumice is quite variable, but that the pumice does not have a pronounced directional permeability (table 8). The physical data also show that the pumice in the upper part of each drill hole tends to be more permeable than that in the lower part, but exceptions do exist (figs. 3-5).

A semilogarithmic plot of the nitrogen permeability and the porosity of the small oriented cores shows that the two do in fact correlate (fig. 6). A least squares line of log Y on X has been drawn through the data points to show the general relationship between these two parameters. Whereas the deviation of the data points from the least squares line is moderate, it is, however, about the same as for similar data on other rock types studied by other investigators. The correlation between nitrogen permeability and porosity of the Southern Coulee pumice appears to be good enough to justify further investigation of the pore geometry of this rock type and to determine the relation between pore geometry and the mechanical or bearing characteristics. Future studies are planned to investigate these relations of pore geometry to other physical characteristics of the pumice.

Mercury capillary pressure curves indicate that the more porous pumice at the Southern Coulee site has a pore system that consists almost entirely or pores large enough that they can be saturated with mercury at pressures less than 1 atm.

S P flow site

Density and porosity measurements on NX cores from the S P flow near Flagstaff, Arizona, indicate that basalt of the S P flow has a lower dry bulk density than does the basalt of the Amboy flow (tables 1 and 9). Also, the grain density of basalt from the S P flow is

significantly lower than the grain density of basalt from the Amboy flow, a fact compatible with the known mineralogical differences of these two flows.

Most of the small oriented cores selected for permeability study had no measurable amount of nitrogen permeability (table 10). However, the five samples obtained from the lower portion of the S P 1 drill hole did have significant amounts of nitrogen permeability. The permeability and porosity values for these five samples indicate, or suggest, that a fair correlation exists between these two parameters for the S P basalt, but since too few permeable samples were available at this time, no correlation has been attempted. In the future, we will try to collect a suite of permeable samples from this site so that correlation studies of permeability and porosity can be conducted.

Mercury capillary pressure curves of the S P basalt indicate that its pore system consists mainly of large and intermediate size pores, with actual pore size varying uniformly throughout the size range.

Summary of physical measurements

The mass physical properties summarized above by site locality represent the initial stage of a study designed to classify the pore system of each rock type being investigated and to relate the geometrical features of each pore system to various engineering properties such as bearing strength, compressive strength, shear strength, and tensile strength. If a good understanding can be obtained of the geometrical characteristics of the pore system, then these data can be correlated with the various engineering properties and a better understanding and capability for predicting the bearing strength characteristics of a given rock type will be possible. More extensive physical properties studies will be continued.

Table 1.--Density-porosity data for NX cores from Amboy, California site

Sample No.	Dry Bulk Density (g per cc)	Saturated Bulk Density (g per cc)	Grain Density (g per cc)	Total Porosity (percent)
AM1-1-14 1/	1.86	2.21	2.87	35.2
AM1-2-17	1.99	2.30	2.92	31.8
AM1-3-18	1.80	2.17	2.89	37.7
AM1-4-26	1.98	2.30	2.90	31.7
AM1-5-29	2.62	2.74	2.97	11.8
AM1-6-35	2.52	2.67	2.96	14.9
AM1-7-39	2.79	3.40	2.97	6.1
Averages	2.22	2.54	2.93	24.2
AM2-1-6	2.41	2.59	2.94	18.0
AM2-2-18	2.35	2.53	2.89	18.7
AM2-3-20	2.46	2.61	2.88	14.6
AM2-4-23	2.50	2.64	2.89	13.5
AM2-5-29	2.76	3.31	2.92	5.5
Averages	2.50	2.74	2.90	14.1
AM3-1-6	2.23	2.47	2.91	23.4
AM3-2-9	2.26	2.49	2.93	22.9
AM3-3-14	2.73	3.35	2.91	6.2
AM3-4-16	2.61	2.73	2.95	11.3
AM3-5-19	2.58	2.70	2.91	11.3

1/ Sample number consists of three parts: drill hole number, sample number in drill hole, and depth of sample.

Table 1.--Density-porosity data for NX cores from Amboy, California site --Continued

Sample No.	Dry Bulk Density (g per cc)	Saturated Bulk Density (g per cc)	Grain Density (g per cc)	Total Porosity (percent)
AM3-6-28	2.18	2.43	2.90	24.8
AM3-7-30	2.60	2.73	2.98	12.8
AM3-8-38	2.77	3.19	2.89	4.2
Averages	2.50	2.76	2.92	14.6
AM4-1-7	2.33	2.54	2.92	20.2
AM4-2-8	2.50	2.65	2.93	14.7
AM4-3-13	2.62	2.73	2.94	10.9
AM4-4-21	2.08	2.37	2.93	29.0
AM4-5-32	2.73	3.51	2.96	7.8
AM4-6-34	2.60	2.73	2.96	12.2
AM4-7-39	2.16	2.43	2.96	27.0
AM4-8-45	2.66	3.52	2.91	8.6
AM4-9-48	2.75	3.42	2.95	6.8
Averages	2.49	2.88	2.94	15.2
Grand Average	2.43	2.74	2.93	17.02

Table 2.-- Density, porosity, and permeability data for small oriented cores from Amboy, California site

Sample No.	Dry bulk Density (g per cc)	Effective Saturated Bulk Density (g per cc)	Effective Porosity (percent)	Nitrogen Permeability (millidarcys)
AM1-1-14-(P) 1/	1.95	2.27	32.0	4.96
AM1-2-17-(P)	2.00	2.20	19.4	NM 2/
AM1-2-17-(N)	2.10	2.27	17.2	NM
AM1-3-18-(P)	1.95	2.28	32.7	NM
AM1-4-26-(P)	2.05	2.24	19.0	NM
AM1-5-29-(P)	2.68	2.69	1.0	NM
AM1-6-35-(P)	2.61	2.68	7.1	NM
AM1-7-39-(P)	2.78	2.79	1.0	NM
AM1-7-39-(N)	2.79	2.80	1.0	NM
Averages	2.32	2.47	14.5	
AM2-1-6-(P)	2.57	2.68	11.2	NM
AM2-1-6-(N)	2.37	2.56	18.8	2.29
AM2-2-18-(P)	2.38	2.50	11.9	NM
AM2-2-18-(N)	2.28	2.45	17.0	0.70
AM2-3-20-(P)	2.53	2.59	6.3	NM
AM2-3-20-(N)	2.55	2.59	4.0	NM
AM2-4-23-(P)	2.48	2.63	15.0	1.34
AM2-4-23-(N)	2.51	2.65	13.8	0.89

1/ Sample number consists of four parts: drill hole number, sample number in drill hole, depth of sample, and (P) indicates core taken parallel to drill hole and (N) indicates core taken normal to drill hole axis.

2/ NM = not measurable; less than about 0.40 millidarcys.

Table 2.--Density, porosity, and permeability data for small oriented cores from Amboy, California site --Continued

Sample No.	Dry bulk Density (g per cc)	Effective Saturated Bulk Density (g per cc)	Effective Porosity (percent)	Nitrogen Permeability (millidarcys)
AM2-5-29-(P)	2.76	2.78	2.0	NM
AM2-5-29-(N)	2.79	2.80	1.0	NM
Averages	2.52	2.62	10.1	
AM3-1-6-(P)	2.14	2.41	26.7	1.34
AM3-1-6-(N)	2.35	2.54	20.0	3.38
AM3-2-9-(P)	2.25	2.45	23.0	1.72
AM3-2-9-(N)	2.31	2.52	21.0	165.8
AM3-3-14-(P)	2.66	2.75	8.9	NM
AM3-3-14-(N)	2.70	2.76	5.9	NM
AM3-4-16-(P)	2.61	2.71	9.9	13.9
AM3-4-16-(N)	2.61	2.71	10.1	23.9
AM3-5-19-(P)	2.58	2.70	11.9	2.06
AM3-5-19-(N)	2.63	2.73	10.0	2.93
AM3-6-28-(P)	2.24	2.44	20.8	NM
AM3-6-28-(N)	2.27	2.47	20.0	NM
AM3-7-30-(P)	2.61	2.67	6.1	NM
AM3-8-38-(P)	2.76	2.77	1.0	NM
AM3-8-38-(N)	2.75	2.75	0.0	NM
Averages	2.50	2.63	13.1	

Table 2.--Density, porosity, and permeability data for small oriented cores from Amboy, California site --Continued

Sample No.	Dry bulk Density (g per cc)	Effective Saturated Bulk Density (g per cc)	Effective Porosity (percent)	Nitrogen Permeability (millidarcys)
AM4-1-7-(P)	2.44	2.60	15.8	2.38
AM4-1-7-(N)	2.08	2.36	28.4	2.35
AM4-2-8-(P)	2.51	2.66	14.6	3.91
AM4-2-8-(N)	2.50	2.64	14.0	1.34
AM4-3-13-(P)	2.60	2.72	11.7	1.39
AM4-3-13-(N)	2.61	2.73	11.7	NM
AM4-4-21-(P)	2.16	2.42	26.0	NM
AM4-5-32-(P)	2.73	2.81	7.8	NM
AM4-5-32-(N)	2.77	2.78	1.0	NM
AM4-6-34-(P)	2.56	2.68	11.7	NM
AM4-6-34-(N)	2.68	2.78	9.8	NM
AM4-7-39-(P)	2.29	2.49	20.0	NM
AM4-8-45-(P)	2.67	2.71	3.9	NM
AM4-8-45-(N)	2.72	2.76	3.9	NM
AM4-9-48-(P)	2.73	2.79	5.8	NM
AM4-9-48-(N)	2.76	2.81	4.9	NM
Averages	2.55	2.67	11.9	- - -
Grand Average	2.49	2.61	12.35	- - -

Table 3.--Density-porosity data for NX cores from Bishop, California site

Sample No.	Dry Bulk Density (g per cc)	Saturated Bulk Density (g per cc)	Grain Density (g per cc)	Total Porosity (percent)
BT1-1-12 1/	1.55	1.92	2.47	37.2
BT1-2-16	1.59	1.93	2.44	34.8
BT1-3-20	1.60	1.95	2.45	34.7
BT1-4-23	1.60	1.93	2.42	33.9
BT1-5-27	1.61	1.95	2.44	34.0
BT1-6-31	1.61	1.96	2.47	34.8
BT1-7-35	1.58	1.94	2.46	35.8
BT1-8-39	1.57	1.92	2.42	35.1
BT1-9-45	1.52	1.89	2.42	37.2
BT1-10-47	1.48	1.86	2.41	38.6
BT1-11-53	1.39	1.80	2.36	41.1
BT1-12-55	1.34	1.77	2.37	43.5
BT1-13-61	1.28	1.74	2.37	46.0
Averages	1.52	1.89	2.42	37.4

1/ Sample number consists of three parts: drill hole number, sample number in drill hole, and depth of sample.

Table 4.--Density, porosity, and permeability data for small oriented cores from Bishop, California site

Sample No.	Dry Bulk Density (g per cc)	Saturated Bulk Density (g per cc)	Effective Porosity (percent)	Nitrogen Permeability (millidarcys)
BT1-1-12-(P) 1/	1.56	1.92	36.0	6.50
BT1-1-12-(N)	1.55	1.91	36.0	19.6
BT1-2-16-(P)	1.57	1.92	35.3	7.58
BT1-2-16-(N)	1.59	1.93	33.7	12.6
BT1-3-20-(P)	1.58	1.92	34.3	20.0
BT1-3-20-(N)	1.59	1.93	34.3	6.35
BT1-4-23-(P)	1.58	1.92	34.3	47.3
BT1-4-23-(N)	1.59	1.92	32.7	23.5
BT1-5-27-(P)	1.62	1.94	31.7	8.34
BT1-5-27-(N)	1.63	1.89	26.1	19.3
BT1-6-31-(P)	1.60	1.93	32.7	10.2
BT1-6-31-(N)	1.61	1.94	32.7	15.5
BT1-7-35-(P)	1.56	1.91	34.7	5.03
BT1-7-35-(N)	1.59	1.92	32.7	10.9
BT1-8-39-(P)	1.56	1.90	33.7	3.35
BT1-8-39-(N)	1.57	1.91	34.0	4.00
BT1-9-45-(P)	1.51	1.86	34.7	4.78
BT1-9-45-(N)	1.51	1.85	33.7	10.5
BT1-10-47-(P)	1.48	1.84	36.4	12.1

1/ Sample number consists of four parts: drill hole number, sample number in drill hole, depth of sample, and (P) indicates core taken parallel to drill hole and (N) indicates core taken normal to drill hole axis.

Table 4.--Density, porosity, and permeability data for small oriented cores from Bishop, California site--Continued

Sample No.	Dry Bulk Density (g per cc)	Saturated Bulk Density (g per cc)	Effective Porosity (percent)	Nitrogen Permeability (millidarcys)
BT1-10-47-(N)	1.47	1.83	36.0	11.9
BT1-11-53-(P)	1.42	1.81	39.0	29.0
BT1-11-53-(N)	1.37	1.78	40.6	34.3
BT1-12-55-(P)	1.35	1.76	41.4	47.5
BT1-12-55-(N)	1.30	1.72	42.4	45.8
BT1-13-61-(P)	1.29	1.72	43.4	66.0
BT1-13-61-(N)	1.30	1.73	43.4	63.9
Averages	1.51	1.87	35.6	20.99

Table 5.--Density-porosity data for NX cores from Sonora Pass, California site

Sample No.	Dry Bulk Density (g per cc)	Saturated Bulk Density (g per cc)	Grain Density (g per cc)	Total Porosity (percent)
SN1-1-2 1/	2.63	2.66	2.70	2.6
SN1-2-7	2.62	2.64	2.66	1.5
SN1-3-11	2.62	2.64	2.67	1.9
SN1-4-16	2.63	2.65	2.69	2.2
SN1-5-20	2.61	2.63	2.66	1.9
SN1-6-24	2.63	2.63	2.64	0.4
SN1-7-28	2.64	2.66	2.69	1.9
SN1-8-32	2.62	2.64	2.67	1.9
SN1-9-37	2.61	2.63	2.67	2.2
Averages	2.62	2.64	2.67	1.8

1/ Sample number consists of three parts: drill hole number, sample number in drill hole, and depth of sample.

Table 6.--Density, porosity, and permeability data for small oriented cores from Sonora Pass, California site

Sample No.	Dry Bulk Density (g per cc)	Saturated Bulk Density (g per cc)	Effective Porosity (percent)	Nitrogen Permeability (millidarcys)
SN1-1-2-(P) 1/	2.63	2.64	1.0	NM 2/
SN1-1-2-(N)	2.61	2.61	0.0	NM
SN1-2-7-(P)	2.62	2.62	0.0	NM
SN1-2-7-(N)	2.61	2.62	0.5	NM
SN1-3-11-(P)	2.61	2.61	0.0	NM
SN1-3-11-(N)	2.61	2.61	0.0	NM
SN1-4-16-(P)	2.63	2.63	0.0	NM
SN1-4-16-(N)	2.63	2.63	0.0	NM
SN1-5-20-(P)	2.61	2.61	0.0	NM
SN1-5-20-(N)	2.59	2.60	0.5	NM
SN1-6-24-(P)	2.62	2.62	0.0	NM
SN1-6-24-(N)	2.64	2.64	0.0	NM
SN1-7-28-(P)	2.64	2.64	0.0	NM
SN1-7-28-(N)	2.68	2.68	0.0	NM
SN1-8-32-(P)	2.61	2.61	0.0	NM
SN1-8-32-(N)	2.62	2.62	0.0	NM
SN1-9-37-(P)	2.61	2.61	0.0	NM

1/ Sample number consists of four parts: drill hole number, sample number in drill hole, depth of sample, and (P) indicates core taken parallel to drill hole and (N) indicates core taken normal to drill hole axis.

2/ NM = not measurable; less than about 0.40 millidarcys.

Table 6.--Density, porosity, and permeability data for small oriented cores from Sonora Pass, California site--Continued

Sample No.	Dry Bulk Density (g per cc)	Saturated Bulk Density (g per cc)	Effective Porosity (percent)	Nitrogen Permeability (millidarcys)
SN1-9-37-(N)	2.61	2.61	0.0	NM
Averages	2.62	2.62	0.1	

Table 7.--Density-porosity data for NX cores from Southern Coulee-Mono Craters, California site

Sample No.	Dry Bulk Density (g per cc)	Saturated Bulk Density (g per cc)	Grain Density (g per cc)	Total Porosity (percent)
SC2-1-10 1/	0.92	1.53	2.35	60.7
SC2-2-14	0.61	1.35	2.34	73.8
SC2-3-36	0.63	1.36	2.34	73.2
SC2-4-38	1.83	2.06	2.37	22.8
SC2-5-50	0.94	1.54	2.36	60.3
SC2-6-59	1.17	1.68	2.40	51.2
SC2-7-71	1.82	2.05	2.36	22.9
Averages	1.13	1.65	2.36	52.1
SC3-1-12	0.60	1.35	2.37	74.7
SC3-2-16	0.50	1.29	2.36	78.9
SC3-3-17	0.70	1.40	2.37	70.4
SC3-4-19	1.13	1.65	2.35	51.9
SC3-5-21	0.97	1.56	2.35	58.8
SC3-6-24	0.75	1.43	2.36	68.4
SC3-7-28	0.76	1.44	2.36	68.0
SC3-8-30	0.50	1.29	2.35	78.8
SC3-9-45	0.49	1.28	2.36	79.2
Averages	0.71	1.41	2.36	69.9

1/ Sample number consists of three parts: drill hole number, sample number in drill hole, and depth of sample.

Table 7.--Density-porosity data for NX cores from Southern Coulee-Mono Craters, California site--Continued

Sample No.	Dry Bulk Density (g per cc)	Saturated Bulk Density (g per cc)	Grain Density (g per cc)	Total Porosity (percent)
SC4-1-10	0.66	1.38	2.32	71.5
SC4-2-14	0.71	1.40	2.32	69.2
SC4-3-17	0.83	1.48	2.36	64.9
SC4-4-19	0.70	1.40	2.34	70.2
SC4-5-24	0.67	1.39	2.36	71.6
SC4-6-25	1.24	1.71	2.36	47.3
SC4-7-32	1.61	1.93	2.36	31.8
SC4-8-46	1.01	1.58	2.36	57.2
SC4-9-52	1.24	1.72	2.36	47.5
SC4-10-65	1.59	1.92	2.36	32.6
SC4-11-95	2.17	2.30	2.50	13.2
SC4-12-96	2.07	2.26	2.55	18.8
SC4-13-116	1.89	2.13	2.49	24.1
Averages	1.26	1.74	2.39	47.7
Grand Average	1.06	1.62	2.37	55.7

Table 8.--Density, porosity, and permeability data for small oriented cores from Southern Coulee-Mono Craters, California site

Sample No.	Dry Bulk Density (g per cc)	Saturated Bulk Density (g per cc)	Effective Porosity (percent)	Nitrogen Permeability (millidarcys)
SC2-1-10-(P) 1/	0.89	1.48	59.2	11.4
SC2-1-10-(N)	0.97	1.52	54.6	12.4
SC2-2-14-(P)	0.55	1.23	68.0	437.0
SC2-2-14-(N)	0.52	1.23	70.8	40.4
SC2-3-36-(P)	0.65	1.32	66.7	128.0
SC2-3-36-(N)	0.56	1.26	69.8	111.0
SC2-4-38-(P)	1.87	2.03	16.3	2.04
SC2-4-38-(N)	1.85	2.00	14.8	346.0
SC2-5-50-(P)	1.08	1.61	52.5	4.47
SC2-5-50-(N)	1.08	1.63	54.6	1.44
SC2-6-59-(P)	1.15	1.63	47.5	1.51
SC2-6-59-(N)	1.18	1.63	44.6	3.85
SC2-7-71-(P)	1.91	2.02	11.2	56.0
SC2-7-71-(N)	1.86	2.02	15.8	1.78
Averages	1.15	1.62	46.2	-

1/ Sample number consists of four parts: drill hole number, sample number in drill hole, depth of sample, and (P) indicates core taken parallel to drill hole and (N) indicates core taken normal to drill hole axis.

Table 8.--Density, porosity, and permeability data for small oriented cores from Southern Coulee-Mono Craters, California site--Continued

Sample No.	Dry Bulk Density (g per cc)	Saturated Bulk Density (g per cc)	Effective Porosity (percent)	Nitrogen Permeability (millidarcys)
SC3-1-12-(P)	0.59	1.23	63.5	203.1
SC3-1-12-(N)	0.59	1.21	62.2	57.4
SC3-2-16-(P)	0.48	1.13	65.3	27.9
SC3-2-16-(N)	0.49	1.13	64.3	26.2
SC3-3-17-(P)	0.61	1.21	60.2	68.7
SC3-3-17-(N)	0.71	1.29	57.6	29.9
SC3-4-19-(P)	1.11	1.52	40.6	NM
SC3-4-19-(N)	1.16	1.54	37.6	3.83
SC3-5-21-(P)	1.00	1.42	42.4	NM
SC3-5-21-(N)	0.92	1.38	45.5	1.63
SC3-6-24-(P)	0.75	1.31	55.6	1.43
SC3-6-24-(N)	0.68	1.26	58.2	2.36
SC3-7-28-(P)	0.68	1.28	59.6	3.73
SC3-7-28-(N)	0.80	1.35	55.1	99.7
SC3-8-30-(P)	0.48	1.16	68.0	33.1
SC3-8-30-(N)	0.48	1.16	67.7	61.1
SC3-9-45-(P)	0.49	1.13	64.3	26.8
SC3-9-45-(N)	0.48	1.14	66.3	54.2
Averages	0.69	1.27	57.4	-

Table 8.--Density, porosity, and permeability data for small oriented cores from Southern Coulee-Mono Craters, California site--Continued

Sample No.	Dry Bulk Density (g per cc)	Saturated Bulk Density (g per cc)	Effective Porosity (percent)	Nitrogen Permeability (millidarcys)
SC4-1-10-(P)	0.68	1.31	62.6	34.6
SC4-1-10-(N)	0.62	1.28	65.7	364.0
SC4-2-14-(P)	0.73	1.36	62.6	117.9
SC4-2-14-(N)	0.75	1.37	61.9	914.6
SC4-3-17-(P)	0.61	1.24	63.4	77.8
SC4-3-17-(N)	1.01	1.44	43.0	2.99
SC4-4-19-(P)	0.65	1.30	64.6	26.3
SC4-4-19-(N)	0.67	1.31	63.6	14.3
SC4-5-24-(P)	0.60	1.24	64.3	29.3
SC4-5-24-(N)	0.72	1.30	57.6	45.4
SC4-6-25-(P)	1.20	1.61	40.9	4.35
SC4-6-25-(N)	1.22	1.62	40.0	1.18
SC4-7-32-(P)	1.59	1.79	19.8	NM 2/
SC4-7-32-(N)	1.59	1.83	23.8	NM
SC4-8-46-(P)	1.02	1.50	48.0	5.25
SC4-8-46-(N)	0.97	1.55	57.6	147.4
SC4-9-52-(P)	1.22	1.62	40.0	4.09
SC4-9-52-(N)	1.26	1.65	38.6	NM
SC4-10-65-(P)	1.60	1.84	23.5	NM
SC4-10-65-(N)	1.60	1.82	21.8	NM

2/ NM = not measurable; less than about 0.40 millidarcys.

Table 8.--Density, porosity, and permeability data for small oriented cores from Southern Coulee-Mono Craters, California site--Continued

Sample No.	Dry Bulk Density (g per cc)	Saturated Bulk Density (g per cc)	Effective Porosity (percent)	Nitrogen Permeability (millidarcys)
SC4-11-95-(P)	2.23	2.30	7.0	NM
SC4-11-95-(N)	2.20	2.29	8.9	NM
SC4-12-96-(P)	2.11	2.24	12.9	4.42
SC4-12-96-(N)	2.12	2.25	12.9	1.36
SC4-13-116-(P)	1.94	2.14	19.8	NM
SC4-13-116-(N)	1.89	2.11	21.8	NM
Averages	1.26	1.67	40.3	- - -
Grand Average	1.06	1.53	47.0	- - -

Table 9.--Density-porosity data for NX cores from the SP Flow site Flagstaff, Arizona

Sample No.	Dry Bulk Density (g per cc)	Saturated Bulk Density (g per cc)	Grain Density (g per cc)	Total Porosity (percent)
SP1-1-13 1/	2.50	2.60	2.79	10.4
SP1-2-18	2.37	2.54	2.85	16.8
SP1-3-21	2.29	2.47	2.80	18.2
SP1-4-22	2.07	2.34	2.82	26.6
SP1-5-27	1.79	2.15	2.80	36.1
Averages	2.20	2.42	2.81	22.0
SP2-1-10	2.08	2.33	2.79	25.4
SP2-2-12	2.24	2.43	2.76	18.8
SP2-3-16	2.43	2.49	2.76	5.8
Averages	2.25	2.42	2.77	16.7
Grand Average	2.22	2.42	2.80	20.0

1/ Sample number consists of three parts: drill hole number, sample number in drill hole, and depth of sample.

Table 10.--Density, porosity, and permeability data for small oriented cores from the SP Flow site, Flagstaff, Arizona

Sample No.	Dry Bulk Density (g per cc)	Saturated Bulk Density (g per cc)	Effective Porosity (percent)	Nitrogen Permeability (millidarcys)
SP1-1-13-(P) 1/	2.50	2.54	3.9	NM 2/
SP1-2-18-(P)	2.37	2.48	10.7	NM
SP1-2-18-(N)	2.35	2.45	10.2	NM
SP1-3-21-(P)	2.27	2.46	18.6	178.3
SP1-4-22-(P)	2.07	2.31	23.8	164.4
SP1-4-22-(N)	2.10	2.31	21.4	136.2
SP1-5-27-(P)	1.82	2.10	28.2	1104.1
SP1-5-27-(N)	1.80	2.09	29.1	699.3
Averages	2.16	2.34	18.2	- - -
SP2-1-10-(P)	2.12	2.25	12.9	NM
SP2-2-12-(P)	2.27	2.44	16.7	NM
SP2-2-12-(N)	2.25	2.40	14.6	NM
SP2-3-16-(P)	2.48	2.51	2.9	NM
SP2-3-16-(N)	2.47	2.50	3.2	NM
Averages	2.32	2.42	10.1	- - -
Grand Average	2.22	2.37	15.1	- - -

1/ Sample number consists of four parts: drill hole number, sample number in drill hole, depth of sample, and (P) indicates core taken parallel to drill hole and (N) indicates core taken normal to drill hole axis.

2/ NM = not measurable; less than 0.40 millidarcys.

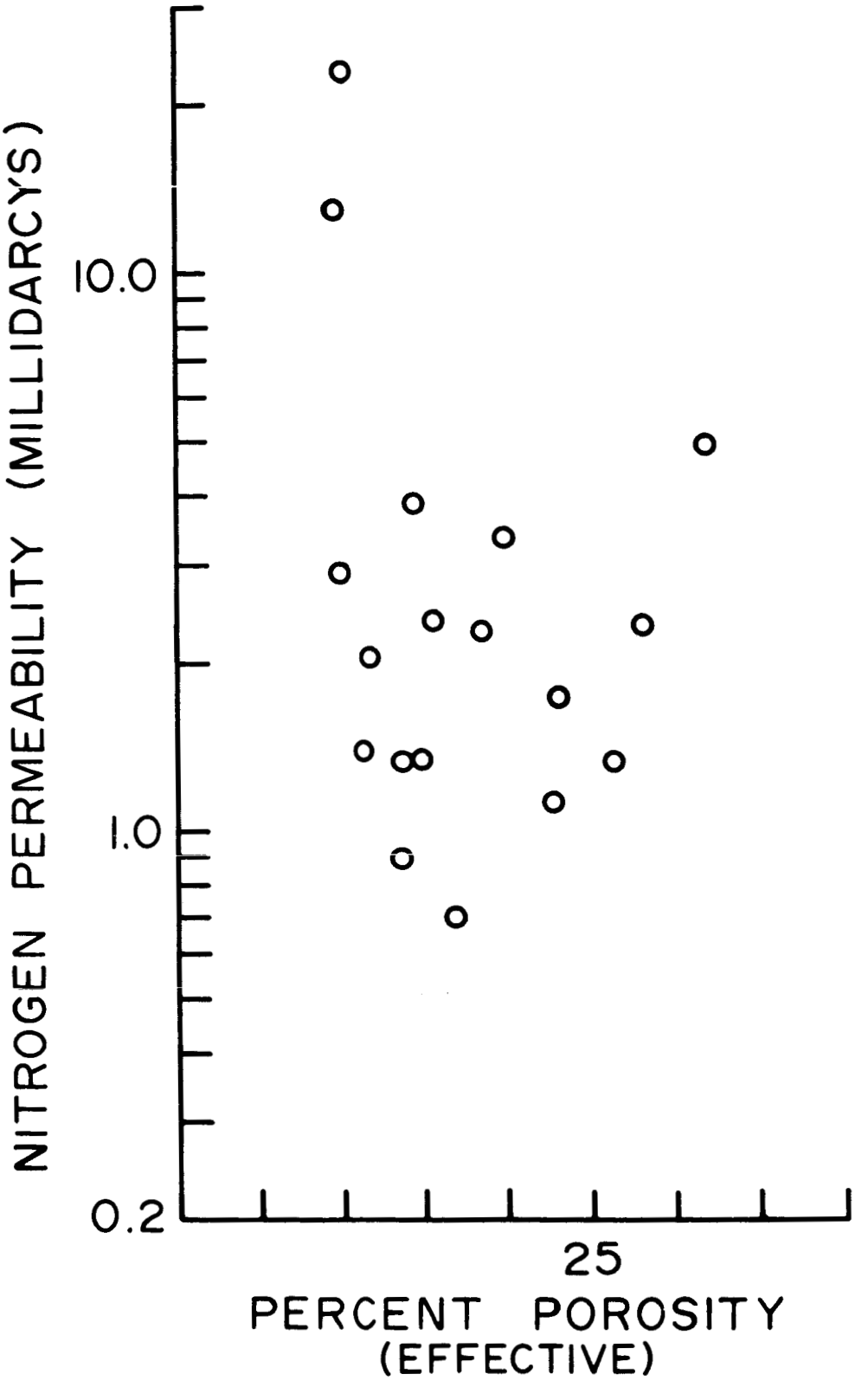

Figure 1.--Porosity and nitrogen permeability of basalt from Drill Holes AM-1 through AM-4, Amboy, California.

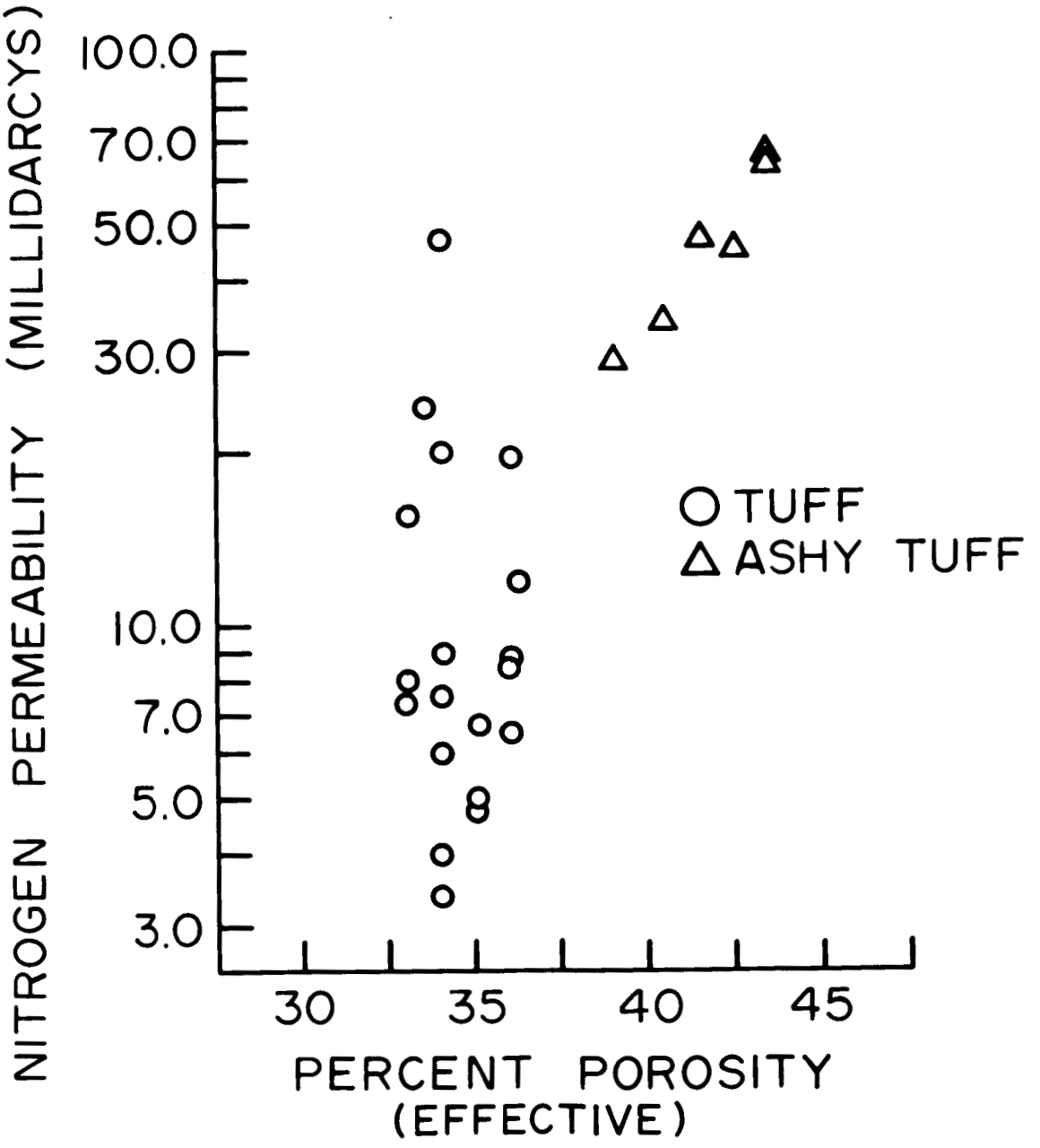

Figure 2.--Porosity and nitrogen permeability of tuff from Drill Hole BT1, Bishop, California.

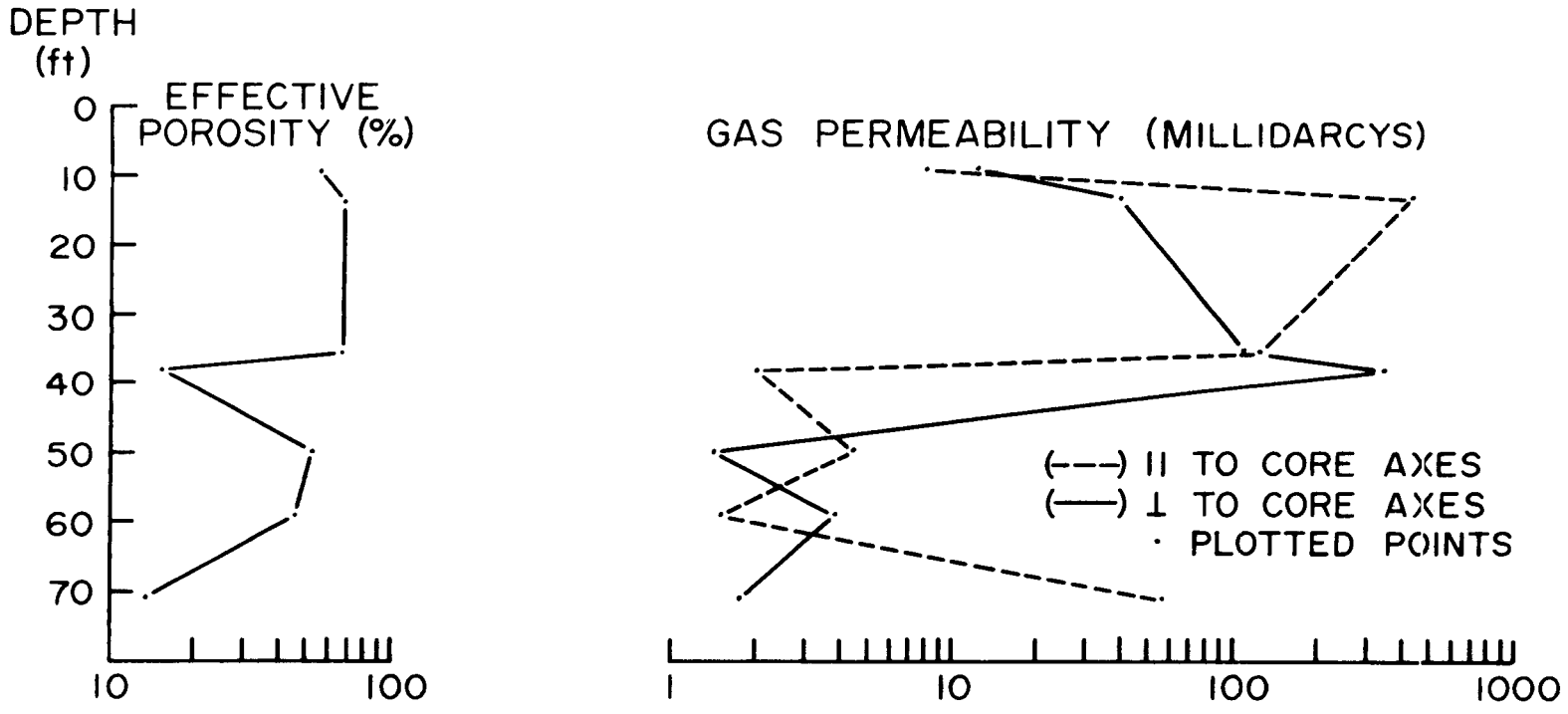

Figure 3.--Distribution of effective porosity and nitrogen permeability of pumice samples in the SC-2 drill hole.

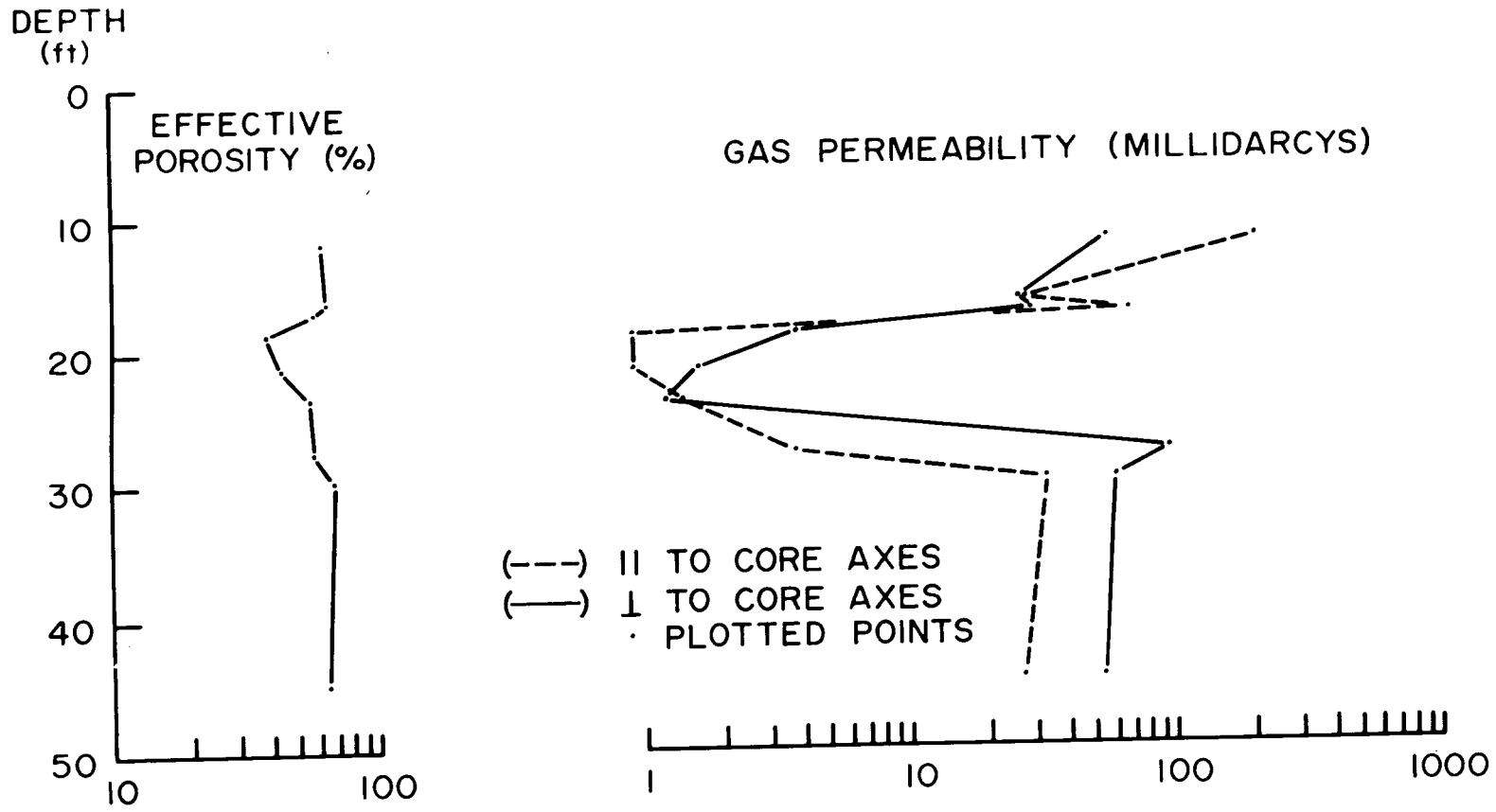

Figure 4.--Distribution of effective porosity and nitrogen permeability of pumice samples in the SC-3 drill hole Southern Coulee-Mono Craters, California.

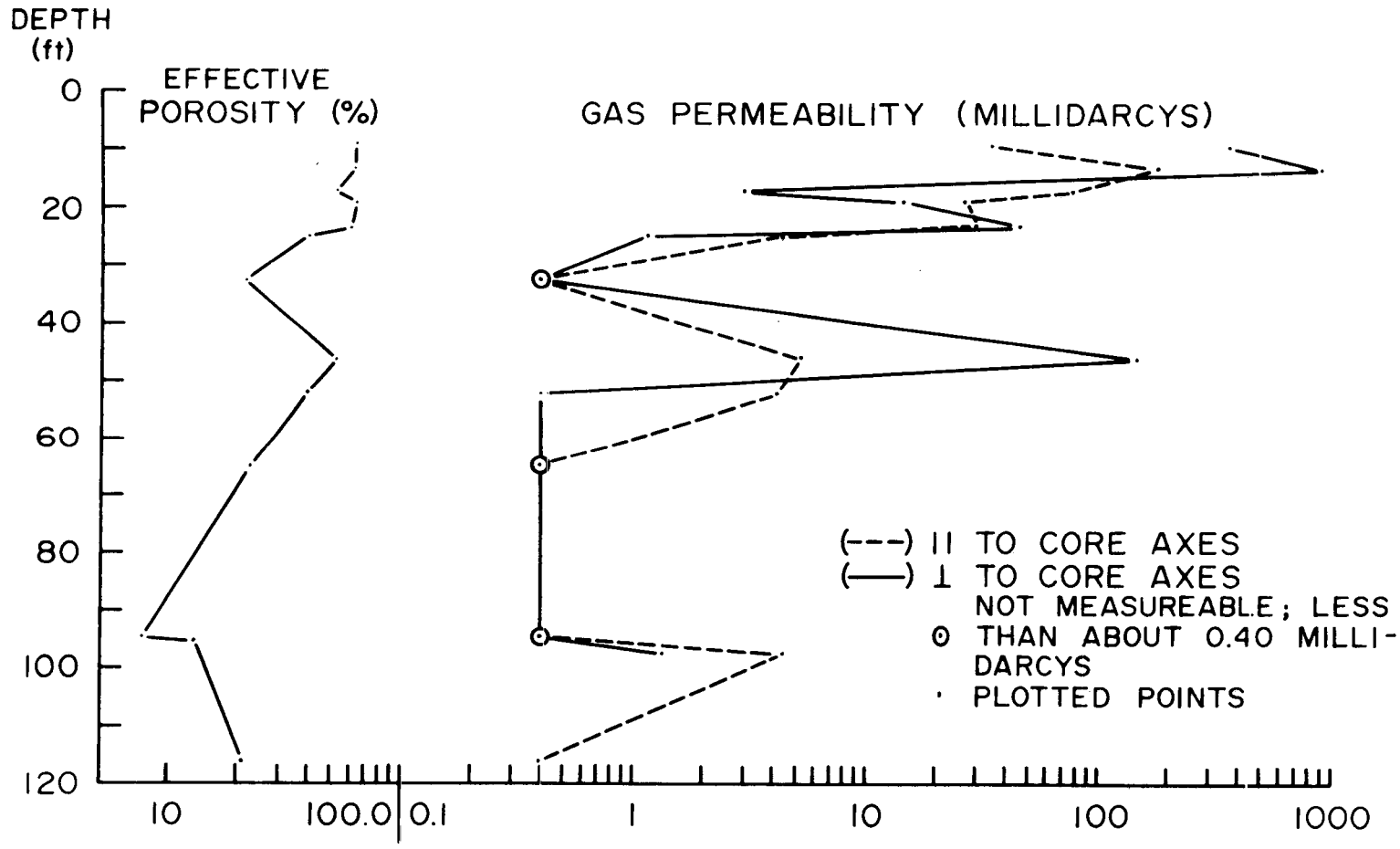

Figure 5.--Distribution of effective porosity and nitrogen permeability of pumice samples in the SC-4 drill hole.

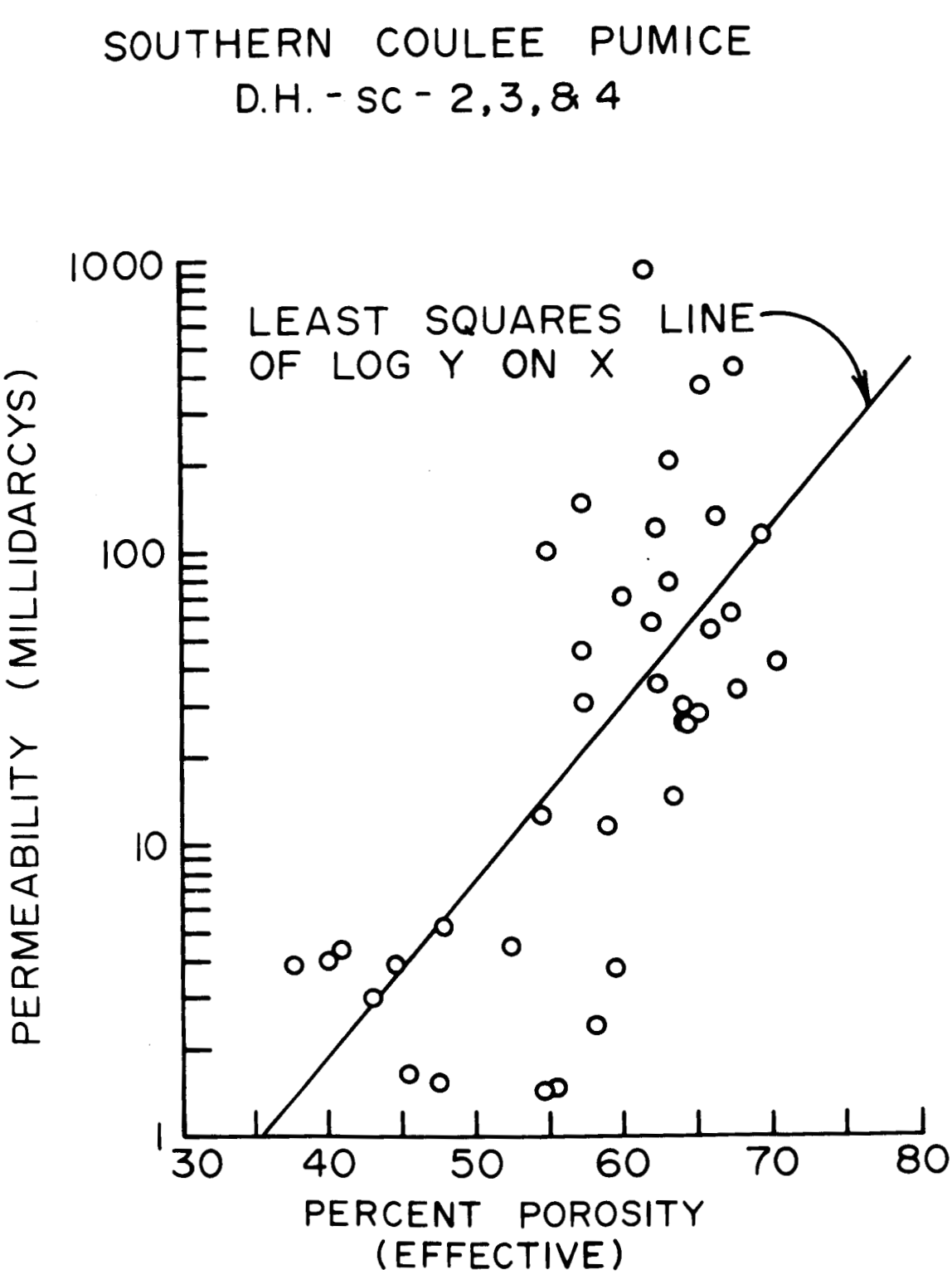

Figure 6.--Effective porosity and nitrogen permeability of pumice from Southern Coulee–Mono Craters site.

SEISMIC SURVEY OF METEOR CRATER, ARIZONA

by R. H. Godson, Hans D. Ackermann, and Joel S. Watkins

ABSTRACT.--Reflection and refraction seismic spreads recorded on the rim and in the bottom of Meteor Crater indicate that the bottom of the pulverized and brecciated zones can be mapped by refraction methods, but that reflections, although present, cannot be interpreted in terms of continuous horizons.

Introduction

Meteor Crater is one of the world's foremost examples of an impact crater. Since most of the large craters observed on the moon are thought to be of impact origin, the U.S. Geological Survey, on behalf of the National Aeronautics and Space Administration, conducted a seismic survey of Meteor Crater as part of its studies of lunar analog structures.

The survey was made to determine the depth and configuration of the bottom of the pulverized or brecciated layer at the center of the crater and of the brecciated layers on the rims, and the seismic velocity and attenuation characteristics of these layers.

Geology

Physiography

Meteor Crater is in the Canyon Diablo region of the southern part of the Colorado Plateau. The surface of the Plateau in the vicinity of the crater has little relief and is underlain by nearly flat-lying beds of Permian and Triassic age. The climate is arid and outcrop exposures are good. The crater lies near the crest of a gentle monoclinal fold, a structure characteristic of this region. The strata are broken by widely spaced northeast-trending normal faults of very little throw, generally some tens of feet up to about a hundred feet. Two mutually perpendicular sets of vertical joints occur in the region of the crater. One set controls the trend of secondary stream courses and the other is subparallel to the normal faults.

Stratigraphy

Pre-Quaternary rocks exposed at Meteor Crater range in age from the Permian Coconino Sandstone to the Triassic Moenkopi Formation. The Moenkopi Formation, a reddish-brown sandstone 10 to 17 m thick, rests on the Kaibab Limestone, which consists of about 82 m of sandy dolomite, dolomitic limestone and some calcareous sandstone. Underneath the Kaibab is the Toroweap Formation--a unit of white to yellowish- or reddish-brown, calcareous sandstone, 3 m thick. The Toroweap Formation is underlain by the Coconino Sandstone, which consists of about 215 to 245 m of fine-grained, white cross-bedded sandstone. Only the upper part of the Coconino Sandstone is exposed in the crater.

The Supai Formation of Pennsylvanian and Permian age, which underlies the Coconino Sandstone, is more than 300 m thick in this region, but only 100 m or so has been penetrated by the drill at the crater. It consists of interbedded red and yellow argillaceous sandstone and subordinate siltstone. The Redwall Limestone lies beneath the Supai Formation.

Quaternary rocks present in and around the crater consist of a complex sequence of debris, breccia, alluvium, and playa and lake beds. The uppermost portion of the rim consists of alluvium and debris from the Moenkopi, Kaibab, Toroweap and Coconino, resting on disturbed Moenkopi and Kaibab strata. The debris layers on the rim are stratigraphically reversed; that is, debris from the Moenkopi rests on the Moenkopi Formation and debris from the Kaibab Limestone rests on the debris from the Moenkopi, etc. No fragments from the Supai Formation are represented in any of the debris.

Pleistocene and Recent alluvium rests unconformably on all of the debris units as well as on bedrock. The alluvium is composed of material derived from all formations represented in the debris and also contains meteorite fragments, lechatelierite and other kinds of fused rock.

The floor of the crater is underlain by Quaternary strata, debris and breccia. Pleistocene talus on the lower parts of the crater walls grades into Pleistocene alluvium on the floor. This alluvium interfingers

with lake beds about 30 m thick at the center of the crater. Several meters of Recent playa beds and alluvium rest on top of the Pleistocene strata.

Underneath the Pleistocene talus and lake beds is a layer of mixed debris about 10 m thick. This layer contains fragments of all the formations that are seen in the crater walls as well as some fused rock and oxidized meteoritic material. Shoemaker (1959) believes this unit was formed by fallout of debris thrown to great height.

The breccia zone which underlies the mixed debris layer consists of shattered blocks of the Kaibab and Coconino Formations. Fused and meteoritic material is also present in this zone, which extends down to a depth of about 210 m near the center of the crater.

Structure of the crater

Meteor Crater is 180 m deep and about 1200 m in diameter with a rim that rises 30 to 60 m above the surrounding plain. The beds near the floor dip gently outward; near the top of the crater the dip becomes quite steep, and in some places rocks of the Moenkopi Formation are overturned. The upturned strata are dissected by a number of small, nearly vertical faults and joints. A number of small thrust faults are also present on the north and west sides of the crater.

Seismic Field Methods

Long refraction methods were carried out in the bottom of the crater and on both the north and south rims. Short reflection and refraction methods were conducted only on the bottom and the south rim.

Reflection methods, south rim

Twenty-two short spreads were recorded to try and obtain reflections from the bottom of the debris layer. Near the rim, where the debris is thickest, the spreads were 50 m long and consisted of 24 geophones with 1.8-m intervals; 300 m from the rim the geophone interval was reduced to 1 m and the spread length to 20 m. All spreads were shot with a blasting cap detonated 3 m below the surface.

Short refraction methods, south rim

Four refraction spreads were also recorded along the above reflection line. These spreads, 140 m long, consisted of 24 geophones at intervals of 6 m. The spreads were recorded from varying offset distances, which depended on the depth to the unbroken Kaibab Limestone. Charge sizes varied from 5 to 15 lb.

Bottom reflection methods

Two reflection lines were recorded on the bottom of the crater. One line had a N-S orientation while the other trended approximately NW-SE. Each line consisted of seven spreads, each made up of 24 geophones at intervals of 4.5 m. Several charge sizes were tried, but 1/16 lb of dynamite gave best results. Shot holes in the middle of spreads were dug by hand to a depth of about 1 m.

Bottom short refraction methods

Two refraction spreads were shot along each reflection line. Each consisted of 24 geophones at 11-m intervals. Spreads were recorded from shots both off the end of the spread and from offset distances varying from 180 to 270 m. Charges for these shots ranged from 10 to 20 lb and were buried to a depth of about 1 m.

Long refraction methods on south rim, north rim, and bottom

Three spreads with long offset shot points were recorded to obtain thicknesses of low velocity zones, both within the crater and radially out from the rim. These consisted of a 2500-m spread extending radially from the south rim, a 2000-m spread extending radially from the north rim, and a 700-m N-S spread in the crater. All three spreads were shot at offsets of approximately 5500 m south and north of the crater center. The two spreads extending from the north and south rims were also shot at their ends and centers.

Offset distances were chosen to insure refractions from a high velocity horizon (Redwall Limestone) at about 700 m below the surface.

Rays traveling up from the Redwall Limestone passed through low velocity zones and from the varying delay times their relative thicknesses were computed.

Results

South rim

For the first 120 or 150 m from the edge of the crater, fair to poor reflections were obtained from the bottom of the brecciated zone. They were, however, difficult to correlate from record to record (fig. 1). From 150 m outward from the crater, the reflections became confused with first-break energy and are difficult to follow from the center of the record to the end traces. However, with a shorter spread it may be possible to map the bottom of the brecciated zone by reflection methods. Continuous reflecting horizons within the brecciated zone may not exist.

The short refraction spreads yielded good results. A good refracting layer was mapped from the edge of the crater outward to the end of the recording spreads (fig. 2). Correlations with a core hole drilled along the recorded line indicates that the refracting layer is about 6 m below the top of the in-situ Kaibab and probably corresponds to the unbroken or slightly broken Kaibab Limestone. Depth of this layer ranged from 90 m at the edge of the crater to 20 m a distance of 520 m from the rim.

The long refraction spread on the south rim was analyzed utilizing the results of the short refraction spreads for near-surface corrections. Preliminary analysis of first arrivals indicated that four distinct seismic horizons exist: a near-surface 800- to 1000-mps (meters per second) layer which thins outward from the crater rim, a 2000- to 2500-mps horizon underlying this, a 2700- to 3200-mps horizon near the surface in the region unaffected by the crater and apparently extending downward about 700 m to the Redwall Limestone, which appears as a 5500- to 5300-mps horizon (fig. 2).

The 2000- to 2500-mps layer may be of considerable interest. In profile it appears as a wedge, thick near the crater rim and thinning outward to zero at about 1000 m from the rim. Physically it may

represent a zone of slightly fractured rock. However, before any real significance is attached to it, velocity distribution outside this zone must be investigated from later recorded arrivals.

North rim

The long offset refraction spread on the north rim did not have accompanying short refraction spreads for accurate near-surface corrections. However, conditions here appear to be similar to those on the south rim.

Bottom

Several reflections were obtained from the spreads recorded, along the N-S line in the bottom of the crater, but they were discontinuous. With few exceptions reflections were poor and difficult to carry from one record to the next. Severe noise trains were observed on the records, and this probably accounts for the discontinuities. More sophisticated recording techniques may improve record quality.

First refraction breaks from the reflection spreads gave information on two shallow beds. The first layer has a thickness of about 1 m, while the second layer is appreciably irregular. The depth of this layer ranges from 3 to 12 m (fig. 2).

The refraction spreads, in addition to confirming information obtained from the shorter reflection spreads, showed the presence of a good refracting layer about 60 m below the bottom of the crater. This layer, with a velocity of 2200 mps, is fairly level and probably corresponds to the present water table beneath the crater floor.

Delay times within the crater from long offset shot points were analyzed utilizing results from the shallow refraction spreads. Typical velocity of water-saturated pulverized material and underlying fractured rock was considered to be 2000 mps. In the center of the crater, thickness of a 2000-mps zone would be approximately 270 m (fig. 2). Inclusion of the 60 m of overlying dry pulverized material gives a total maximum thickness of approximately 330 m of pulverized, brecciated and highly fractured rock. Thickness of this zone decreases rapidly away from the center. Midway between the center and both the north and south

rims, combined thickness is approximately 150 m, a decrease of about 180 m, or slightly over 50 percent. Configuration of this zone further outward from the center could not be accurately determined.

Reference

Shoemaker, E. M., 1959, Impact mechanics at Meteor Crater, Arizona: U.S. Geol. Survey open-file report, 55 p., 7 figs.

1

FIGURE 1.

REFLECTION RECORDS

METEOR CRATER, SOUTH RIM

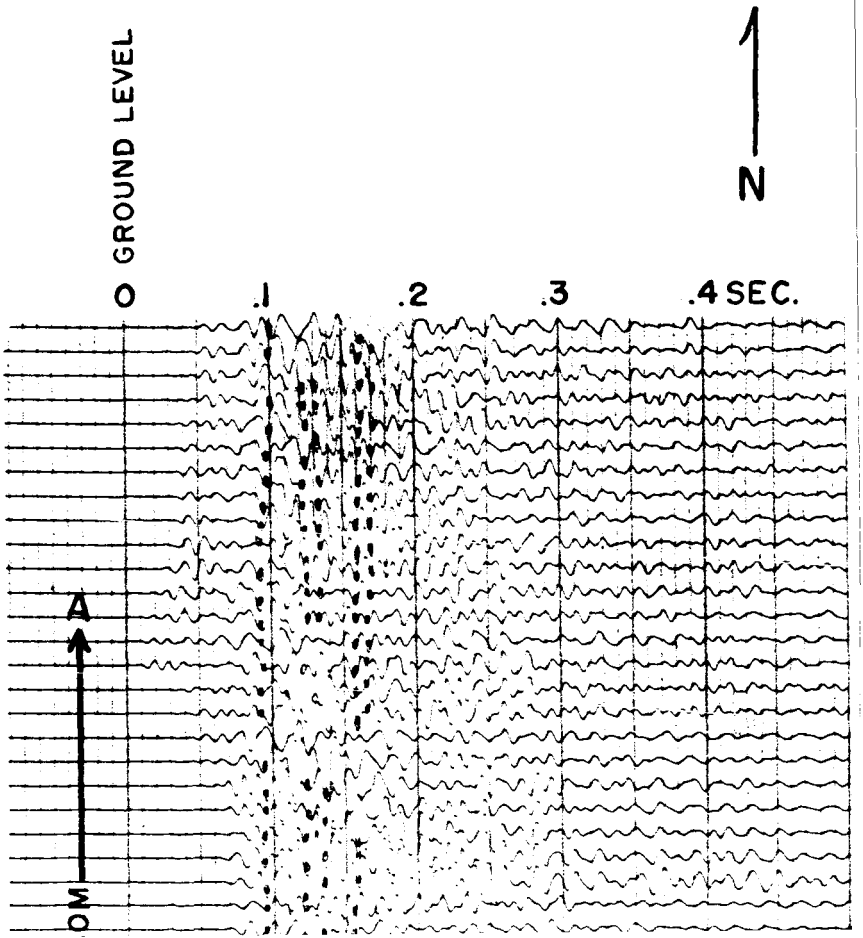

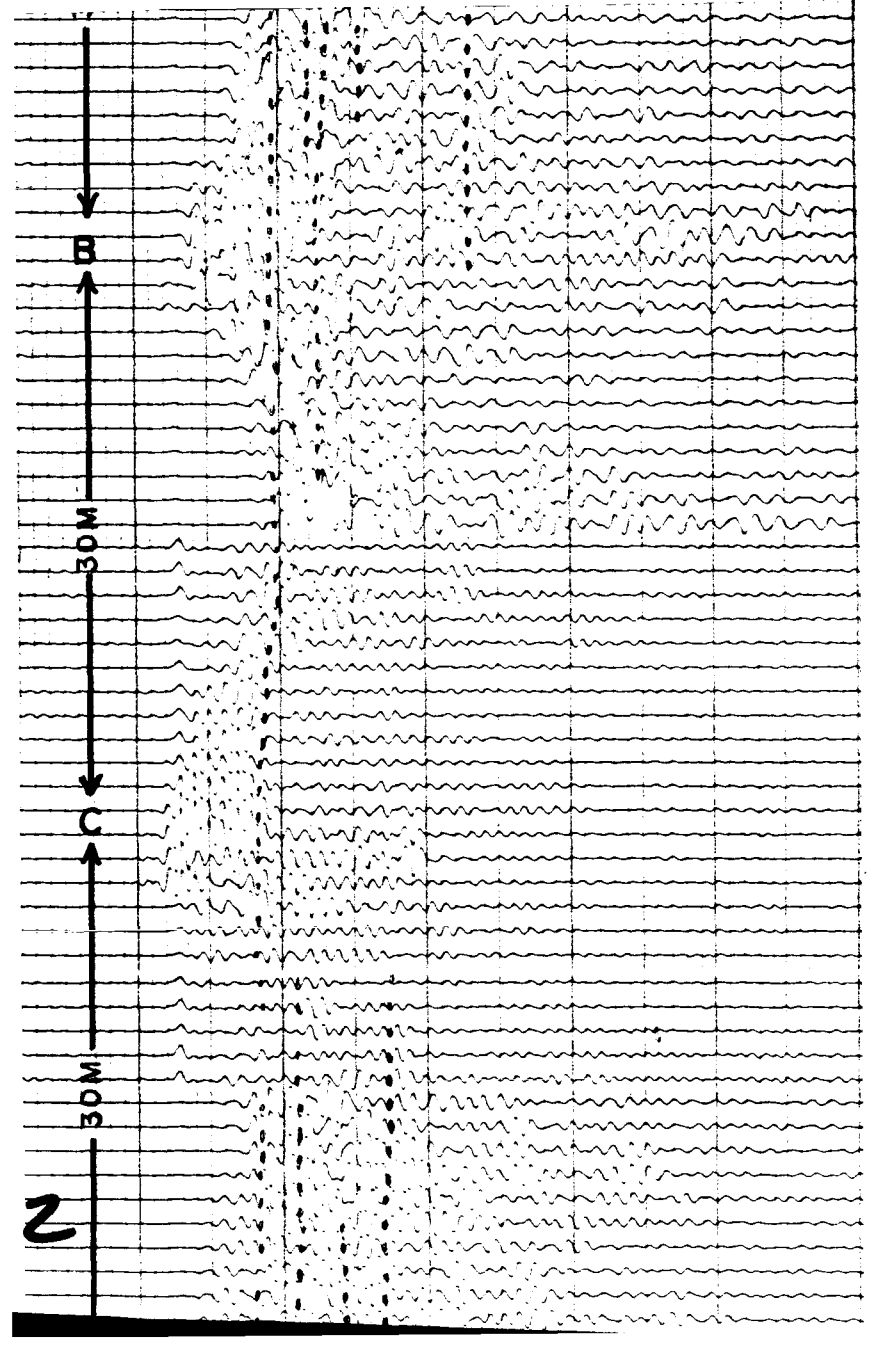
B
30M
C
30M
2

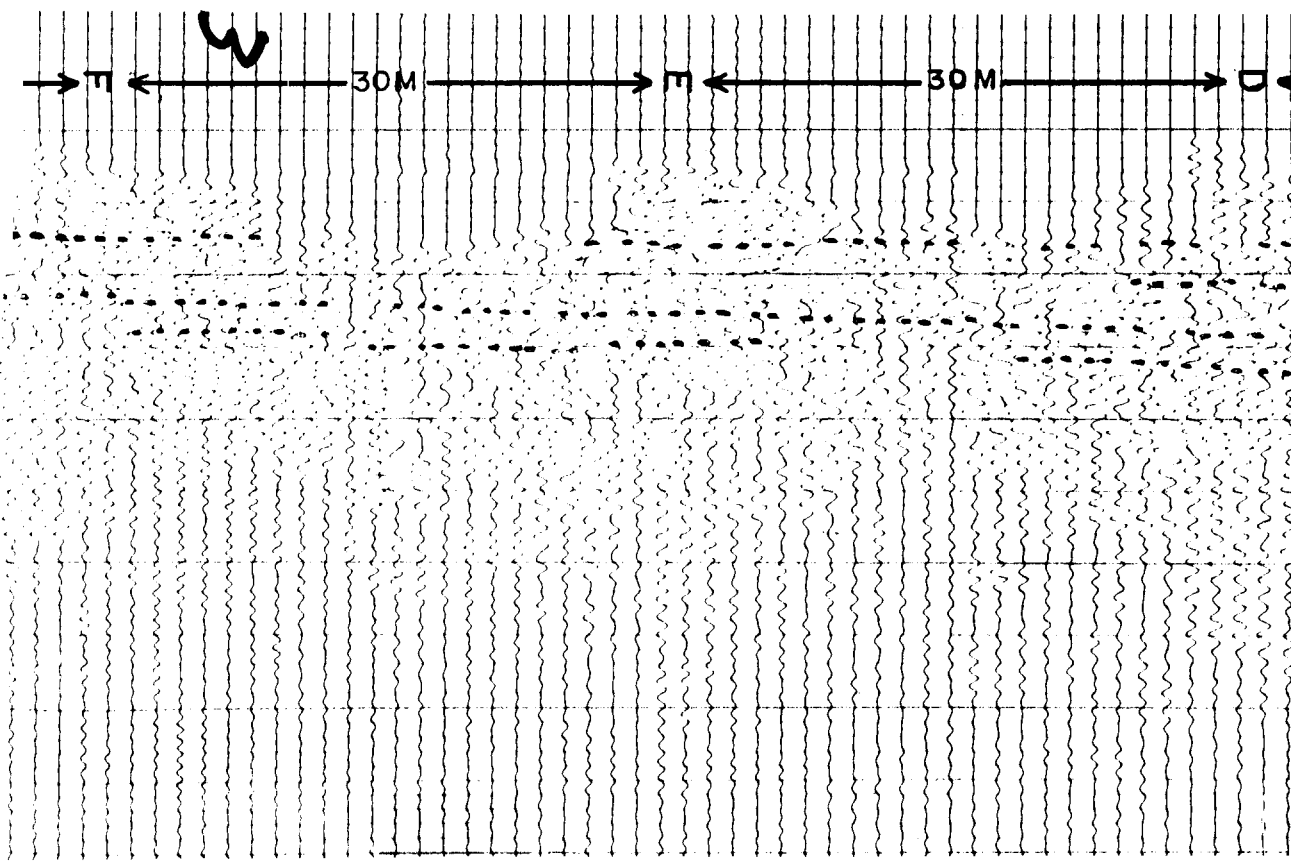
30M
30M

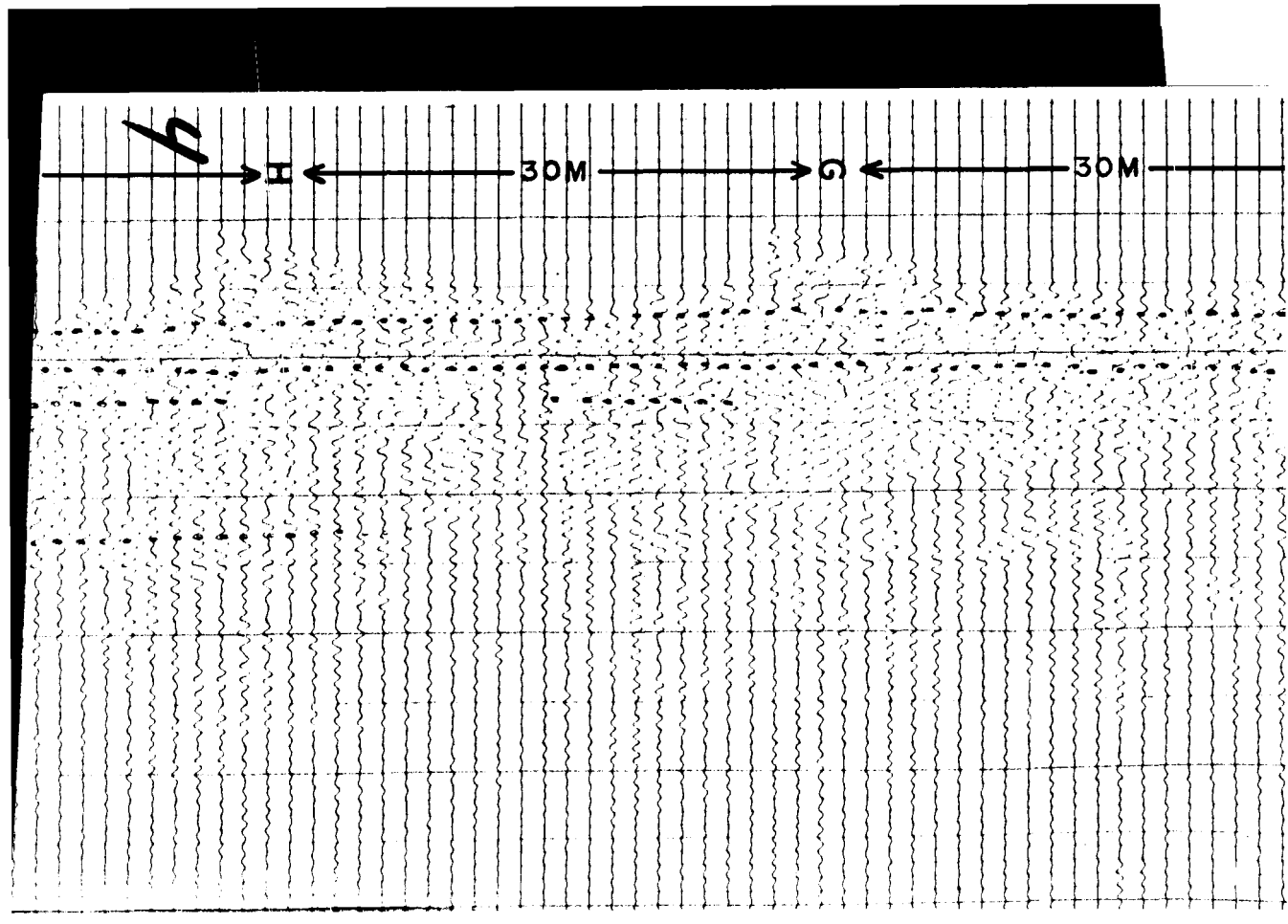
b
H
30M
G
30M

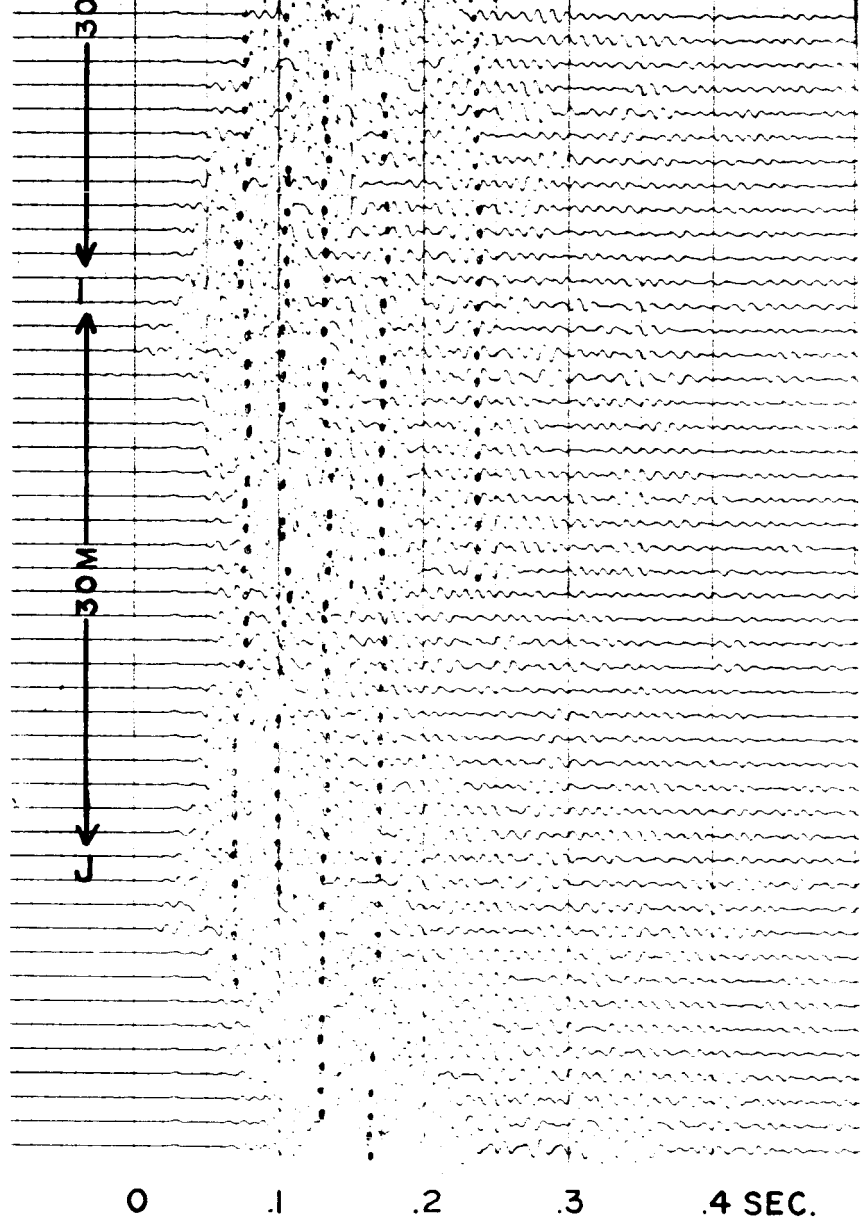

5

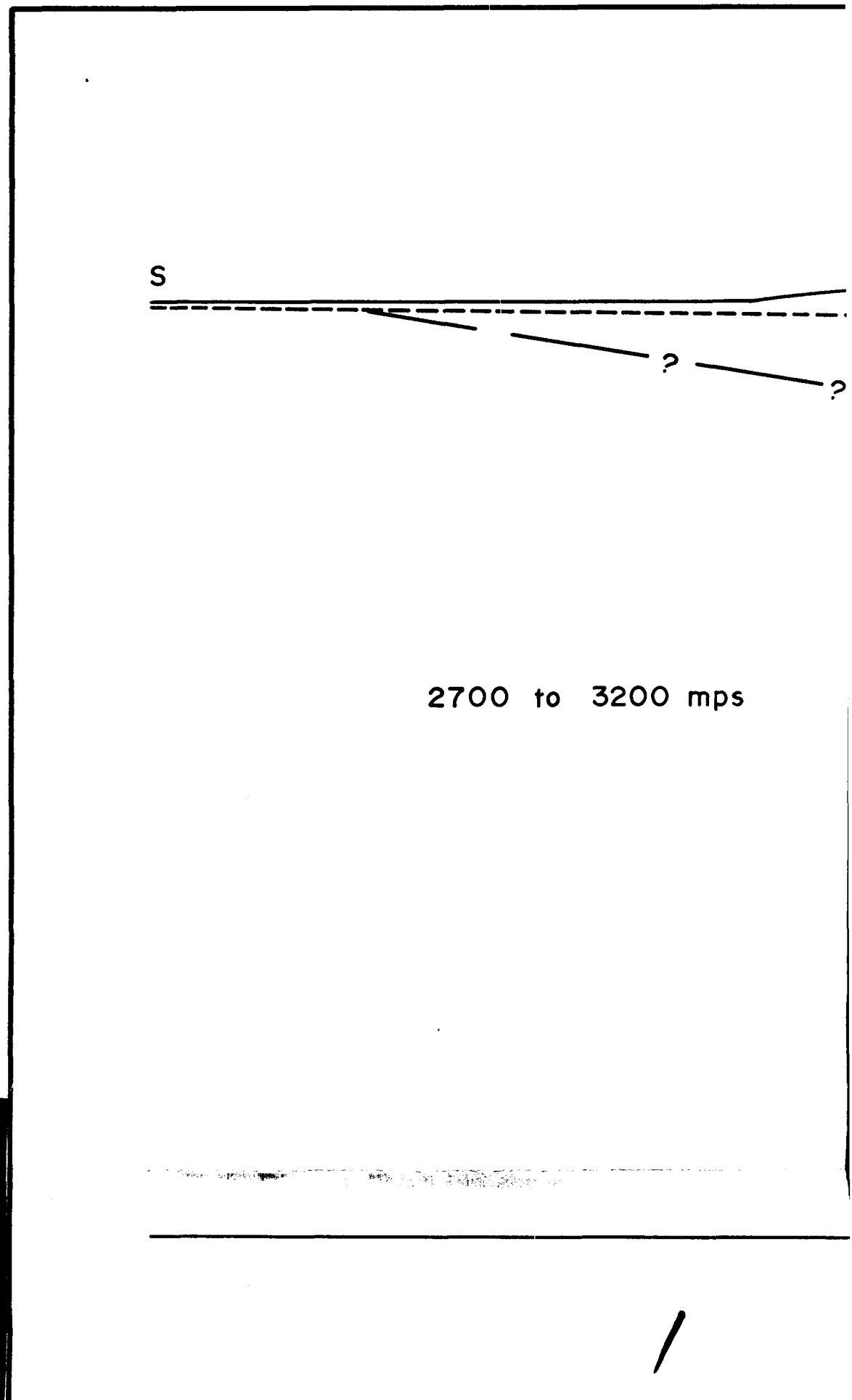

Figure 2. Preliminary geologic cross se

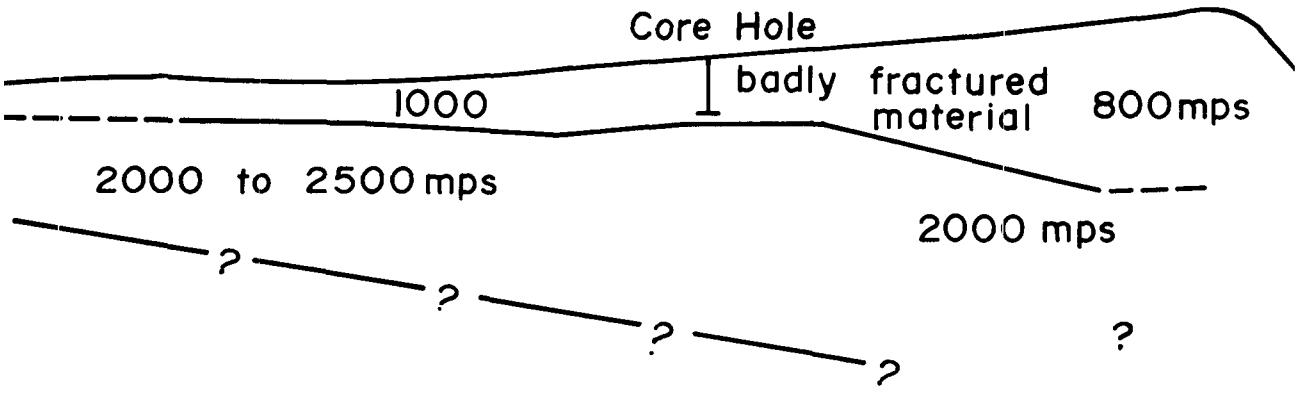

2

tion inferred from seismic refraction data at Met

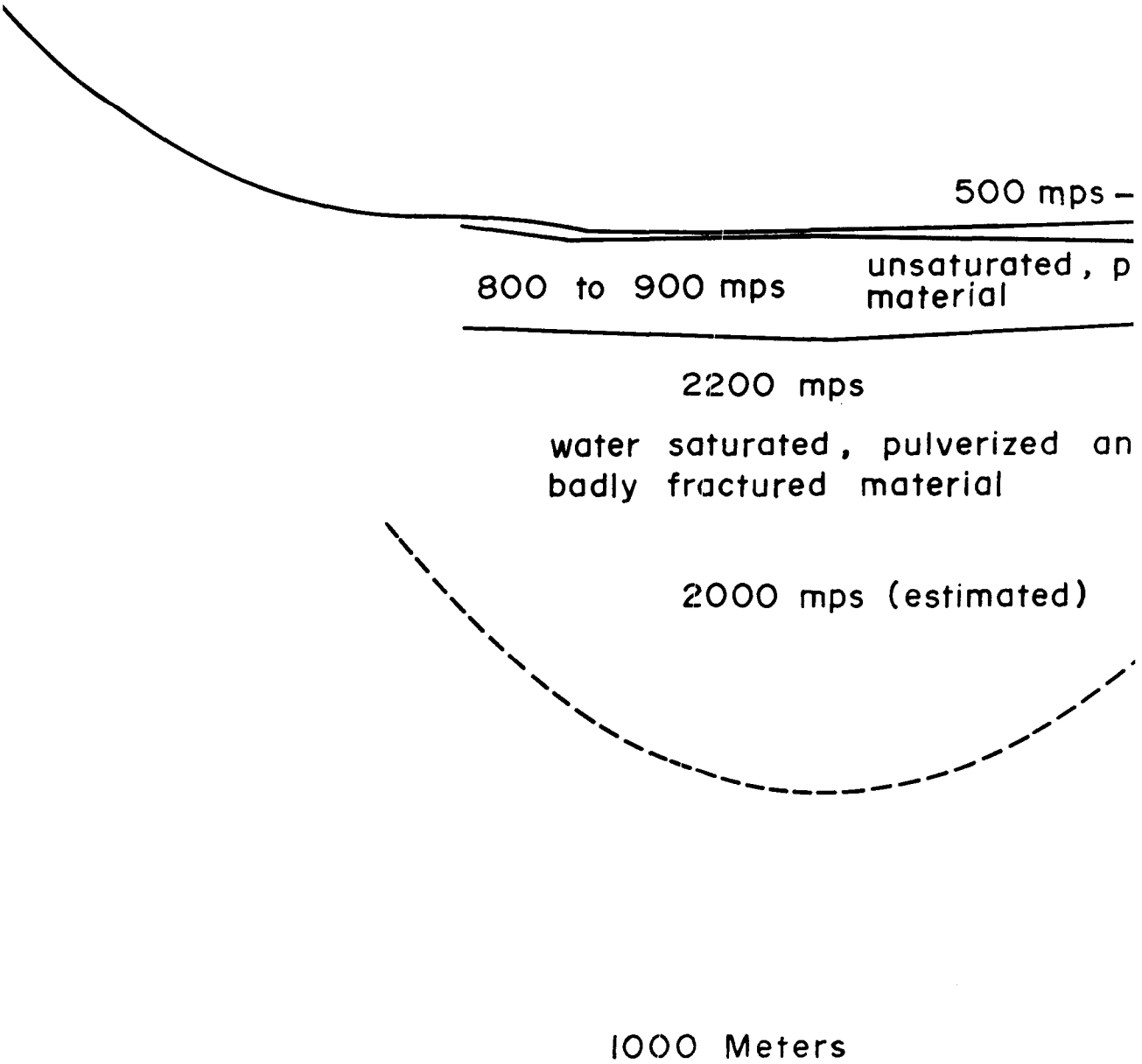

1000 Meters

5500 to 5800 mps

or Crater, Arizona.

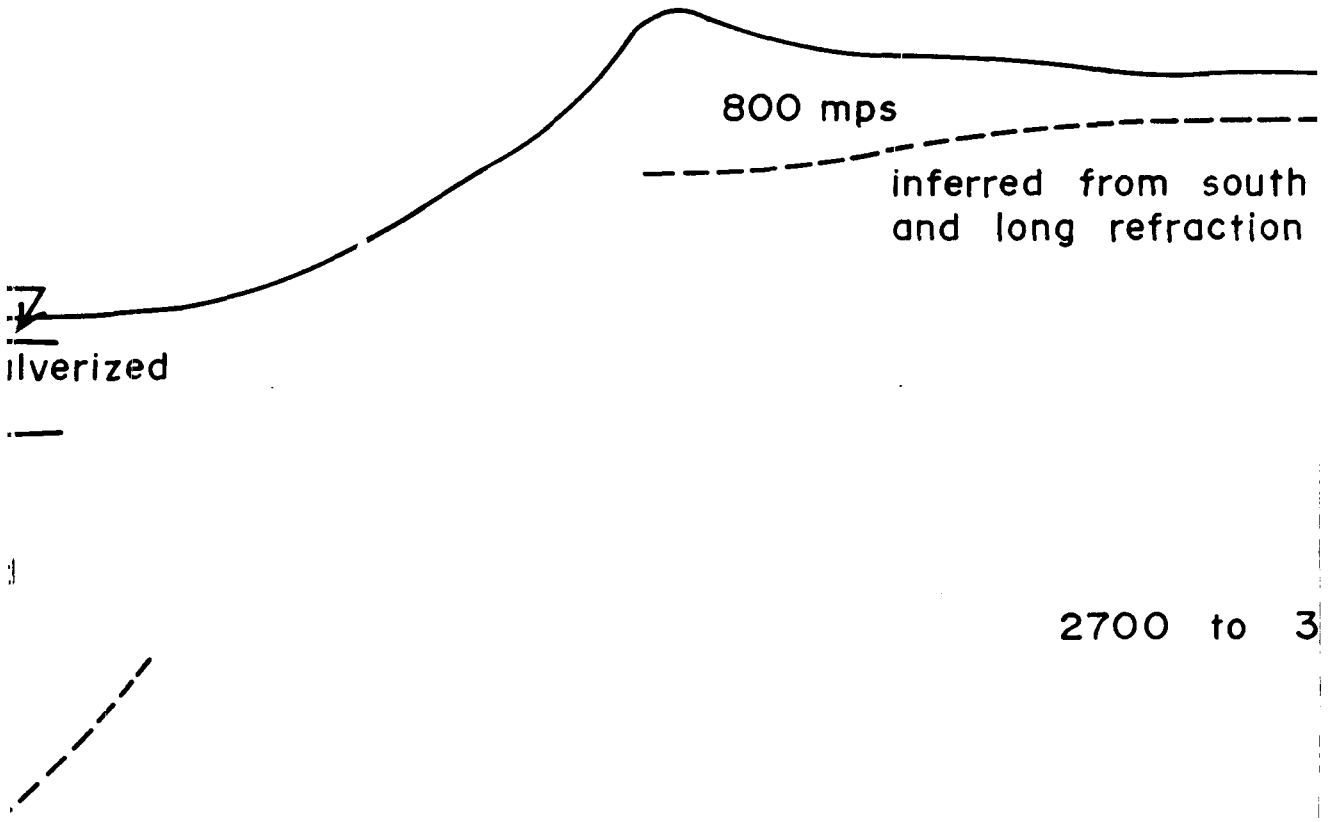

2700 to 3

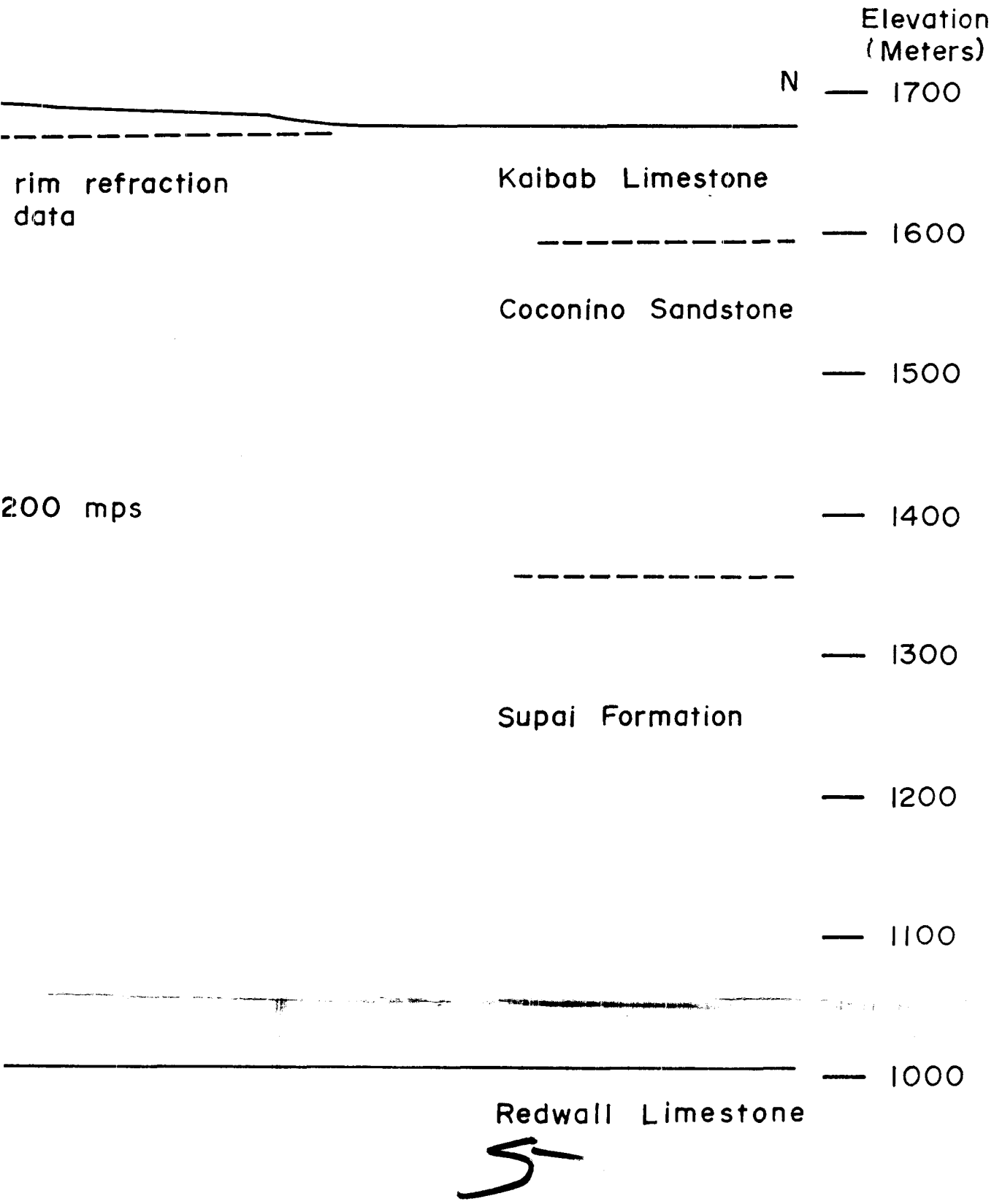
Elevation
(Meters)
N
1700
rim refraction
data
Kaibab Limestone
1600
Coconino Sandstone
1500
200 mps
1400
1300
Supai Formation
1200
1100
1000
Redwall Limestone
5

SOUTHERN COULEE REFRACTION STUDIES

by Jerry H. Hassemer, Joel S. Watkins, Richard H. Godson,
and Hans D. Ackermann

ABSTRACT.--Seismic refraction data from accessible portions of Southern Coulee of the Mono Craters show surface velocities ranging from 160 to 600 mps and velocities ranging up to 2000 mps at depth. Zones with distinctive vertical velocity distributions correlate in varying degrees with lothologic and morphologic units inferred from geologic mapping and with coring data.

Seismic data indicate relatively higher velocity media at shallow depths (less than 20 m) beneath the dome and adjacent portions of the flow. No significantly higher velocity media were indicated to depths of 60 m beneath the talus slope on the flow at 200 to 300 m from the dome.

Higher velocities are thought to represent harder, denser material underlying a frothy, low-density crust.

Introduction

Southern Coulee of the Mono Craters consists primarily of rhyolitic pumice with local occurrences of obsidian. The surface of the Coulee (or flow) is generally covered with blocks of pumice ranging in density from 0.51 to 2.01 g per cc, and in size from a few centimeters to a meter or more. Locally the pumice is covered with ash, which was less than 5 m thick where depth was seismically determined. Extremely low densities of the pumice and evidence that the surface of lava extruded into the lunar vacuum may be highly scoriaceous or pumiceous recommends this site as one of the most promising lunar analogs conveniently available for study.

R. A. Loney conducted geologic field surveys and analyses of aerial photography of the Coulee in Fiscal Year 1965, reporting his preliminary interpretation of the field data in a previous In Situ Physical Properties Quarterly Report (Loney, 1964). A topographic map, scale 1:5000, contour interval 20 ft, was subsequently prepared by topographers of the Branch of Astrogeology. The map will be published as part of a final report on Southern Coulee, but preprints are available upon request.

Seismic field studies were begun on the trafficable portion of the

Coulee during the summer of 1964 and completed during the summer of 1965. The present report describes observed P-wave velocity variations and subsurface geologic structure inferred from velocity data. A brief summary of relations between seismically indicated structure and Loney's (1964) inferences of surface lithology and morphology is also included.

A separate report in this volume (Roach and others) includes comprehensive data on density, porosity, permeability, and pore geometry determined from cores taken during the summer of 1965.

Seismic Data

On the basis of distribution of seismic velocities recorded at various profile locations and inferred subsurface structure, the studied portion of Southern Coulee can be divided into four different zones (fig. 1).

Zone 1. Surface velocities of 500 to 540 mps with no deeper layers detected.

Zone 2. Surface velocities of 160 mps underlain at shallow depths (less than 5 m) by a 350-mps layer. At depths of 8 to 17 m a third layer with a minimum velocity of 725 mps occurs.

Zone 3. Surface velocities of 350 to 500 mps underlain by a 1000- to 1350-mps layer at depths between 2 and 21 m.

Zone 4. Surface velocities of 350 to 600 mps underlain by a 1500- to 2000-mps layer at 20 m or less.

Figures 2 and 3 are diagrammatic sections along the spreads showing depths to the various layers inferred from the seismic data.

Profile and spread designation

Each profile consists of 3 superimposed spreads of 175, 70, and 35 m, each with a common end geophone. Each spread was given a letter designation, hence a complete profile designation consists of 3 letters, for example, profile A B C consists of the 35-m spread A, the 70-m spread C, and the 175-m spread B. Spread HH is an anomalous 325 m in length. Shorter spreads provide detailed data on near-surface materials, whereas longer spreads gave more generalized information on deeper structure.

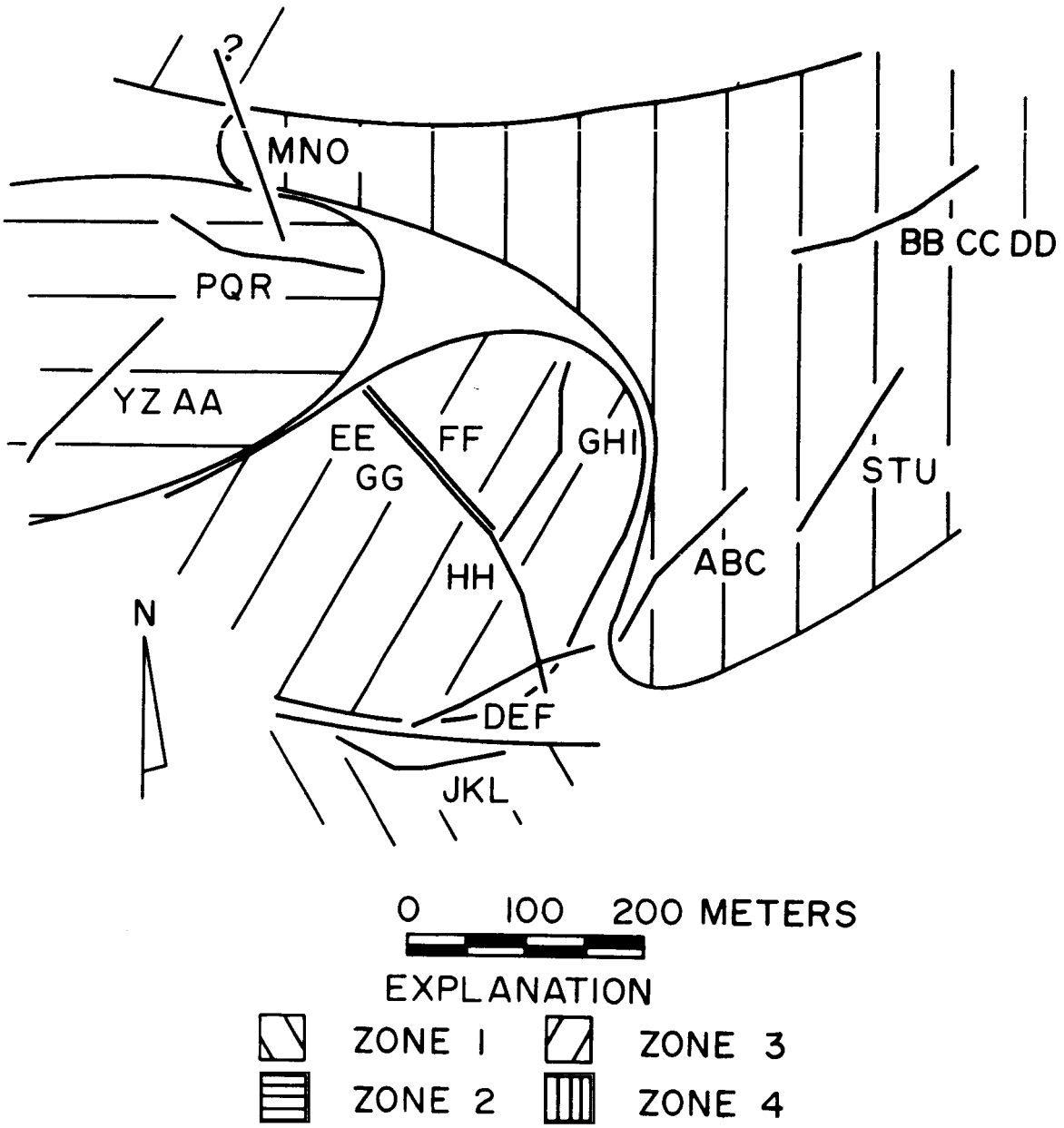

Figure 1.--Seismic zones, profile and spread locations at Southern Coulee-Mono Craters, California. See figures 4 and 5 for location of spreads relative to the areal distribution of lithologic and morphologic units at Southern Coulee.

Characteristics of zones

Interpretation of seismic data from Southern Coulee is ambiguous to some extent because velocities are not distributed according to simple geometries of classical refraction theory. Multiple spreads and multiple shot points employed in the field surveys alleviate some ambiguity, however.

Zone 1. Zone 1 is near the edge of the crater, consists of material having velocities of 500 to 540 mps and includes only the profile J K L. Profile J K L data indicates no significantly faster layers to a minimum depth of 50 m.

Zone 2. Zone 2 typically has a surface layer with a velocity of 160 mps correlative with 2 to 5 m of ash observed in the area. The 160-mps velocity is the lowest observed in situ during Project operations. Slightly lower velocities are reported in the literature, however (for example, Domzalski, 1956). Beneath is a 10-m layer with velocities ranging from 350 to 440 mps. The deepest layer in the zone has a minimum velocity of 725 mps.

Profiles Y Z AA, P Q R, and the southern end of profile M N O are within zone 2. The highest zone 2 velocity, 880 mps, was observed on profile Y Z AA.

Zone 3. Zone 3 typically consists of a surface layer whose velocity varies from 350 to 500 mps underlain by a 1000- to 1400-mps layer. Profiles A B C, S T U, BB CC DD and the central portion of profile M N O are within this zone. Zone 2 velocities immediately below the ash layer are approximately the same as those surface velocities of zone 3, but velocities of deeper layers in both zones differ somewhat. Zone 2 may be an ash-covered facies of zone 3.

High attenuation and local noise along profile A B C prohibited accurate plotting of arrival times beyond 80 m from shot points. However, two shorter spreads at the southern end of this profile indicate a 500-mps layer underlain by a 700-mps layer dipping northward (fig. 3). A 1000-mps layer is observed at a depth of 21 m on the southern end and at a depth less than 5 m at the north end of this profile. High-energy attenuation and noise also negated usefulness of reversed parts of S T U

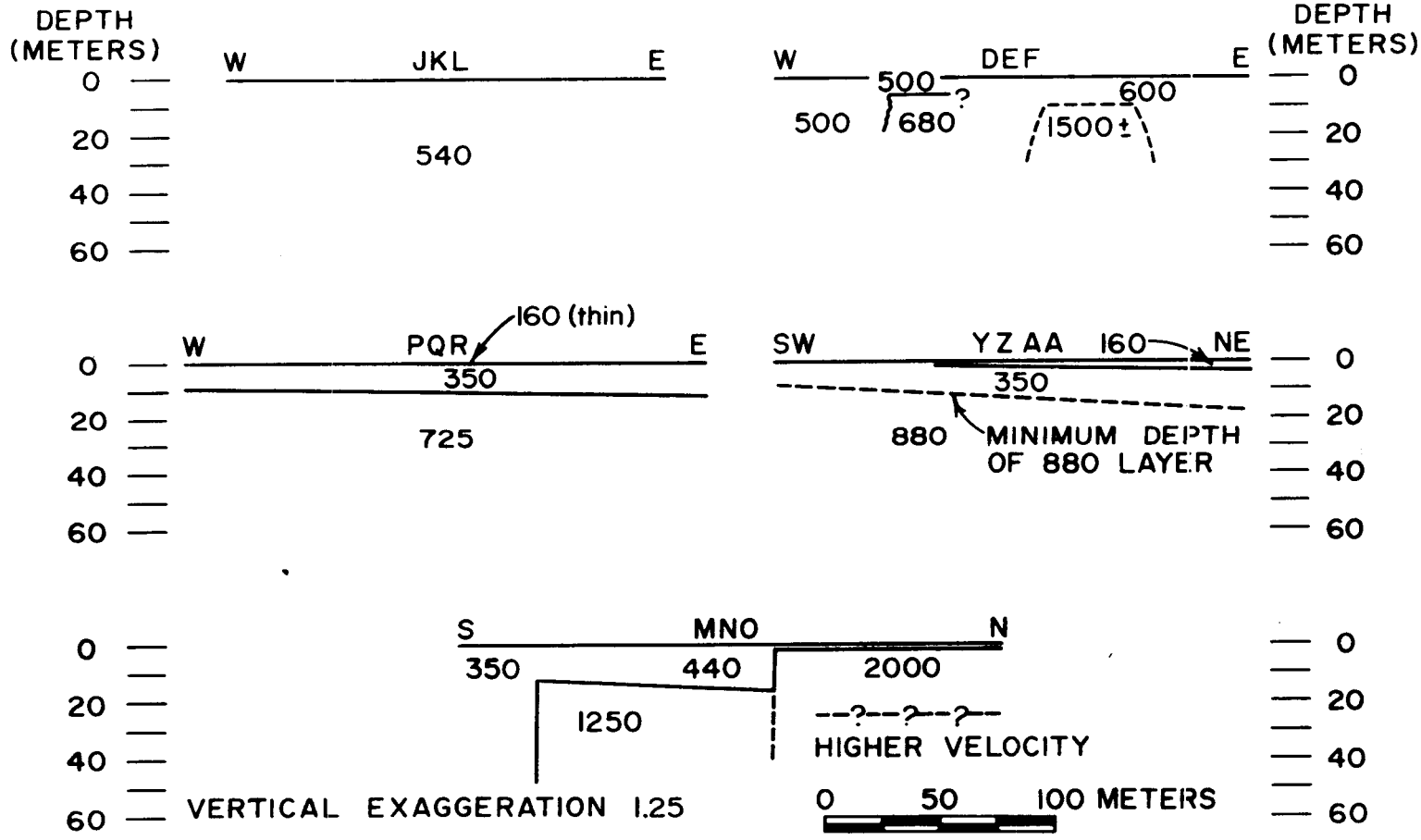

Figure 2.--Diagrammatic sections of profiles J K L, Y Z AA, P Q R, M N O, and D E F. Velocities shown are in meters per second.

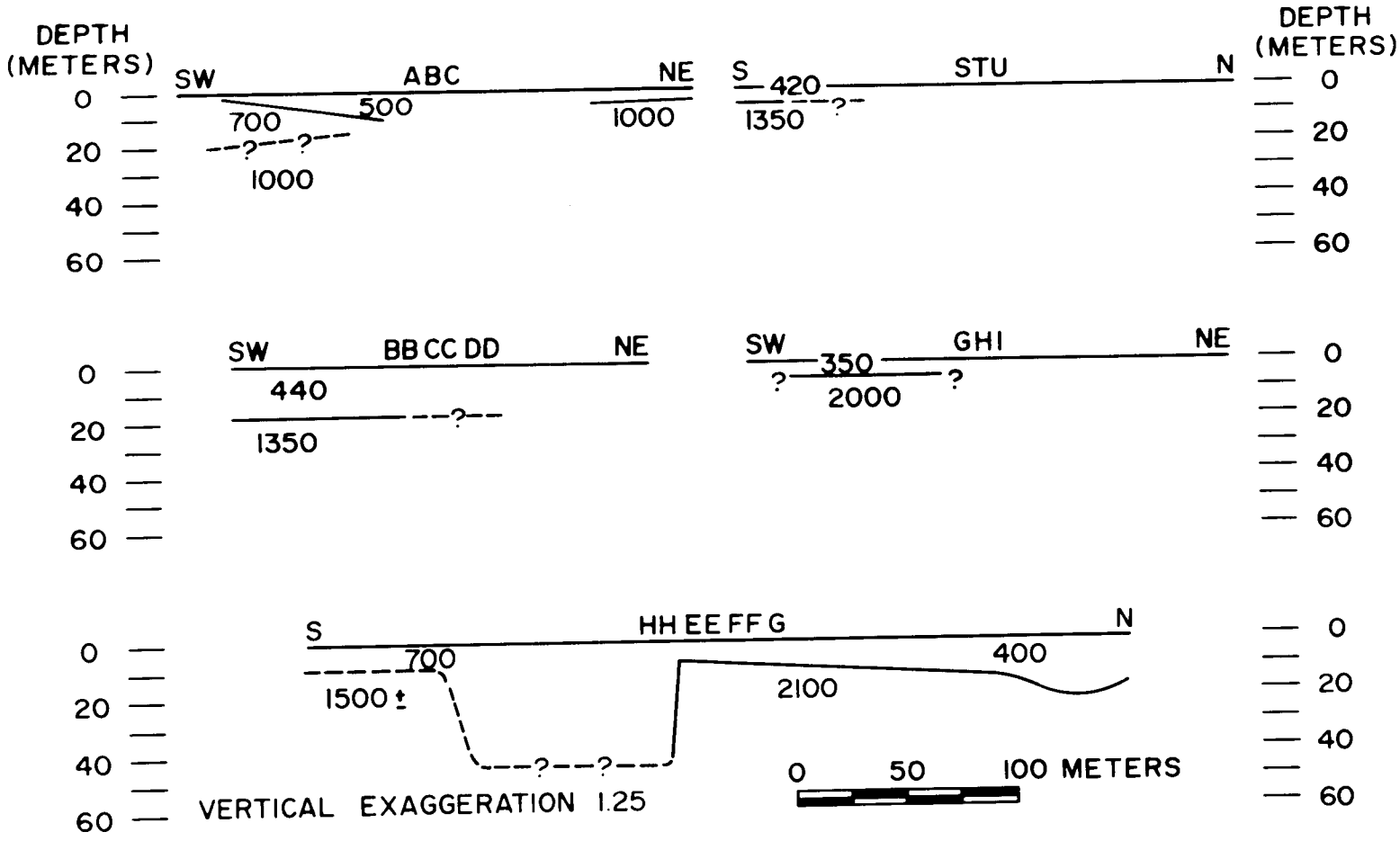

Figure 3.--Diagrammatic sections of profiles A B C, S T U, BB CC DD, G H I and EE FF GG and spread HH. Velocities shown are in meters per second.

and BB CC DD. However, if apparent velocities are approximately the same as true velocities in these profiles, then the 420-mps layer is 6 m thick on S T U and the 440-mps layer is 18 m thick on the southwest end of BB CC DD. A 1350-mps layer underlies 420 to 440 mps materials on both profiles.

Low-velocity material in the central portion of M N O (fig. 2) is underlain by a 1250-mps layer at a depth of about 15 m. The low-velocity material thickens under the southern end. The 2000-mps layer observed on the north end was not detected on the south end.

Zone 4. Zone 4 is characterized by low velocity (400 to 700 mps) surface material underlain in part by a 1500- to 2000-mps material. G H I, EE FF GG, and the 325-m profile HH, lie entirely within this zone. The north end of M N O is shown (fig. 1) but data justifying this relationship are limited.

As in some other areas, reversals did not yield first breaks which could be picked with confidence, and only shorter spreads were used to determine thicknesses of the 350-mps layer along profile G H I (fig. 3). Apparent velocities observed along this profile suggest that a 1000-mps layer may be present below the 350-mps layer; if so, the 2000-mps layer is deeper than indicated in figure 3.

High attenuation and local noise on HH resulted in weak first breaks, but first troughs indicate a thickening of the 500- to 540-mps layer near the southern end of the spread.

On the north end of M N O, the 2000-mps layer is within 2 m of the surface (fig. 2), but in the center of M N O, the 2000-mps layer disappears as 440-mps surface material thickens. The record from the south shot point suggests that a layer with a velocity greater than 2000 mps may exist at a minimum depth of 25 m near the southern end.

Relation of Seismic and Geologic Data

Figures 4 and 5 show the relation of refraction profiles to lithologic and morphologic units of the Southern Coulee as mapped by Loney (1964). The lithologic units defined by Loney were defined on the basis of densities of surface materials because there were few definitive

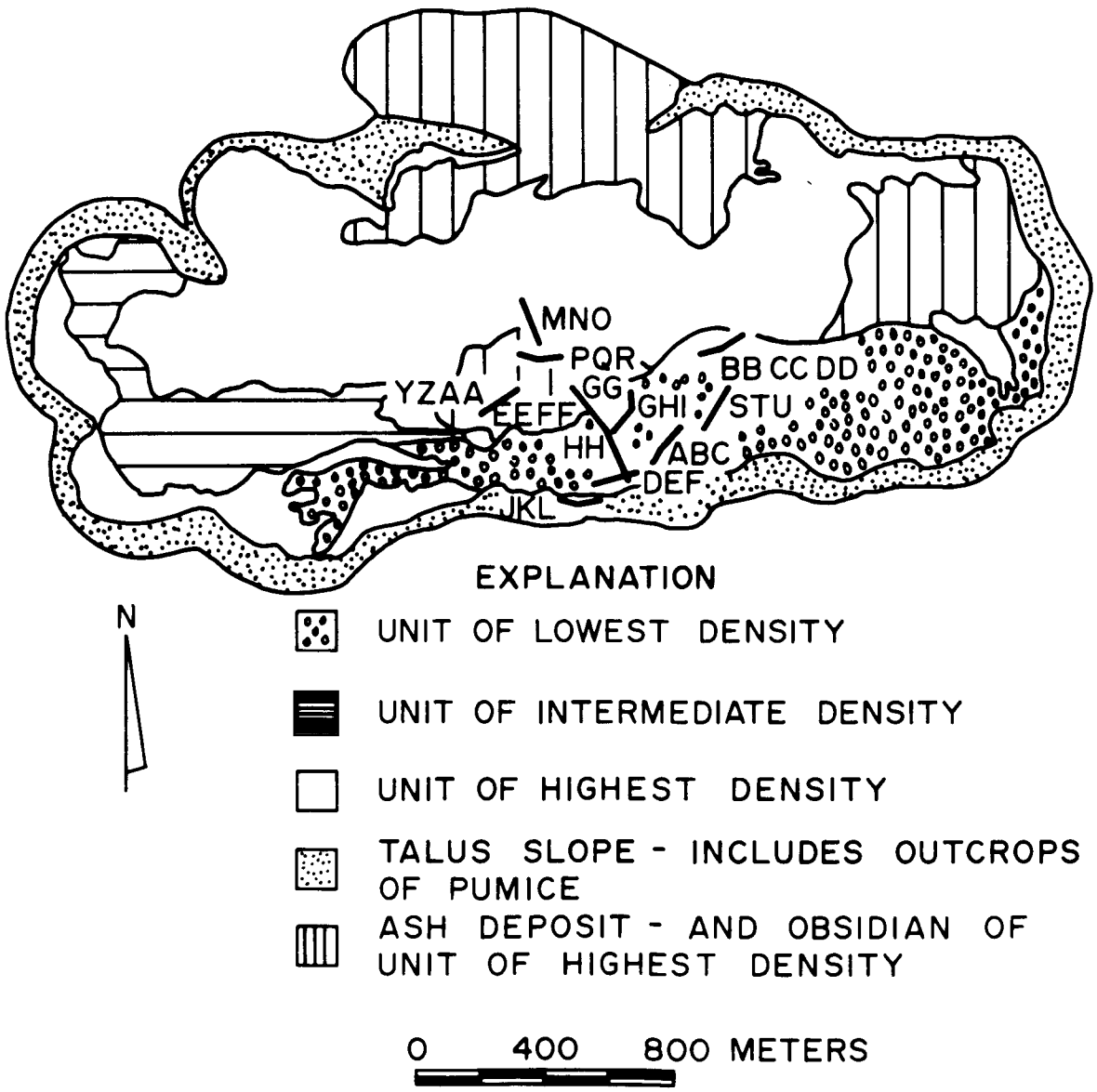

Figure 4.--Relation of refraction profiles and lithologic units of the Southern Coulee (after Loney, 1964).

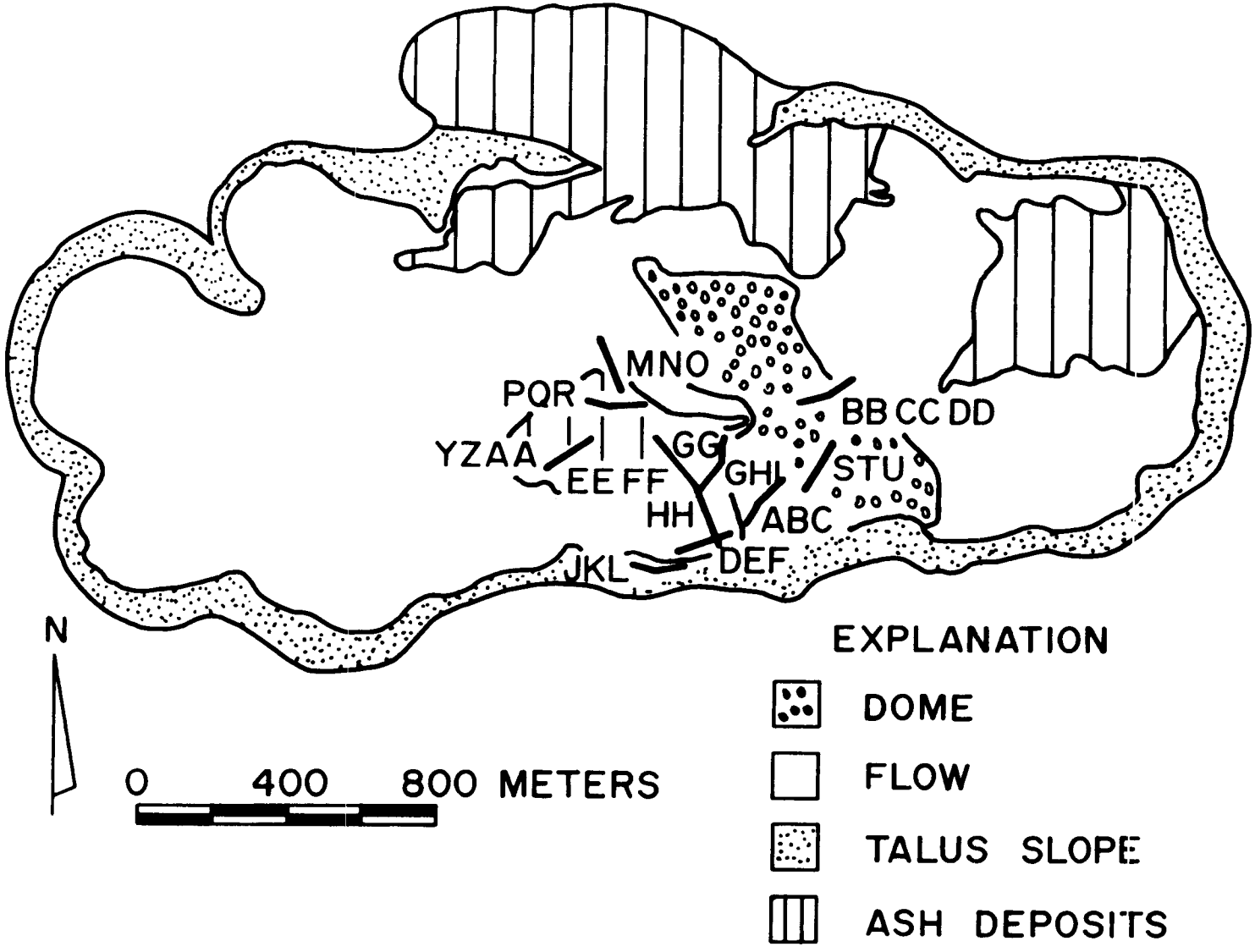

Figure 5.--Relation of refraction profiles and morphologic units of the Southern Coulee (after Loney, 1964).

differences in chemical composition of the materials and because flow rocks mineralogically consisted largely of glass.

Seismic profiles are limited to the accessible portion of the flow, which in turn is determined by roads built by the U.S. Pumice Supply Company for quarrying pumice. Low-density pumice has the greatest value, consequently roads are generally restricted to this area. Only part of one profile, M N O, is located on the unit of highest density; no profiles are located on the unit of intermediate density; and only J K L is located on the talus slope. Most of the remaining data are from the unit of lowest density, although P Q R and Y Z AA as well as parts of M N O and EE FF GG are located on an ash deposit. Data from the north end of M N O, which is located on the unit of highest density, indicate a 2000-mps layer at a depth of about 2 m, a velocity consistent with higher density material.

The two profiles entirely within the ash deposit, P Q R and Y Z AA have 160-mps surface velocities, which are correlative with the ash deposits. M N O, and EE FF GG and HH are also in part on the ash deposits, but data suggest that the ash is too thin (less than 2 m thick) to be detected. The one profile on the talus, J K L, has a velocity of 540 mps, which is within the general range of the low-density materials.

Six profiles located on the low-density unit have surface velocities ranging from 350 mps on G H I to 700 mps on the southern end of A B C. Surface velocities tend to be slightly lower in the northern portions of the unit, that is, the northern part of EE FF GG and HH (400 mps), G H I (350 mps), BB CC DD (440 mps) and S T U (420 mps) relative to velocities in the southern part of the unit where velocities of 700 mps are observed on the southern end of EE FF GG, HH, southern end of A B C; and on D E F, where surface velocities range from 500 to 600 mps. These profiles are widely dispersed, however, and the apparent areal variation of velocities may be coincidental.

In general, seismic zone 1 (with the exception of part of M N O), is correlative with the talus slope, zones 3 and 4 are crudely correlative with the unit of lowest density with the exception of the southern end of M N O. Zone 2 is correlative with the ash deposit.

Relationships between seismically inferred zones and the morphologic units, however, are also correlative. Three profiles, BB CC DD, S T U, and A B C constituting the bulk of zone 4 data, lie mostly on the dome. These spreads have surface velocities ranging from 420 to 720 mps and overlie a layer whose velocity is 1000 to 1350 mps at depths ranging from 4 to 20 m below the surface.

The one profile on the talus J K L is unique in that no high-velocity layer was found. Its surface velocity, 540 mps, is not significantly different from surface velocities on the dome or the flow, however. Data from the western end of D E F suggest that it may also lie on the talus slope, although its mapped location is on the flow.

Profiles EE FF GG, HH, G H I, and M N O lie, for the most part, on outcrops of the flow. Surface velocities range from 350 to 700 mps. The surface layer is underlain by an irregular layer whose depth ranges from 2 to more than 40 m below the surface and whose velocity ranges from 1250 to 2100 mps. Structure beneath the eastern end of profile D E F seems similar to that of the other four profiles on the flow in that its surface layer (600 mps) is underlain by a 1500-mps layer which rises to within about 10 m of the surface.

Hence zone 3 profiles are generally correlative with flow rocks. The profile M N O is anomalous as in the case of the lithologic units.

Profiles Y Z AA and P Q R (zone 2) are also thought to lie on flow rocks (the thin layer of ash is ignored) but differ significantly from the previously described profiles on the flow. Surface velocities for Y Z AA, P Q R, and part of the western half of D E F range from 350 to 500 mps and are underlain at depths of 6 to 20 m by a layer ranging in velocity from 680 to 800 mps (the extreme western end of D E F revealed no deeper layer, and this may indicate that this portion of the spread lies on the talus slope rather than on the main part of the flow).

The presence of a layer with a velocity over 1000 mps at relatively shallow depths in the dome, and a layer with similar velocities present at irregular depths beneath profiles EE FF GG, HH, G H I, M N O, and the eastern end of profile D E F suggests that the dome and parts of the flow immediately adjacent to it, are underlain by denser intrusive material.

The lower velocities observed in profiles P Q R, Y Z AA, and part of D E F, suggest that the main mass of the flow consists of material of lower densities extending to a minimum depth of 50 or 60 m.

In summary, seismic zone 1 data indicate that the talus slope is not underlain by higher velocity materials to depths of 60 m, zone 2 data suggest that flow rocks at some distance from the dome have velocities less than 800 mps to depths of 60 m, and zone 3 data suggest that the higher velocity material observed at shallow depths in the dome (zone 4) extends irregularly beneath flow rocks near the dome.

References

Domzalski, W., 1956, Some problems of shallow refraction investigations: Geophys. Prosp. v. 4, no. 2, p. 140-166.

Loney, R. A., 1964, Geology--Southern Coulee site, in Watkins, J. S., Loney, R. A., Whitcomb, J. H., and Godson, R. H., Investigation of in situ physical properties of surface and subsurface site materials by engineering geophysical techniques--Project quarterly report, Oct. 1 to Dec. 31, 1964, p. 5-36.

SH-WAVE INVESTIGATIONS OF SHALLOW IN SITU MATERIALS

by James H. Whitcomb

ABSTRACT.--SH-wave propagation through shallow (less than 30 m deep) in situ materials has been studied at a number of sites using the angular transducer technique of detection (Whitcomb, 1965).

In situ elastic moduli were calculated using dry bulk density (from core and hand samples), P-wave velocity, and SH-wave velocity. Preliminary analysis of the relationship of the elastic moduli and SH-wave velocity show that the shear modulus can be estimated by the relation

$$\ln\mu = 2.35 \ln\beta + 7.50,$$

where μ is the shear modulus (x 10^{10} dynes/cm^2) and β is SH-wave velocity (mps). Similarly, Young's modulus can be estimated by

$$\ln E = 2.07 \ln\beta + 9.80,$$

where E is the Young's modulus (x 10^{10} dynes/cm^2).

Laboratory-determined elastic moduli for three of the sites were plotted with the same scale as in situ values. These laboratory data plot in a group near the in situ data of the most competent rock, namely a homogeneous, solid granite, instead of near their respective in situ values. It is inferred from this observation that fracturing and associated voids, instead of rock composition, are dominant factors controlling elastic properties of near-surface in situ geologic materials.

The degree of fracturing and associated voids of the sites are related to the parameter θ where θ = dry bulk density/Poisson's ratio.

Introduction

Whitcomb (1965) showed that SH waves can be detected by instruments that measure angular ground motion of in situ materials. This ability is based on a mathematical characteristic of body wave transmission, the cross-product or curl of compressional waves is zero and that of shear waves is not zero. Eight angular accelerometers with a sensitivity of 0.1 mv/rad/sec^2 were used in an array for the detection of direct and refracted SH waves.

After testing different types of energy sources, a small, buried explosive proved to be the most practical means for generating SH waves. Except in volcanic ash sites, the small explosive was placed in the rock to cause fracturing, an effect that almost always successfully generated SH waves in solid materials.

SH-wave investigations of the in situ sites are incomplete; however, many data already gathered permit preliminary calculations of some of the physical parameters for the sites. Because field work is incomplete and the present need is for simplicity, an average of the various calculated physical parameters is used for each site.

In this report, the sites studied for SH waves are briefly described and average physical parameters, calculated from data gathered both in situ and in the laboratory from hand and core samples, are given. A parameter is developed which is applicable to determining the degree of fracturing and associated voids in an in situ material.

SH-Wave Test Sites

Brief descriptions of the sites that have been studied in the SH-wave investigation are given below. More complete descriptions of the general geology at each site can be found in Watkins and others (1964, 1965a, 1965b). Here, the name of each site is preceded by its initials, which are used in the illustrations of this report for brevity and clarity.

SG--Sonora Granite. This granite is coarsely porphyritic, pale pink, generally unweathered, nearly homogeneous, and sparsely jointed.

KL--Kaibab Limestone. The unit consists of a sequence, 80 m thick, of limestone beds and interbedded limestone - clastic beds of Permian age.

MMH--Middle Mesa. This site consists of a cross-bedded, slightly cemented sandstone. The bedding is horizontal and fracturing is slight.

MMT--Middle Mesa. This site consists of a cross-bedded, slightly cemented sandstone. Prominent cross-bedding planes are vertical and there are extensive vertical fracture planes perpendicular to the seismic spread.

BT--Bishop Tuff. This rock is a partially welded, rhyolitic tuff of Pleistocene age, 30 to 60 m thick. The upper 10 or 15 m is welded, hard, and dense, but material beneath is unwelded and less dense to an unknown depth. The upper 10 to 15 m of tuff is a well-indurated rock and is tightly jointed in polygonal columns about 0.7 m in diameter.

KB--Kana-a Basalt. This is a Recent aa lava flow composed of olivine basalt whose upper surface consists of jagged, spinose, vesicular,

clinkery blocks and plates of lava that grade at depth into a fairly massive basalt with varying degrees of vesicularity.

KA--Kana-a Ash. This material overlies the Kana-a Basalt and consists of volcanic ash deposits up to 13 m thick at the study site.

MT--Mono Tuff. This rock is found at depth beneath thick deposits of volcanic ash at the Mono Ash site. It is assumed to be similar to Bishop Tuff material.

MA--Mono Ash. This material consists of a thick layer of white pumiceous ash and lapilli.

SC--Southern Coulee. The site consists of loosely piled angular blocks of rhyolitic pumice and obsidian.

In Situ Elastic Moduli

Table 1 shows average values of density, SH-wave velocity, P-wave velocity, Poisson's ratio, shear modulus, Young's modulus, and bulk modulus calculated for the test sites described in the previous section. Because density, SH-wave velocity, and P-wave velocity are data parameters that can be measured directly, it is natural to examine calculated physical parameters of in situ materials as functions of one or more of the three original parameters. Because this investigation is concerned primarily with SH waves, all physical properties are treated in the illustrations as a function of β, the SH-wave velocity.

Dry bulk densities of ash deposits were calculated from cylindrical samples taken from the surfaces of the deposits; all other dry bulk densities were calculated from hand and core specimens from the sites. Thus, the density values in the table are not actually in situ values, that is, they do not represent a large sample of in situ material which includes voids between blocks.

Figure 1 shows a plot of dry bulk density as a function of β. It is seen that, in general, density increases as β increases; but points are widely scattered.

Figure 2 illustrates a plot of Poisson's ratio as a function of β. Poisson's ratio is one of the more significant of the elastic moduli because of its high sensitivity to changes in the ratio of β to P-wave velocity; the graphical spread of data reflects this sensitivity. At

Table 1. In situ physical properties

	Density g per cc	SH-Wave Velocity (mps)	P-Wave Velocity (mps)	Poisson's Ratio	Shear Modulus ($\times 10^{10}$ dynes/cm^2)	Young's Modulus ($\times 10^{10}$ dynes/cm^2)	Bulk Modulus ($\times 10^{10}$ dynes/cm^2)
Sonora Granite	2.64	2800	5110	0.285	20.7	53.2	41.2
Kaibab Limestone	2.24	1100	1900	0.245	2.71	6.75	4.41
Middle Mesa H	1.97	800	1210	0.115	1.26	7.74	2.05
Middle Mesa T	1.97	500	980	0.320	0.482	1.32	1.22
Bishop Tuff	1.52	880	1400	0.170	1.18	2.76	1.39
Kana-a Basalt	2.51	440	760	0.245	0.486	1.21	0.790
Mono Tuff	1.6 ?	500 ?	780 ?	0.150 ?	.40 ?	9.20 ?	0.438 ?
Mono Ash	1.26 ?	250	460	0.295	0.079 ?	0.204 ?	0.166 ?
Southern Coulee	1.06	240	540	0.375	0.061	0.168	0.224
Kana-a Ash	1.08	200	370	0.295	0.043	0.111	0.090

the lowest values of β, Poisson's ratio appears to be increasing to the theoretical limit of 0.5 for decreasing values of β. A general low is shown around the β = 1000 mps area of the curve followed by the single value of .285 for granite at β = 2800 mps. At present, a preliminary estimate of Poisson's ratio as a function of β for an average near-surface material would be: an approach to 0.5 for values of β lower than 150 mps, a decrease to about 0.2 in the vicinity of β = 1000 mps, and an increase to 0.25 to 0.30 for values of β above 2000 mps.

Figure 3 is a plot of the shear modulus as a function of β. Shear modulus is governed by the equation

$$\mu = \rho\beta^2,$$

where μ is the shear modulus, and ρ the density. Because the magnitude of ρ varies little compared to that of β for the samples, μ exhibits a direct relationship to β when plotted logarithmically. If ρ were constant the equation for the relationship would be

$$\ln\mu = 2\ \ln\beta + C.$$

However, the equation of a straight line, fitted to the data by eye, has the form

$$\ln\mu = 2.35\ \ln\beta + 7.50,$$

which seems to be a reasonable relationship for estimating shear modulus (x 10^{10} dynes/cm^2) from β (mps) pending more field data.

Young's modulus as a function of β is plotted in figure 4. Behavior of this parameter as a function of β is very similar to that of the shear modulus, and yielding an eye-fitted, straight-line equation of

$$\ln E = 2.07\ \ln\beta + 9.80,$$

where E is Young's modulus (x 10^{10} dynes/cm^2).

Figure 5 is a plot of bulk modulus as a function of β. Although the data are scattered, the bulk modulus shows a general increase with β.

Laboratory Elastic Moduli

Laboratory determinations of dynamic and static elastic moduli have been completed at this writing for the Sonora Granite, Kaibab

Limestone, and Kana-a Basalt among the sites studied for SH waves. Dry bulk density, SH-wave velocity, P-wave velocity, Poisson's ratio, shear modulus, Young's modulus, and bulk modulus for the dynamic determinations are given in table 2. Static determinations of Poisson's ratio, shear modulus, Young's modulus, and bulk modulus are given in table 3.

Poisson's ratio, shear modulus, Young's modulus, and bulk modulus are plotted as a function of the dynamic determination of β in figures 6, 7, 8, and 9, respectively, for cores from the three sites. For easy comparison, scales of these illustrations are the same as those plotted for the in situ values.

Because of the present scarcity of data, no conclusions have been formed as to the relationship of laboratory moduli to in situ values. However, laboratory values plot in a group in the vicinity of the data from the most competent in situ rock, the Sonora Granite. This observation may suggest that fracturing and associated voids, instead of rock composition, are dominant factors controlling in situ physical properties of near-surface geologic materials.

Fracturing Parameter

Fracturing and associated voids are dominant factors controlling in situ physical properties of materials. A singular example of the effects of fracturing on the elastic moduli is the divergence of data from the two Middle Mesa sites; the MMH site has almost no, but the MMT site has numerous, vertical fractures perpendicular to the seismic spread. The fractures cause a radical change in the transmission of SH waves through this structure.

A useful fracturing parameter that separates sites according to their degree of fracturing and associated voids is

$$\theta = \frac{\rho}{\sigma}$$

where θ is the fracturing parameter, ρ is dry bulk density, and σ is Poisson's ratio. This parameter is plotted as a function of β for both in situ and laboratory data in figure 10. Figure 10 is divided into four sections representing the following degrees of fracturing: (1) none

Table 2. Laboratory dynamic elastic moduli

	Density (g per cc)	SH-Wave Velocity (mps)	P-Wave Velocity (mps)	Poisson's Ratio	Shear Modulus ($x10^{10}$ dynes/cm^2)	Young's Modulus ($x10^{10}$ dynes/cm^2)	Bulk Modulus ($x10^{10}$ dynes/cm^2)
Sonora Granite	2.64	2460	3760	.124	16.1	36.0	16.6
Kaibab Limestone	2.24	2540	4100	.187	15.4	37.4	21.8
Kana-a Basalt	2.51	2050	3430	.220	11.2	26.8	15.7

Table 3. Laboratory static elastic moduli

	Poisson's Ratio	Shear Modulus ($x10^{10}$ dynes/cm^2)	Young's Modulus ($x10^{10}$ dynes/cm^2)	Bulk Modulus ($x10^{10}$ dynes/cm^2)
Sonora Granite	.148	7.37	18.4	9.23
Kaibab Limestone	.208	15.1	37.1	26.8
Kana-a Basalt	.160	11.9	27.7	14.5

observed, highly competent rock; (2) slight to moderate; (3) moderate to heavy; and (4) loosely piled blocks and ash.

Where near-vertical fracturing dominates in a test site material, the parameter calculated from a spread perpendicular to the fracturing will give a lower value than the parameter from a spread parallel to the fracturing. This effect, caused by impedance to SH waves traversing fracture planes, can be used to determine the direction of maximum fracturing by varying the direction of the seismic spreads.

It is interesting to note the results from the Kana-a Basalt site which, because of its jumbled and platy surface, leads one to the assumption that the rock is heavily fractured. However, the fracturing parameter θ plots in a range indicating slight to moderate fracturing, which is confirmed by penetration of solid vesicular basalts beneath the surface of the flow during drilling (Watkins and others, 1965).

Conclusions

Although this study is not yet completed, some preliminary conclusions have been reached. The most obvious is that SH-wave data, along with P-wave and density data, can potentially give significant information about in situ physical properties of materials, even though parameters such as the elastic moduli do not theoretically apply to these nonelastic media.

Data from sites studied thus far show that fracturing and associated voids, and not rock composition, are dominant properties controlling the in situ physical parameters of shallow (less than 30 m) geologic materials. The degree of fracturing and associated voids of the sites can be qualitatively related to a parameter θ, defined as

$$\theta = \frac{\rho}{\sigma} .$$

This θ can be used as a relative measure of fracturing of rocks encountered during lunar and terrestrial surveys, and can be used to determine direction of dominant vertical or nearly vertical fracture planes in near-surface rocks.

The shear and bulk moduli, because their values for the test areas

can be closely approximated by SH-wave velocity alone, may be useful diagnostic parameters in preliminary seismic surveys.

References

Watkins, J. S., De Bremaecker, J. Cl., Godson, R. H., and Loney, R. A., 1964, Investigation of in situ physical properties of surface and subsurface site materials by engineering geophysical techniques--Project quarterly report, July 1 to Sept. 30, 1964.

Watkins, J. S., De Bremaecker, J. Cl., Loney, R. A., Whitcomb, J. H., and Godson, R. H., 1965a, Investigation of in situ physical properties of surface and subsurface site materials by engineering geophysical techniques--Project annual report, FY 1965.

Watkins, J. S., Loney, R. A., Whitcomb, J. H., and Godson, R. H., 1965b, Investigation of in situ physical properties of surface and subsurface site materials by engineering geophysical techniques--Project quarterly report, Oct. 1 to Dec. 31, 1964.

Whitcomb, J. H., 1965, Shear-wave detection, in Watkins, J. S., De Bremaecker, J. Cl., Loney, R. A., Whitcomb, J. H., and Godson, R. H., 1965, Investigation of in situ physical properties of surface and subsurface site materials by engineering geophysical techniques--Project annual report, FY 1965, p. C-1 - C-10.

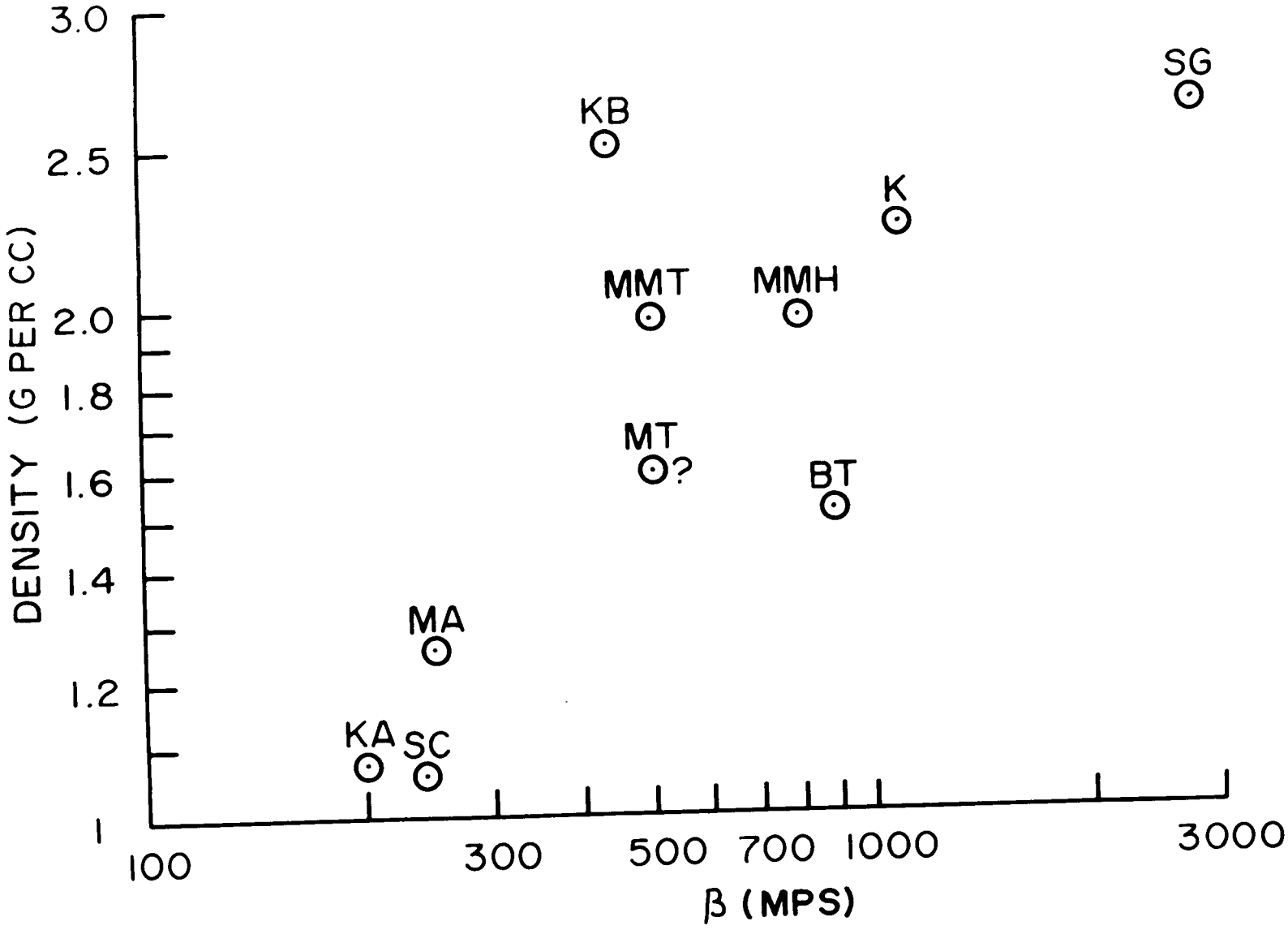

Figure 1.--Dry bulk density vs. SH-wave velocity.

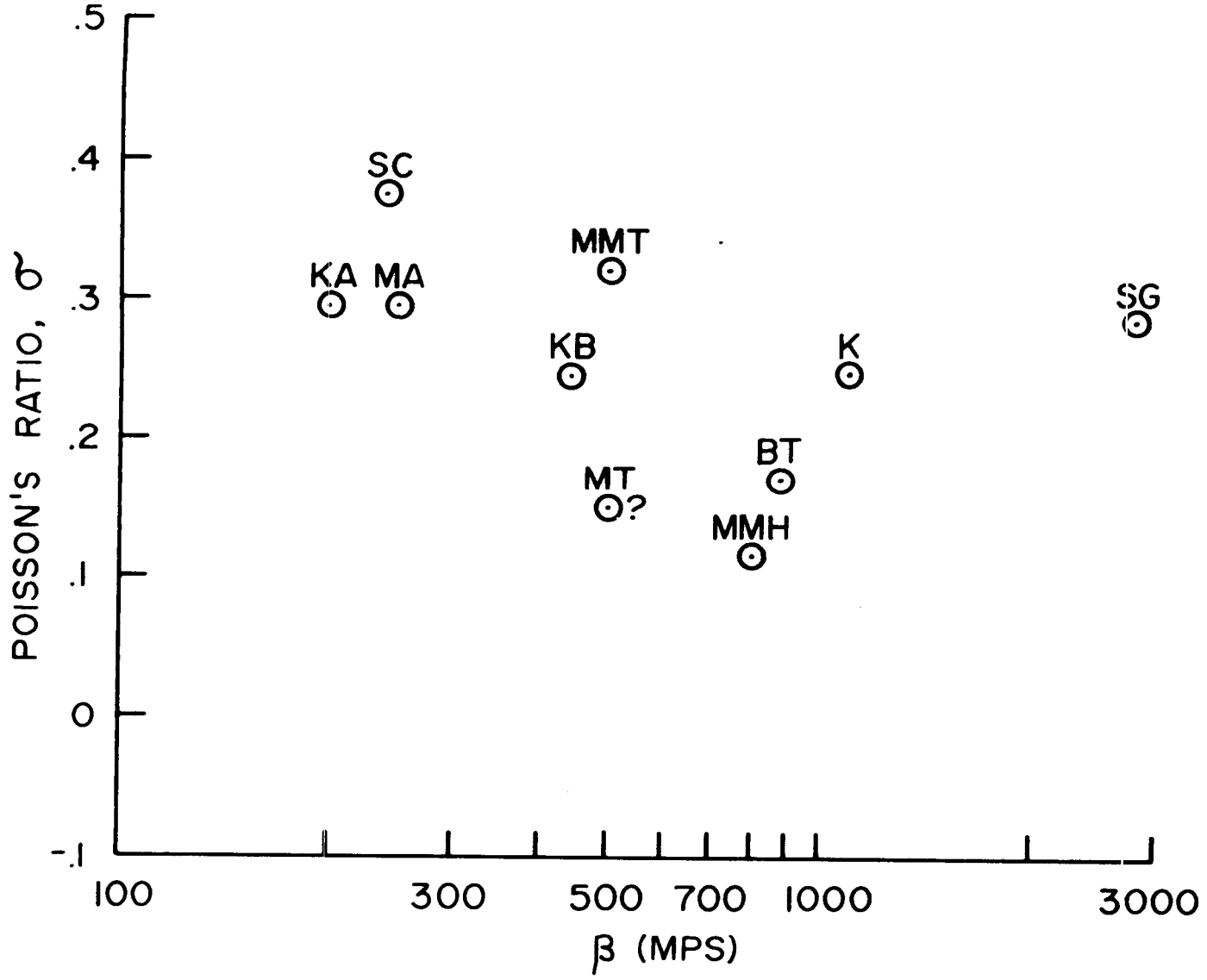

Figure 2.--In situ Poisson's ratio vs. SH-wave velocity.

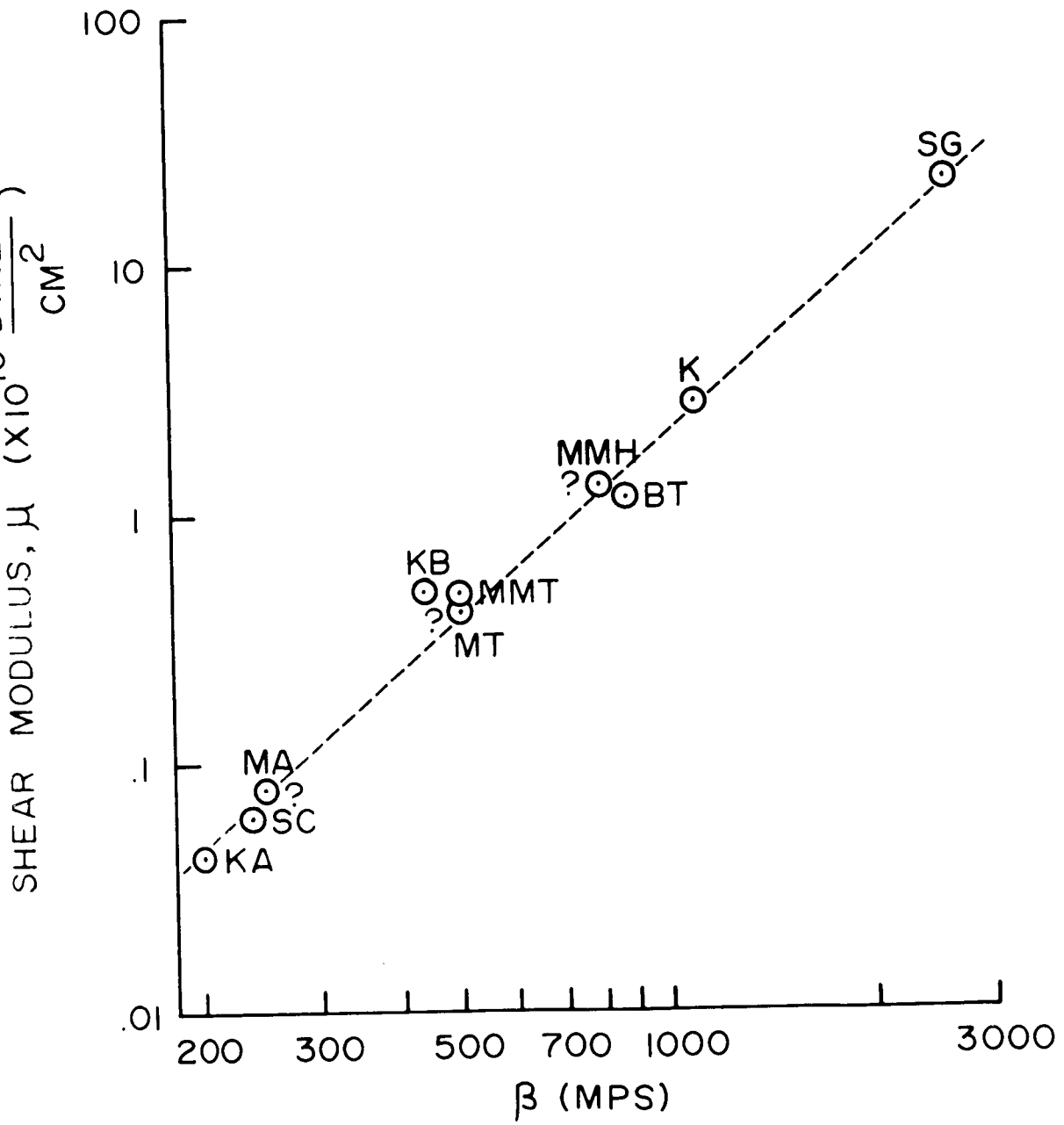

Figure 3.--In situ shear modulus vs. SH-wave velocity.

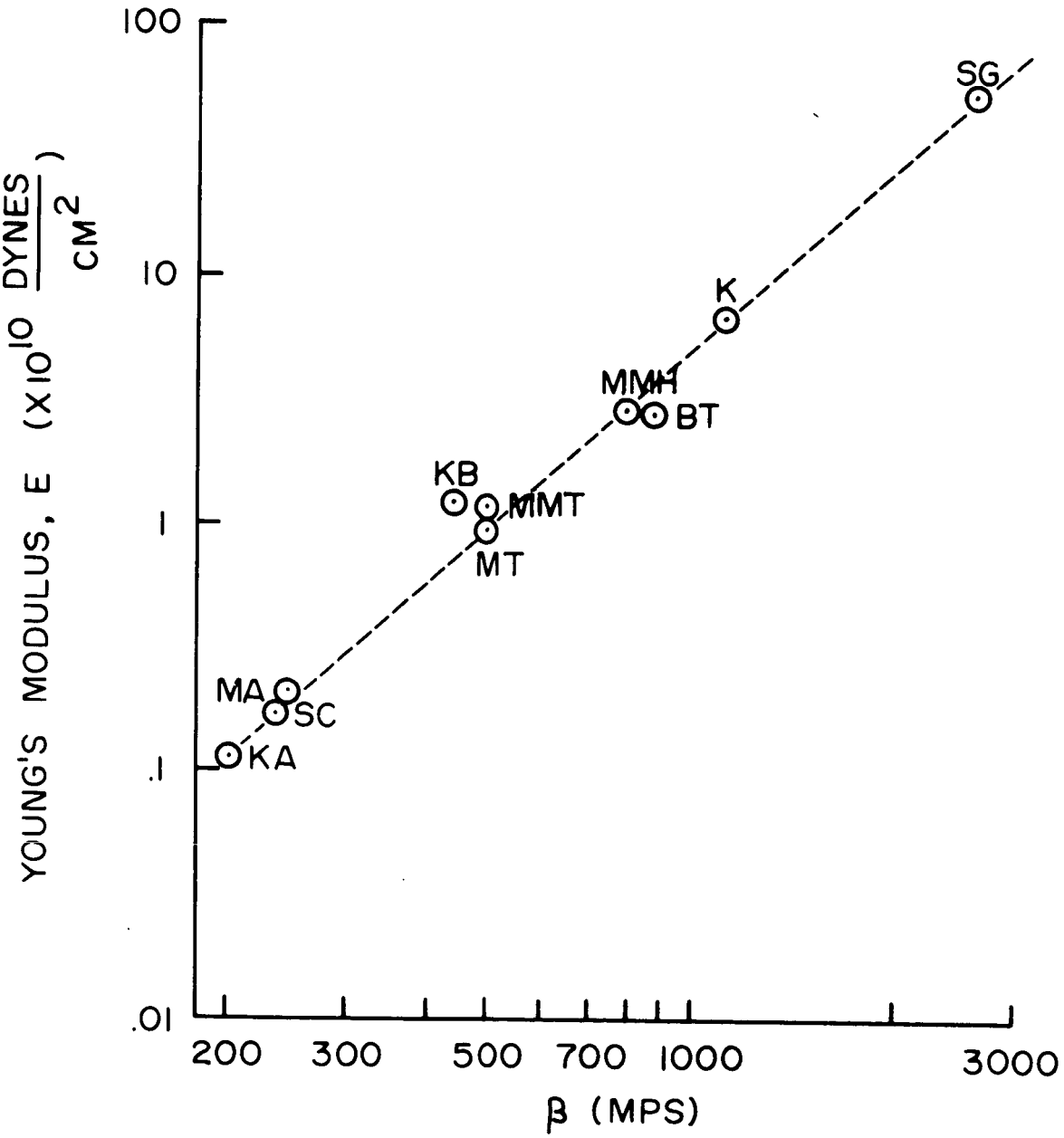

Figure 4.--In situ Young's modulus vs. SH-wave velocity.

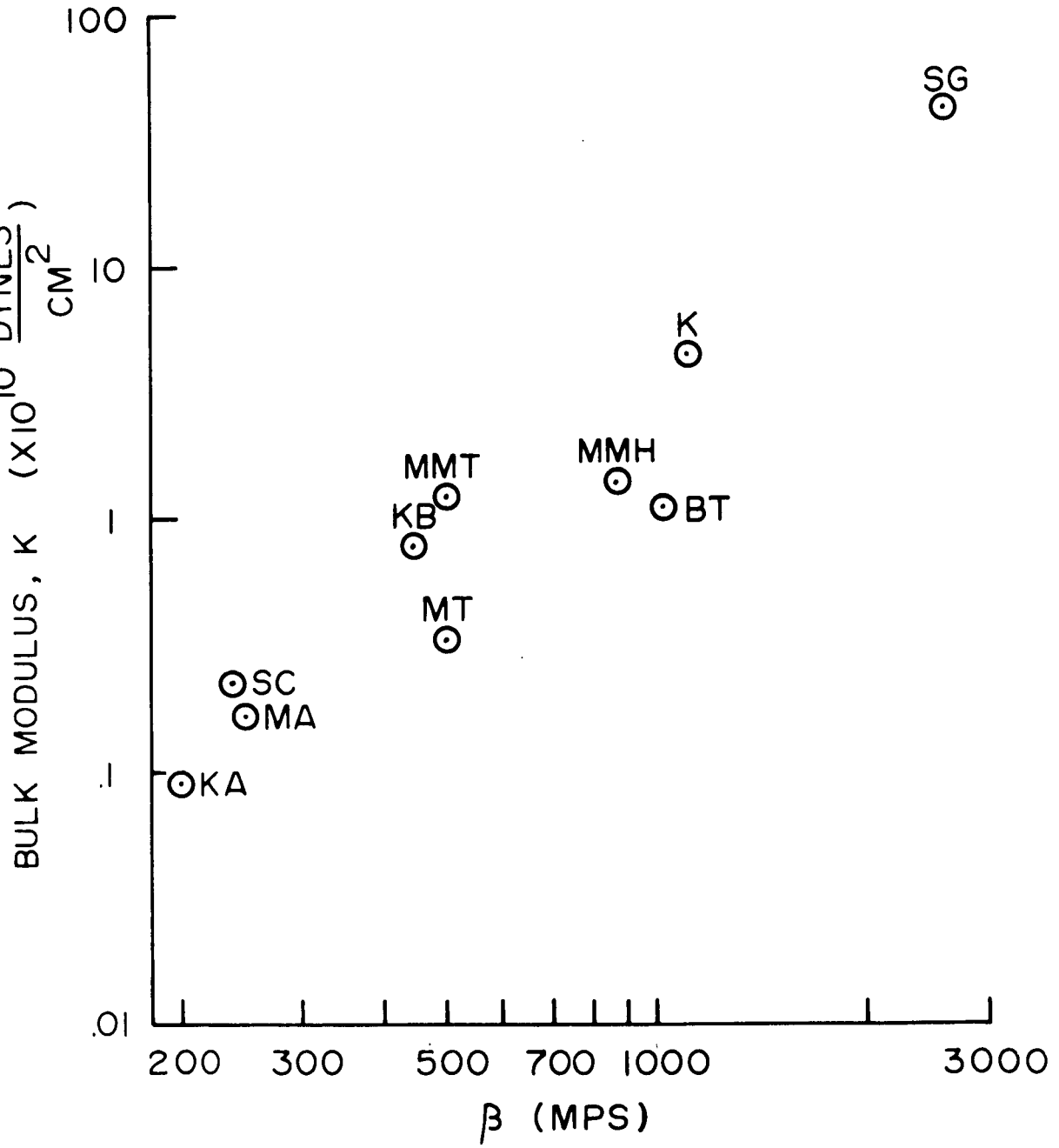

Figure 5.--In situ bulk modulus vs. SH-wave velocity.

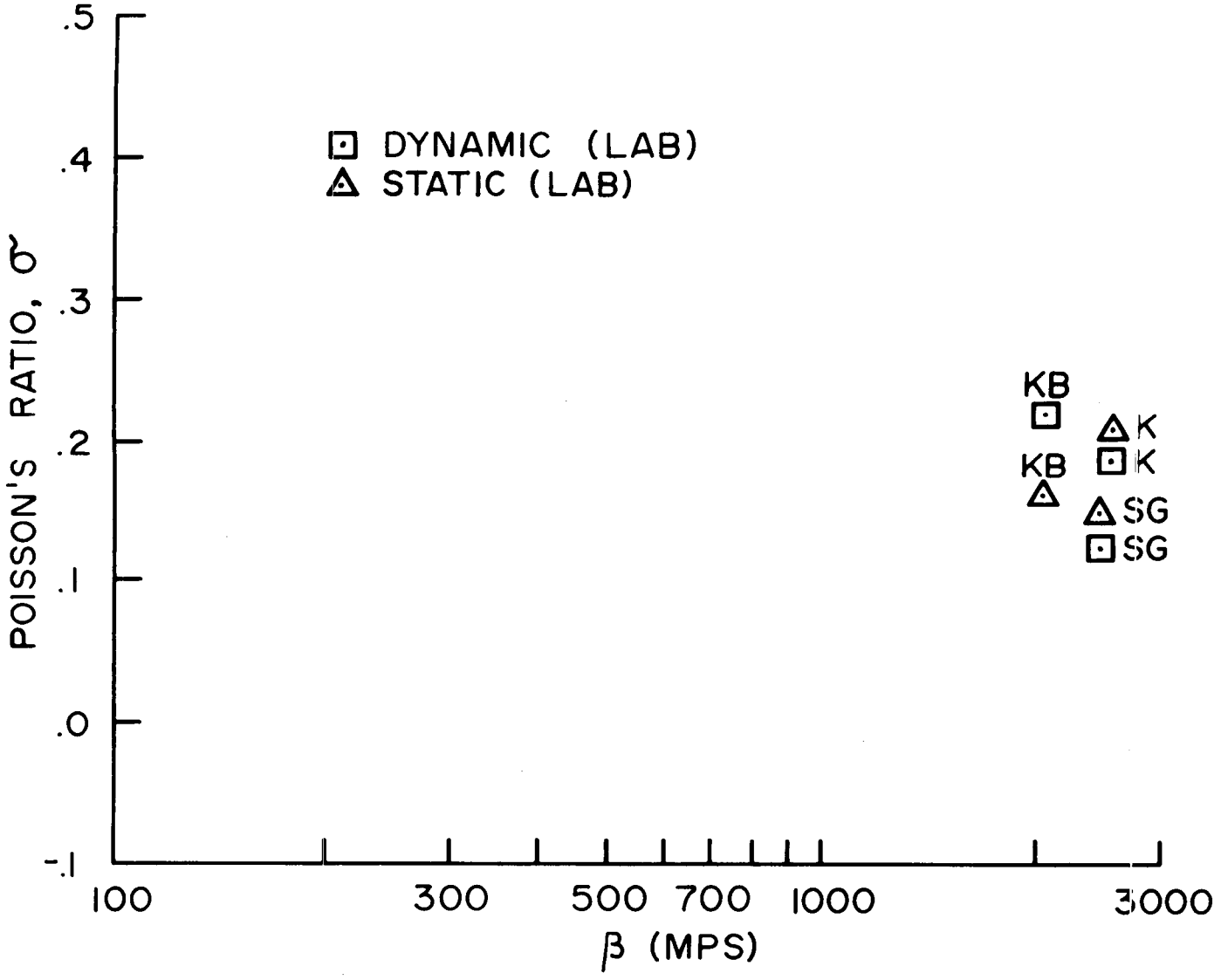

Figure 6.--Laboratory Poisson's ratio vs. SH-wave velocity.

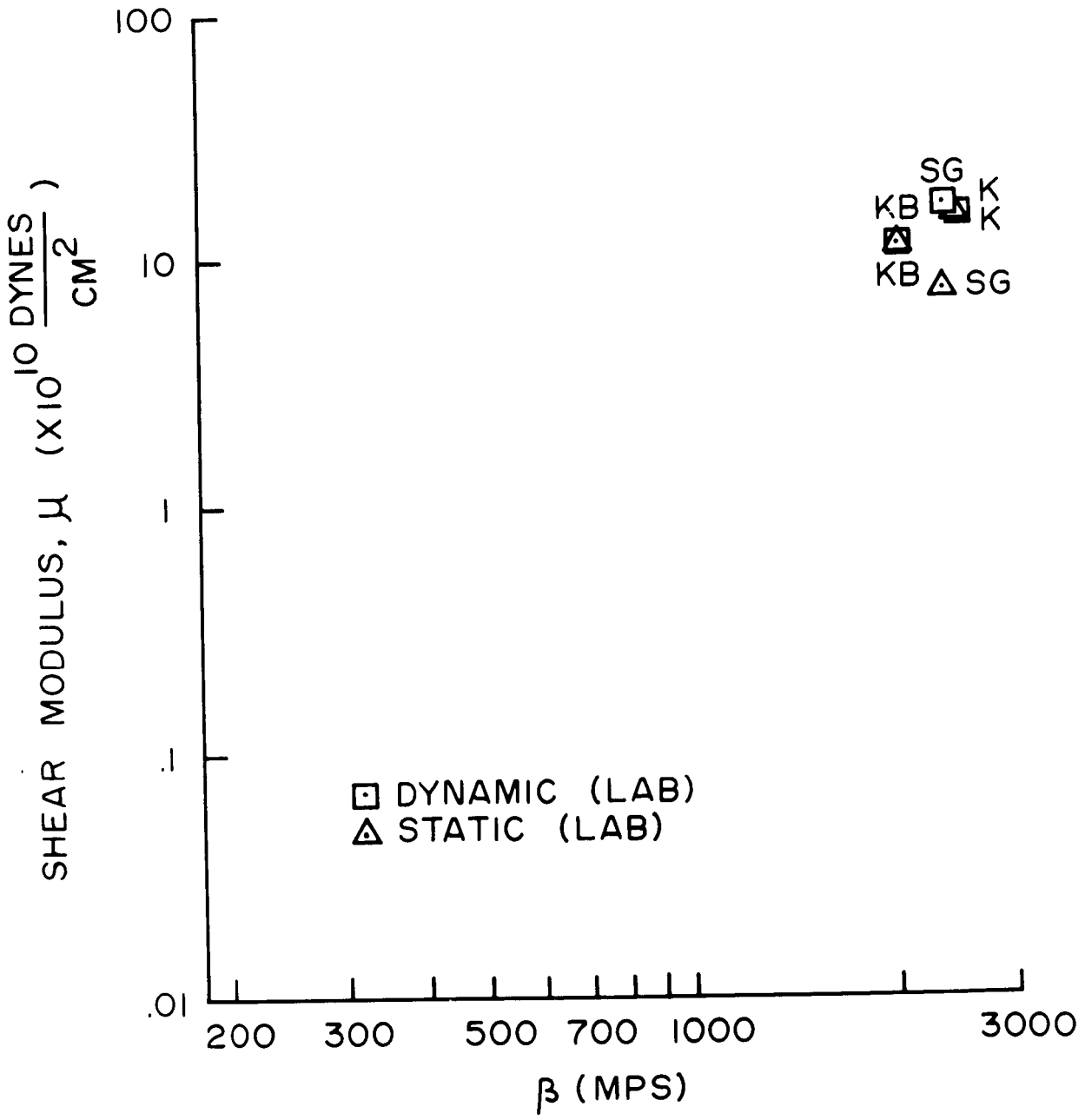

Figure 7.--Laboratory shear modulus vs. SH-wave velocity.

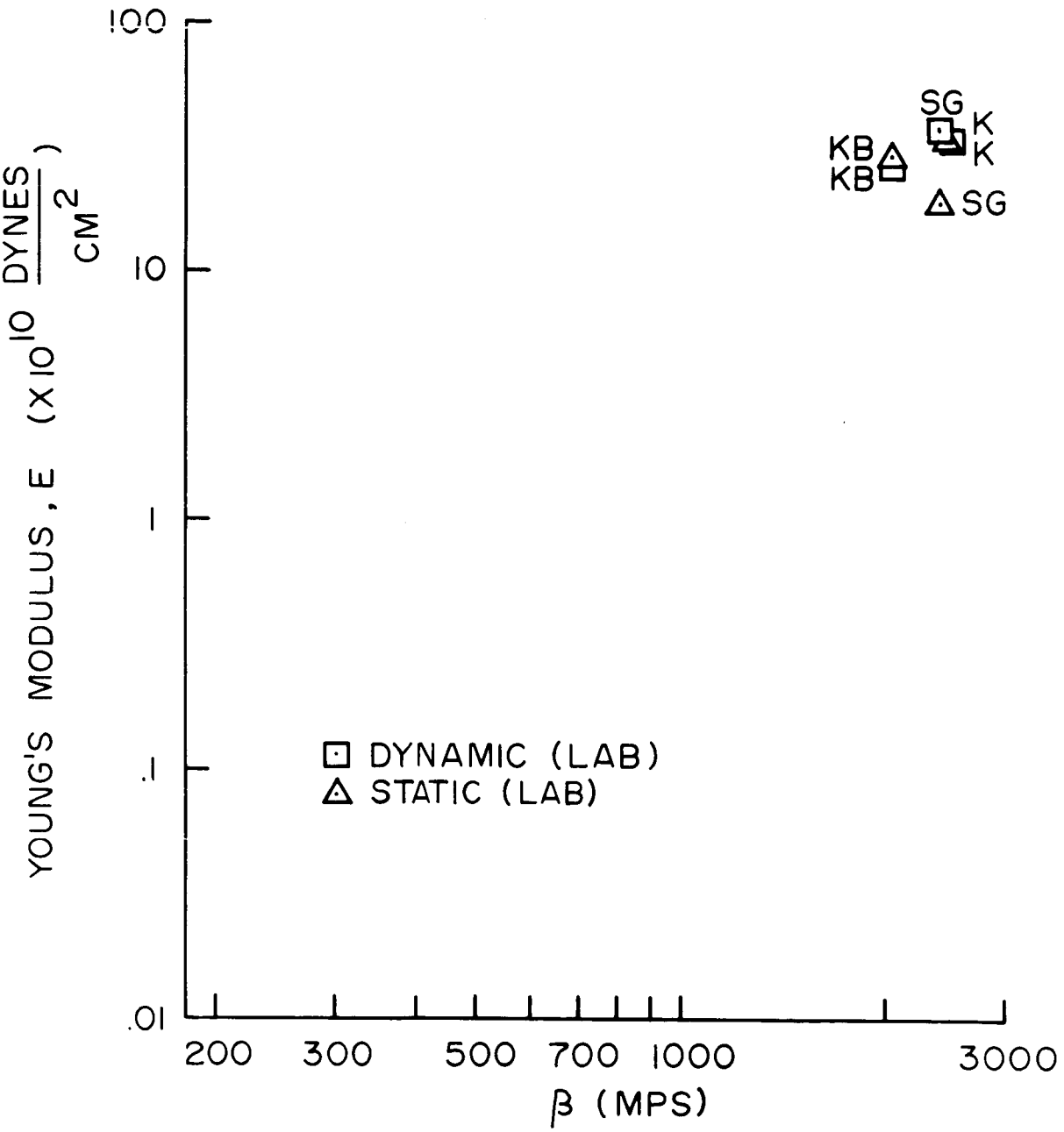

Figure 8.--Laboratory Young's modulus vs. SH-wave velocity

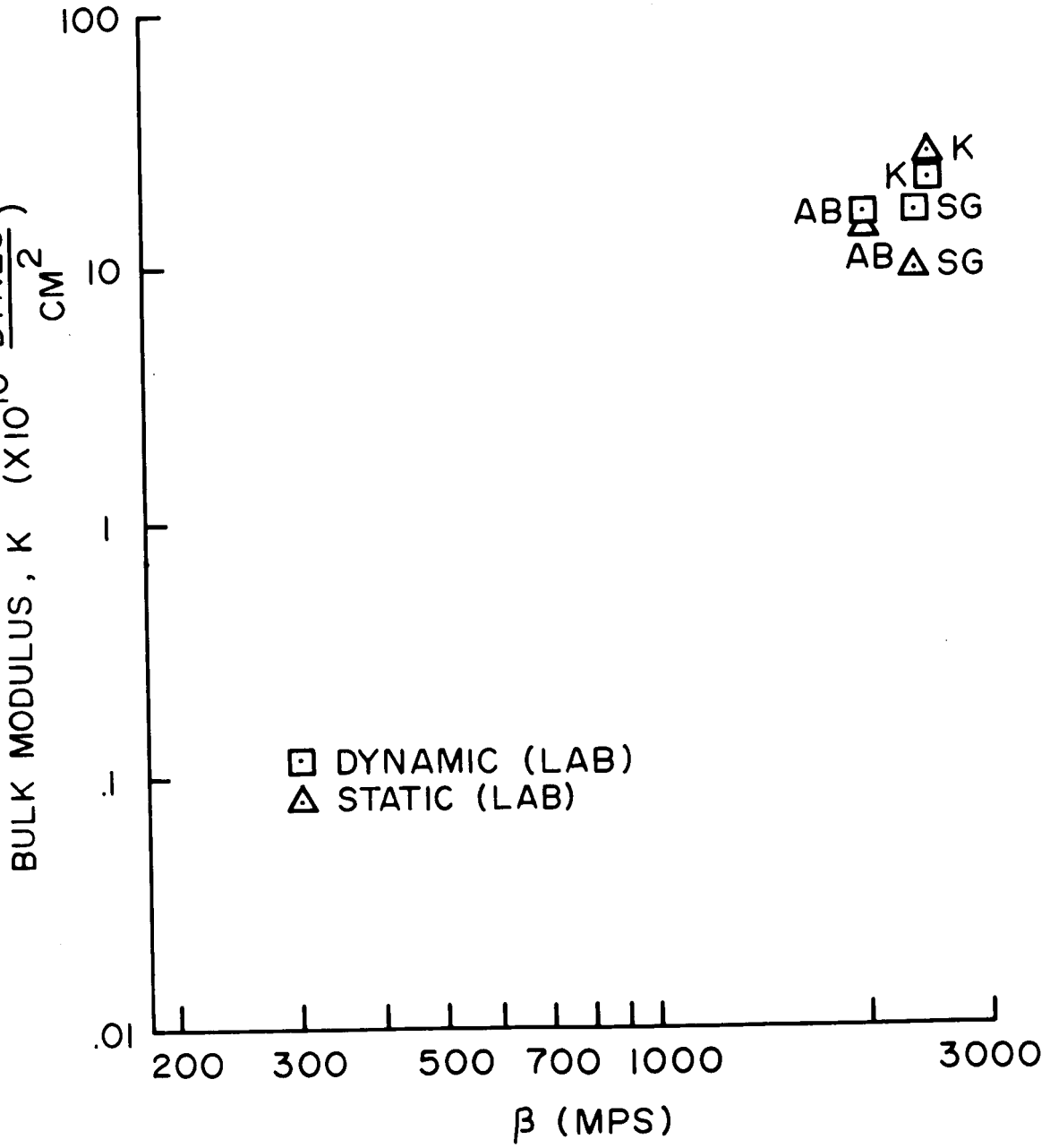

Figure 9.--Laboratory bulk modulus vs. SH-wave velocity

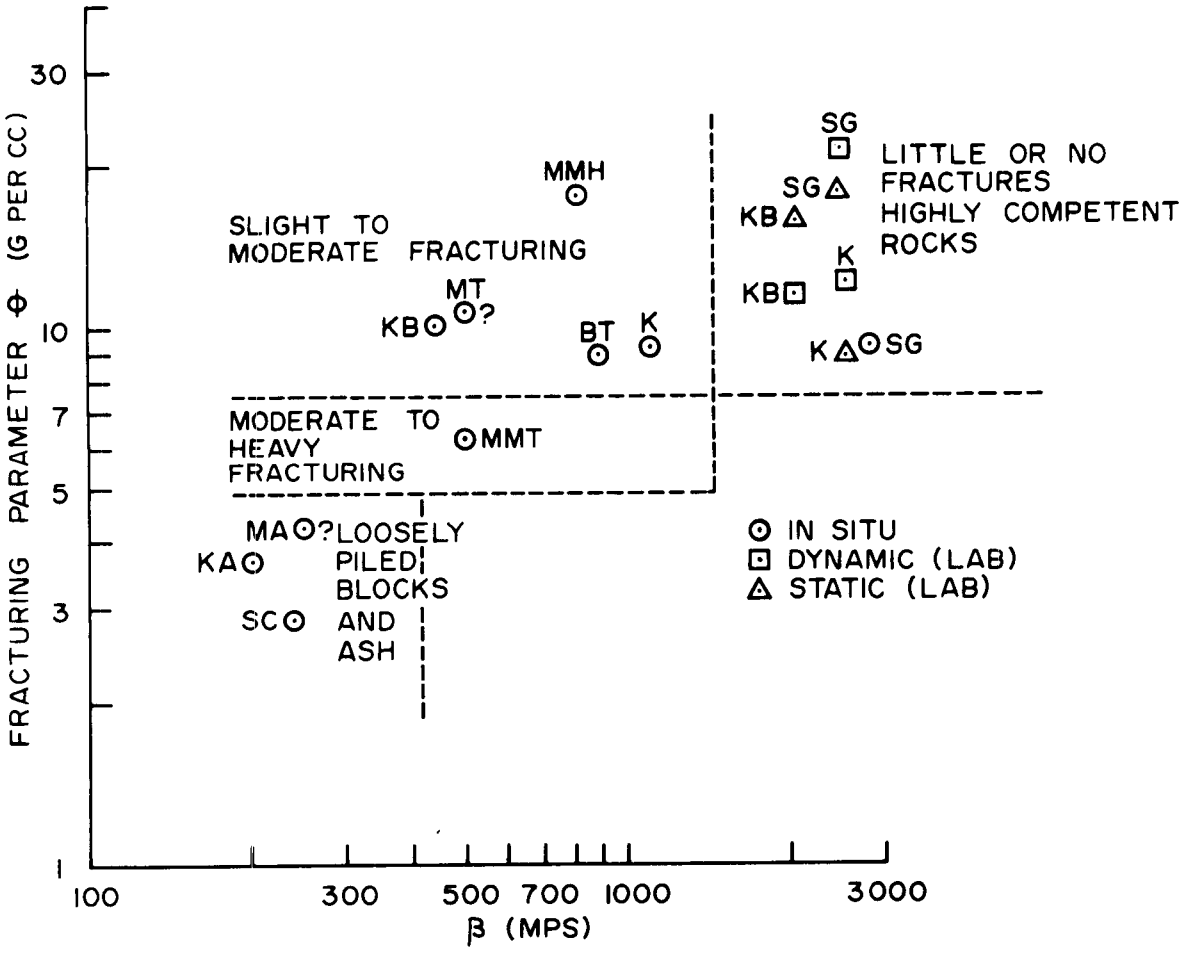

Figure 10.--Fracturing parameter as a function of SH-wave velocity.

IN SITU BULK DENSITY MEASUREMENT AT S P FLOW, ARIZONA

by Lawrence A. Walters

ABSTRACT.--Recent excavations at S P flow, an andesitic basalt flow of Recent age, have shown that the in situ bulk density of materials lying within 3 m of the surface was 1.23 g per cc, although the bulk density of the individual blocks of andesitic basalt was 2.22 g per cc. If the same packing arrangement were employed with low density pumice blocks, such as those of the Mono Craters, California, where densities as low as 0.49 g per cc have been observed, the in situ bulk density would be approximately 0.3 g per cc.

Introduction

In situ bulk density measurements were made on S P flow as part of the continuing program of study of the interrelationships of various physical parameters of lunar analog materials.

Studies of compressional wave seismic velocities as a function of bulk densities suggested that the in situ bulk density of the upper part of the S P flow should be lower than the average density of 2.22 g per cc determined for individual blocks of the lava. Numerous voids existed between the blocks of lava on the surface of the flow, but their amount and variation with depth of the voids was not known.

Location and Geologic Setting

S P flow is a thoroughly fractured, blocky, andesitic basalt flow located in the northern part of the San Francisco volcanic field (fig. 1). The flow extends 4.5 miles north from the base of S P Crater and its maximum is about 1.5 miles wide. The maximum thickness probably does not exceed 200 ft. The S P Crater, a contemporary cinder cone, is the source of the flow. Sabels (1960) dated the flow at about 1300 years.

The flow consists of loosely packed, angular, polygonal blocks of lava that range in size from less than 1 inch to greater than 5 ft in their largest dimension. Abundant fines consisting of ash and residual weathering products are found in the voids between the blocks of lava.

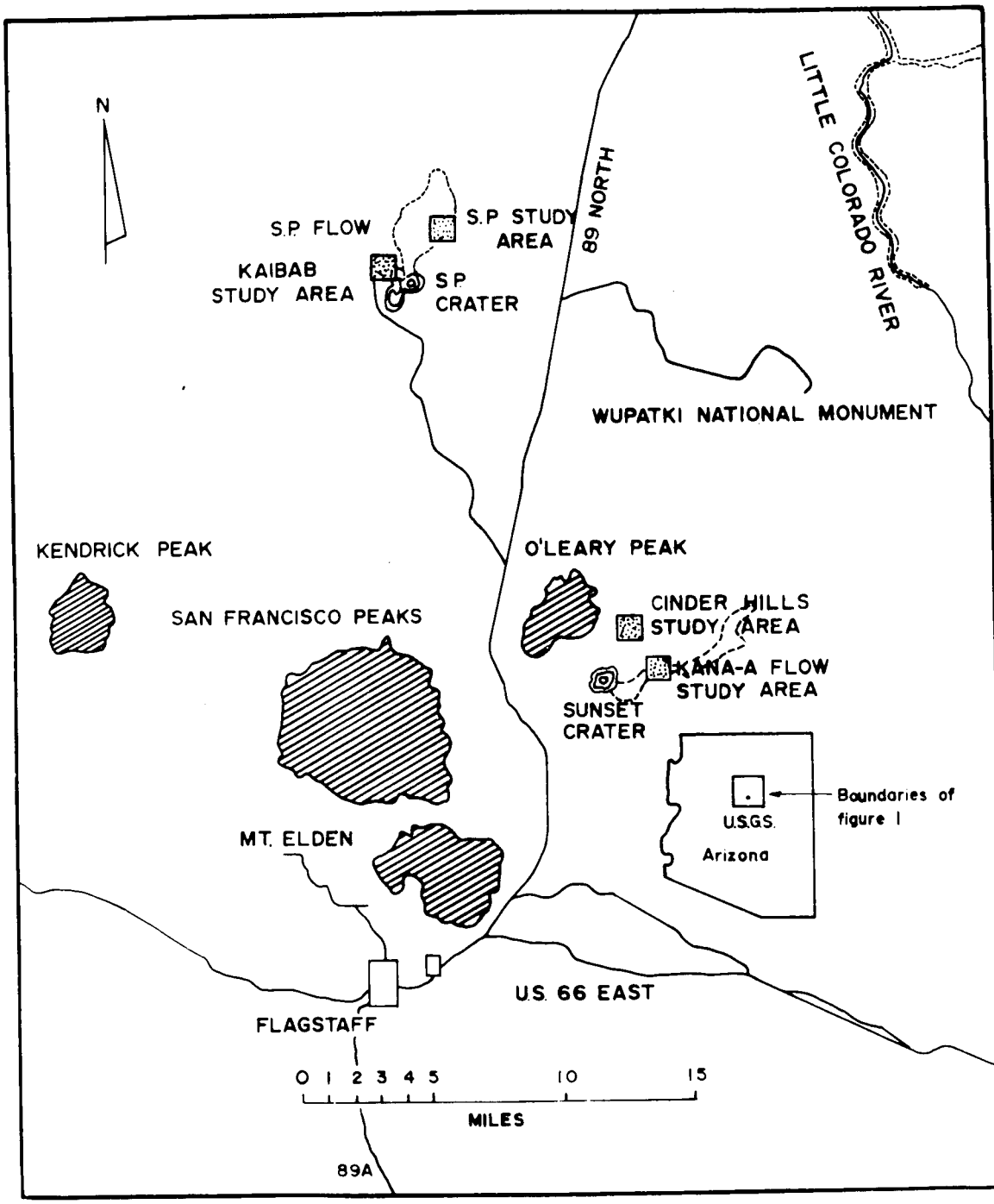

Figure 1.--Location of S P flow relative to prominent terrain and cultural features of north-central Arizona.

The lava is dark gray to black and at places weathers to reddish brown.

Petrographic Description

Modal composition of the S P andesitic basalts is as follows: andesine (An_{40-48}; 26 percent); diopsidic augite ($2V_z = 56^o-62^o$; 24 percent); olivine (2 percent); brown glass ($n_D = 1.540 \pm .003$; 36 percent); vesicles (12 percent); and magnetite (trace) Loney (1965). In general, the rock is a fine-grained andesitic basalt with small, flattened vesicles. It has a porphyritic hyalopilitic texture in which brown glass occupies the interspaces between the laths of plagioclase and the prisms of pyroxene. The vesicularity of the rocks ranges from almost zero to greater than 50 percent.

Techniques

An area was selected where the compressional wave velocity of the upper unit of the flow was low and where relief was minimal. A level frame of 2 in. x 6 in. boards, 10 ft x 10 ft was erected (fig. 2a). The frame was braced and the corners and braces were cemented to the surface of the flow.

A thin piece of canvas was placed over the lava inside the frame, making certain that it conformed very closely to the actual relief on the top of the flow. A thin plastic tarp was placed on top of the canvas and the edges draped over the upper edge of the wooden frame. Water was pumped into the plastic pool until the highest point on the flow was just covered by water (fig. 2b). The level of the water with respect to the wooden frame and the volume of the water were recorded.

The tarps were removed, and the rock bounded by the frame was excavated to a depth of 9.5 ft (fig. 2c) and weighed. The freezing of moisture within the flow attached fines to adjacent blocks of lava and none of the fines were lost due to sifting ahead of the level of excavation.

As the excavation progressed, the walls were sprayed at night with a fine mist of water from a fruit sprayer. This water froze to the outer surface of the walls and cemented the loose blocks together, thus

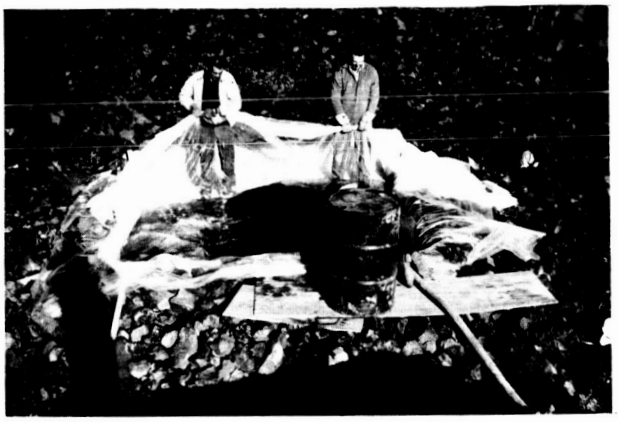

Figure 2.--Photographs showing excavation at S P flow. Top left, erection of rigid reference frame; top right, volume measurement of irregular surface of the flow; bottom left, cross section of lava flow in the wall of the excavated pit; bottom right, excavated pit, lined with plastic, being filled with water.

stabilizing the walls and preventing cave-ins. Additional water was pumped into the flow a few feet behind the walls of the pit to provide additional support when it froze. During the day, white tarps were placed over the iced walls to prevent the black rocks from absorbing enough heat to cause melting. This technique was successful on all walls except the north wall, which melted because of long exposure to the sun each day. Additional cribbing of 2 in. x 6 in. timber was needed to stabilize this wall.

The completed pit was lined with canvas tarps. A 30 ft x 32 ft plastic tarp was placed on top of the canvas and its edges draped over the wooden frame (fig. 2d). The plastic-lined pit was filled with water to the same level relative to the frame as it was before excavation. The water level was measured at eight places around the frame. Six measurements were identical, but two on the northeast corner indicated that that corner had settled .25 inches. Since it is reasonable to assume that the corner would only move differentially, the six identical measurements indicate that most of the frame remained stationary. The volume of water needed to just completely cover the top of the flow before the excavation was subtracted from the volume needed to fill the pit to the same level after the excavation.

Results

The excavation yielded 37,819.5 lb of material and the volume of the pit was 487.7 cu ft.

If the plastic and canvas tarps did not conform exactly to the configuration of the pit, the above measured volume would be too small relative to the actual volume. It does not seem likely that the above measurement could be in error by more than 5 cu ft. Therefore, the maximum volume of the pit could not be greater than 492.7 cu ft.

The scales used in weighing the excavated material were accurate to ± 0.5 lb in 250-lb lots, since 160 lots were weighed, the figure of 37,819.5 lb is accurate to ± 80 lb.

Hence, the bulk density measurement has the following range of error:

$$\frac{37{,}819.5 \text{ lb rock}}{487.7 \text{ cu ft}} \times .01602 = 1.24 \text{ g per cc}$$

$$\frac{37{,}739.5 \text{ lb rock}}{487.7 \text{ cu ft}} \times .01602 = 1.24 \text{ g per cc}$$

$$\frac{37{,}819.5 \text{ lb rock}}{492.7 \text{ cu ft}} \times .01602 = 1.23 \text{ g per cc}$$

$$\frac{37{,}739.5 \text{ lb rock}}{492.7 \text{ cu ft}} \times .01602 = 1.23 \text{ g per cc.}$$

Hence, the bulk density of the upper 9.5 feet of the S P flow appears to be 1.235 ± .005.

Conclusions

This measurement suggests that it may be possible to account for the low-density layer thought to exist on the lunar mare surfaces without invoking extraterrestrial processes. At S P flow, the bulk density of materials lying within 3 m of the surface was 1.23 g per cc although the bulk density of individual blocks of lava was 2.22 g per cc. If these blocks were replaced in the same packing arrangement by pumice blocks, whose individual bulk densities range down to 0.49 g per cc, the average bulk density of the composite blocks could be approximately 0.3 g per cc.

References

Loney, R. A., 1965, The Kana-a flow, an alkali basalt of the San Francisco volcanic field, Arizona, in Watkins, J. S., De Bremaecker, J. Cl., Loney, R. A., Whitcomb, J. H., and Godson, R. H., 1965, Investigation of in situ physical properties of surface and subsurface site materials by engineering geophysical techniques--Project annual report, FY 1965, p. D-1 - D-48.

Sabels, B. E., 1960, Late Cenozoic volcanism in the San Francisco volcanic field and adjacent areas in north-central Arizona: Univ. of Arizona, unpublished doctor's thesis.

AUTOMATIC DATA PROCESSING

by Jean Claude De Bremaecker and James H. Whitcomb

ABSTRACT.--Computer programs have been written for the digital analysis of seismic data. These programs provide spectral analysis, single or multichannel filtering, velocity filtering, cross correlation, autocorrelation and computation of the true ground motion.

For maximum flexibility, subroutines, which perform the actual computations on the seismic data, are controlled by main-line programs which can be changed to suit the programmer's needs with little programming effort.

The subroutines and/or main-line programs, written in FORTRAN IV for a CDC 3600, are available upon request.

Introduction

Our aim has been to provide all of the programs necessary for the usual treatment of seismic data in digital form. Broadly speaking, this includes spectral analysis, single or multichannel filtering, velocity filtering, cross correlation, autocorrelation and computation of the true ground motion. Other aspects of data analysis may be added as the need arises. General references on spectral analysis are Blackman and Tukey (1959), Lee (1961), and Lanczos (1956).

Project philosophy in programming has been to subroutinize operations in order to provide maximum flexibility and to make "debugging" easier. The subroutines and/or main-line programs, written in FORTRAN IV language for a CDC 3600, are available upon request. Descriptions of the subroutines and their functions are given, followed by some examples of the use of these subroutines in main-line programs.

Subroutines

UNPACK

The family of subroutines titled UNPACK reads and stores a group of analog traces in digital form. Individual traces are then unscrambled from their original data form and stored in a matrix in the computer,

making them ready for further computations. The UNPACK family of subroutines is a prerequisite for any analysis of the seismic data and is the first subroutine incorporated in any main-line program.

TRNSFRM

This subroutine computes the amplitude spectrum of a function which is, in this case, the digitized seismic trace. The method uses an approximation to the integral known as "Filon's method." The method is given in many textbooks on numerical analysis which deal with quadratures (Hamming, 1962).

CHANCOR

The object of the CHANCOR subroutine is to correct the obvious digitization errors in the digitized seismic record. In general, the method computes the standard deviation of all the digitized values and then compares each value for validity with the magnitude of five times the standard deviation. If one or two errors in a row are detected, they are smoothed over, using adjacent values, but if three or more errors are detected, the record is discarded and no computations are made.

DETREND

In order to eliminate errors caused by a biasing of the data in computations, a least squares straight line is calculated for the seismic trace data. The least squares line is subtracted from the data prior to analysis by another subroutine or the main-line program.

CONVO

This subroutine permits filtering data by even filters. The process in digital analysis is called convolution or rectangular integration and its analog equivalent can be thought of as a frequency filter of variable bandpass width and shape. The shape of the filter can be varied by the programmer and a relatively narrow bandpass response can be obtained.

PYSLICE

The subroutine, PYSLICE, velocity-filters adjacent seismic traces of a record as described in Embree and others (1963). The general operation of PYSLICE is to filter, using the CONVO subroutine, traces of the seismic record by a given, even filter. Then, amplitudes of adjacent traces are added with various time shifts to provide the velocity filtering effect.

AUTOCOR

AUTOCOR computes the autocorrelation function for a given window and given maximum phase shift of the seismic trace. Digitally, the process simply multiplies a time window by the same window at various phase shifts. The function has no real physical significance in itself, but may prove useful for interpretation of seismic data.

CROCOR

Crosscorrelation of adjacent traces is computed by CROCOR, given a specified time window and maximum phase shift. The function thus provides a measure of continuity of signal from trace to trace; however, as in AUTOCOR, it has no physical significance except as an aid to interpretation.

Main-Line Programs

The subroutines described in the previous section can be called by a main-line program that is written to perform one or more digital analysis computations on a record. These main-line programs are flexible and can be revised with little effort on the programmer's part. Examples of main-line programs in use are given below.

ATTNALN

The purpose of the ATTNALN is to find the amplitude spectra for a given time window of all the traces of any number of successive digitized analog records. The program uses UNPACK, CHANCOR, DETREND, and TRNSFRM in succession for each analog record.

CORLAT

The autocorrelation function for a given time window for each trace of any number of successive digitized analog records is computed using UNPACK, CHANCOR, and AUTOCOR in succession for each analog record.

References

Blackman, R. B., and Tukey, J. W., 1959, The measurement of power spectra from the point of view of communications engineering: New York, Dover Pubs., 190 p.

Embree, Peter, Burg, J. P., and Backus, M. M., 1963, Wideband velocity filtering--the Pie-slice process: Geophysics, v. 28, no. 6, p. 948-974.

Hamming, R. W., 1962, Numerical methods for scientists and engineers: New York, McGraw-Hill, 309 p.

Lanczos, Cornelius, 1956, Applied analysis: New York, Prentice-Hall, 539 p.

Lee, Y. W., 1961, Statistical theory of communication: New York, John Wiley & Sons, 509 p.

PLANS FOR THIRD QUARTER, FISCAL YEAR 1966

by Joel S. Watkins

Operations in the third quarter of Fiscal Year 1966 will be strongly oriented toward determining in situ seismic and engineering properties of low-density materials. One promising site which is yet to be reconnoitered is the Lompoc site in Southern California, which consists of a thick accumulation of diatomaceous earth. Loess in the Denver region, mine tailing dumps at borax and bentonite mines also seem promising as models for study of very low-density materials. As this report is being prepared, preliminary data from White Sands, New Mexico, indicate that the bulk density of gypsum sands is somewhat higher than anticipated; consequently, no further study is anticipated for that site.

An extensive suite of SH-wave measurements will be conducted on several of the sites not previously examined. Because the SH-wave detection technique utilizing angular accelerometers was discovered long after the inception of the P-wave velocity attenuation and frequency measurements, several of the earlier P-wave study sites have yet to be studied for SH-wave characteristics.

Coring is now under way at the south rim of Meteor Crater and is expected to be finished sometime near the end of February. Coring will then start at Middle Mesa and will be followed by coring at Sierra Ancha.

Automatic data processing and petrographic analyses of geologic data will continue along lines indicated in the introduction. Completion goals for all petrographic analyses and computer programs are June 1, 1966.

Physical properties of available cores will be measured during this quarter and physical properties measurements from all test sites will be completed by June 1, 1966.